https://ntrs.nasa.gov/search.jsp?R=19790017336 2020-03-21T21:51:18+00:00Z

NASA Contractor Report 159040

LOW ENERGY PROTON RADIATION DAMAGE TO (AlGa)As–GaAs SOLAR CELLS

(NASA-CR-159040) LOW ENERGY PROTON RADIATION DAMAGE TO (AlGa)As-GaAs SOLAR CELLS Final Report, 5 Jul. 1978 - 5 Jan. 1979 (Hughes Research Labs.) 106 p HC A06/MF A01 CSCL 10A G3/44 N79-25507 Unclas 26428

Robert Loo, Sanjiv Kamath, and Ronald Knechtli

Hughes Research Laboratories

3011 Malibu Canyon Road

Malibu, CA 90265

January 1979

Contract NAS1–15443

Final Report

For period 5 July 1978 through 5 January 1979

National Aeronautics and Space Administration

Langley Research Center
Hampton, Virginia 23665

HUGHES

HUGHES AIRCRAFT COMPANY
RESEARCH LABORATORIES

LOW ENERGY PROTON RADIATION DAMAGE TO (AlGa)As-GaAs SOLAR CELLS

Robert Loo, Sanjiv Kamath, and Ronald Knechtli

JANUARY 1979

Contract NAS1-15443
FINAL REPORT

For period 5 July 1978 through 5 January 1979

Prepared for
NASA
Langley Research Center
Hampton, VA 23665

TABLE OF CONTENTS

SECTION 1

INTRODUCTION AND SUMMARY

The objective of this contract was to evaluate the performance of (AlGa)As-GaAs solar cells irradiated by low-energy protons (50 keV, 100 keV, and 290 keV) and to compare it to the performance of silicon solar cells under the same conditions. This study is an extension of the work previously done under contract to NASA Langley on high-energy proton irradiation at 15.4 MeV and 40 MeV (contract No. NAS1-14727).

The low-energy proton irradiation was performed at Hughes Research Laboratories (HRL) using an ion-implantation machine. Both the GaAs and Si solar cells were mounted side by side on aluminum plates. They were irradiated in vacuum (~10^{-6} Torr) at room temperature. The fluence over the target plate was uniform within $\pm$5 percent.

Figure 1 shows the (AlGa)As-GaAs solar cell structure used for this study. The n^+ concentration for the substrate is >5 x 10^{17} cm^{-3} with Te as the dopant. The n buffer layer concentration is 1 x 10^{17} cm^{-3} and the thickness is greater than 10 μm. The Be-doped p^+ (AlGa)As window layer is grown by infinite solution epitaxy on GaAs. Its carrier concentration is 1 x 10^{18} cm^{-3}. During (AlGa)As window layer growth, a p-n junction is formed by Be diffusion from the (AlGa)As layer into the n buffer layer. The carrier concentration of the p diffused layer also is 1 x 10^{18} cm^{-3}. The thickness of the (AlGa)As window layer is 0.5 μm or less, and the junction depth for these cells is controllably held close to 0.5 μm. A shallow junction depth has been shown to enhance the resistance to radiation damage (see Appendix A). The remaining parts of the baseline structure are self-explanatory. The AuZn contacts are about 3000 to 4000 Å thick with a silver overlay about 4 μm thick. The n contact is AuGeNi (~5000 Å) with Ag overlay. The anti-reflection (AR) coating is Ta_2O_5. The cells used for the proton damage studies have a power conversion efficiency of approximately 16 percent with no cover glass protection.

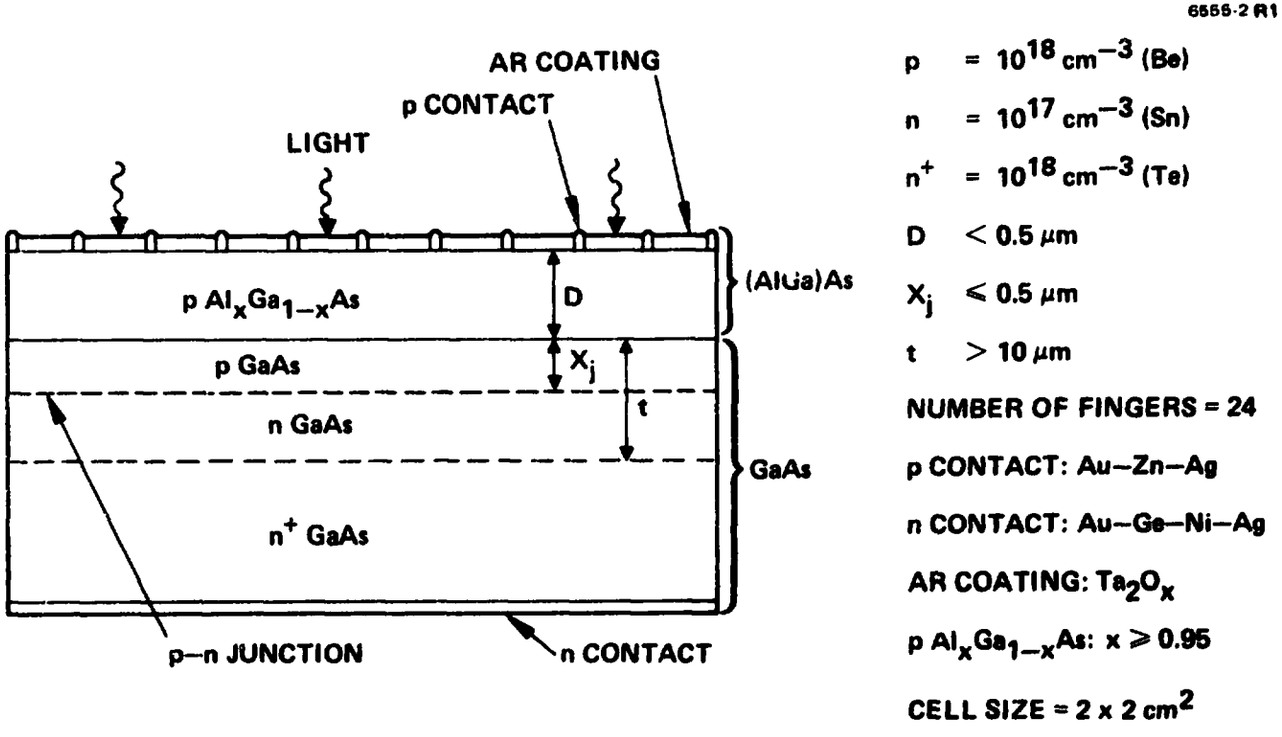

Figure 1. (AlGa)As-GaAs solar cell structure used in proton irradiation experiment.

Table 1 gives the full matrix of tests performed on the GaAs and silicon solar cells. In addition, three GaAs solar cells were protected with 12-mil-thick cover glass and then irradiated under the same conditions as the others to verify the shielding effect of glass against low-energy protons.

Figure 2 shows the penetration range of protons bombarding GaAs and silicon as a function of proton energy. The low-energy protons do not penetrate far into the cell, and the physical damage they create is close to the surface of the cell. Also, low-energy protons produce nonuniform damage; when they are stopped in a solar cell, most of the damage is concentrated at the end of the proton track. Since 50-keV protons are stopped about 0.5 μm below the surface, most of the damage is produced in the (AlGa)As and in the p^+ Be-diffused GaAs layer before the protons reach the junction. The 100-keV protons are stopped about 1.0 μm below the surface, creating damage close to the junction. The 290-keV protons penetrate deeper into the cell and are stopped ~2.5 μm below the surface, causing damage throughout the active region of the GaAs solar cells. Since the Si solar cells have junction depths between 0.2 μm and 0.3 μm, all the low-energy protons penetrate beyond the junction and cause most of the damage in the base p region.

The results of low-energy proton irradiation tests are summarized in Figure 3. It shows the percentage of remaining maximum power output versus proton fluence for the GaAs and silicon solar cells specified in Table 1. The loss in power in the silicon cells (the dotted line) is mainly due to the reduction in the open-circuit voltage and fill factor (FF). As shown in Section 2 (Table 3) and discussed below, the GaAs cells also suffer losses in V_{oc} and FF but suffer mostly from a reduction in short circuit current I_{sc}. The three GaAs solar cells protected by a cover glass show no sign of degradation.

Table 2 gives the critical fluence for GaAs and silicon solar cells. Figure 4 shows the percentage of remaining solar cell power output versus proton energy for low-energy protons. For practical space missions, the effect of high-energy protons have to be considered as well as the effect

Table 1. Proton Irradiation Test Matrix for the (AlGa)As-GaAs and Silicon Solar Cells

Energy, keV	Fluence, p/cm^2	(AlGa)As-GaAs Solar Cells		Silicon Solar Cells[a]	
		Number of Cells	Cell Number	Number of Cells	Cell Number
50	1×10^9	2	2266, 2295		
	1×10^{10}	2	2266, 2295		
	1×10^{11}	3+1	2406, 2407, 2411 2402[b]	3	3, 6, 9
	1×10^{12}	3+1	2426, 2427, 2428 2402[b]	3	10, 11, 12
100	1×10^9	2	2302, 2307		
	1×10^{10}	2	2302, 2307		
	1×10^{11}	3+1	2417, 2419, 2420 2430[b]	3	2, 5, 8
	1×10^{12}	3+1	2429, 2432, 2456 2430[b]	3	13, 14, 15
290	1×10^9	2	2370, 2375		
	1×10^{10}	2	2370, 2375		
	1×10^{11}	3+1	2421, 2422, 2424 2446[b]	3	1, 4, 7
	1×10^{12}	3+1	2457, 2477, 2311 2446[b]	3	16, 17, 18

[a] n on p, ~0.2 to 0.3 μm junction depth, 2.2 cm x 2.0 cm, 12-mil-thick high-efficiency silicon solar cells with SiO_x AR coating, no cover glass protection.

[b] Cell Numbers 2402, 2430, 2446 have 12-mil-thick cover glass protection.

6483

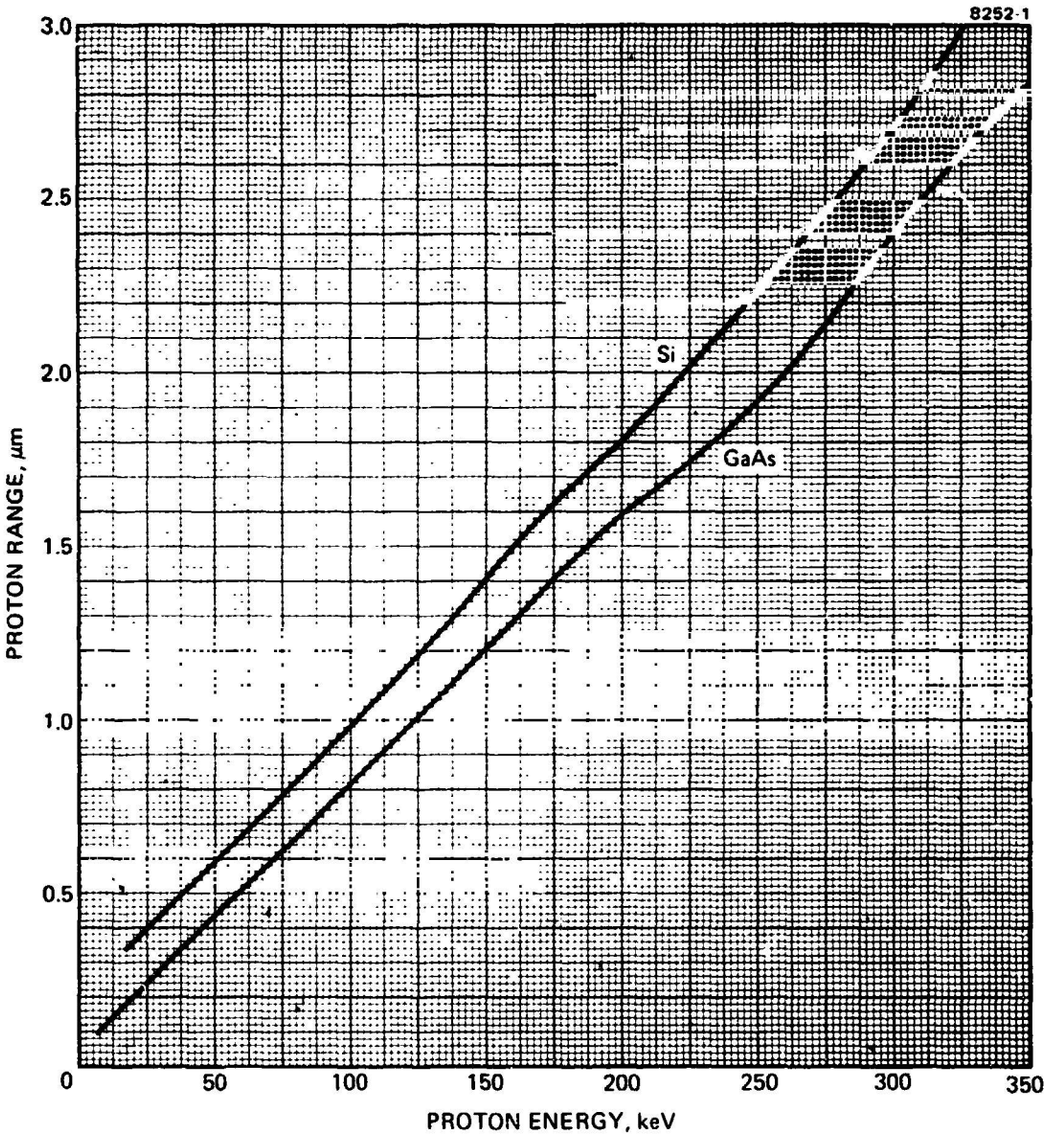

Figure 2. Proton energy versus projected range in GaAs and Si.

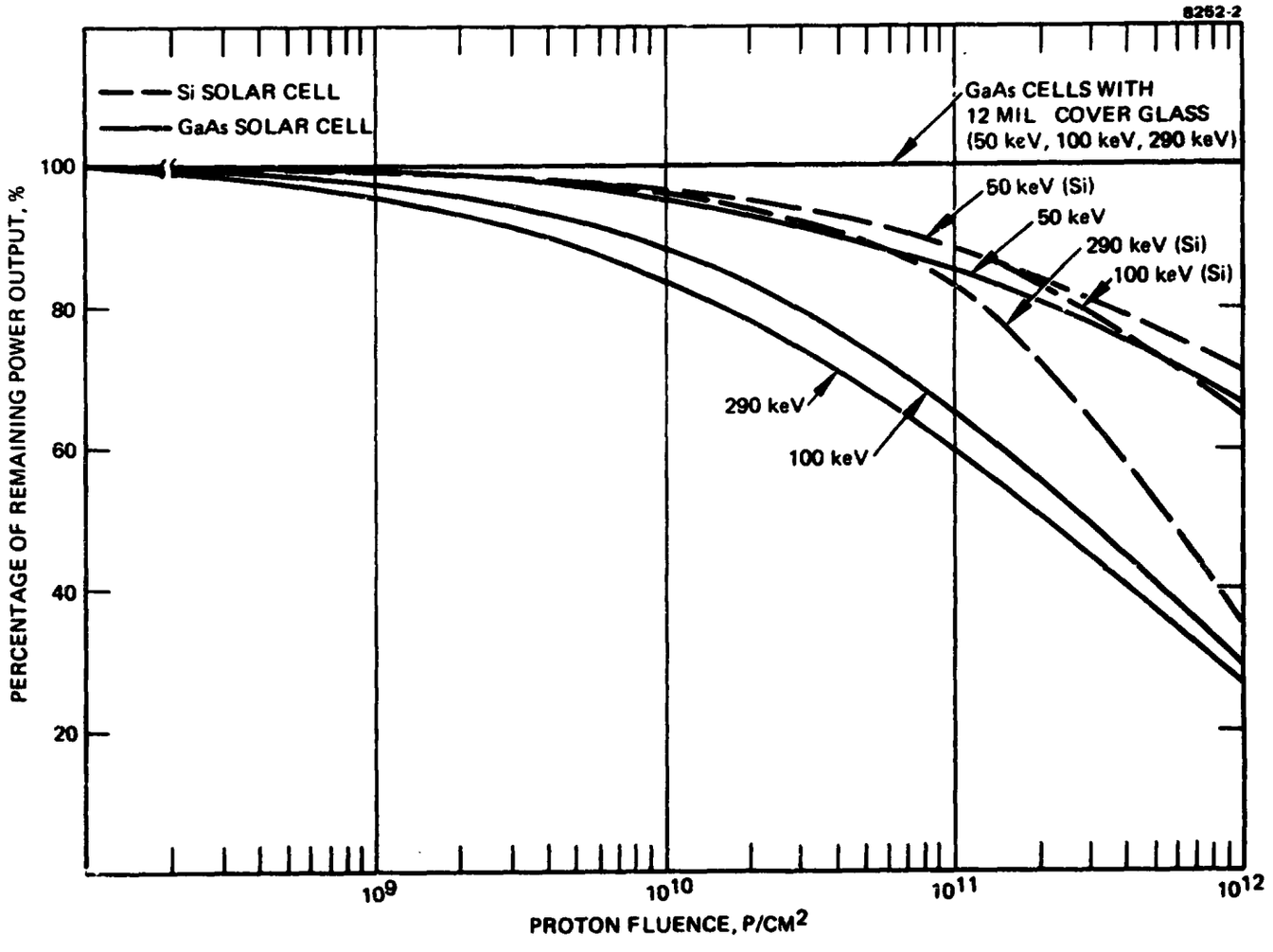

Figure 3. Percentage of remaining solar cell power output versus proton fluence.

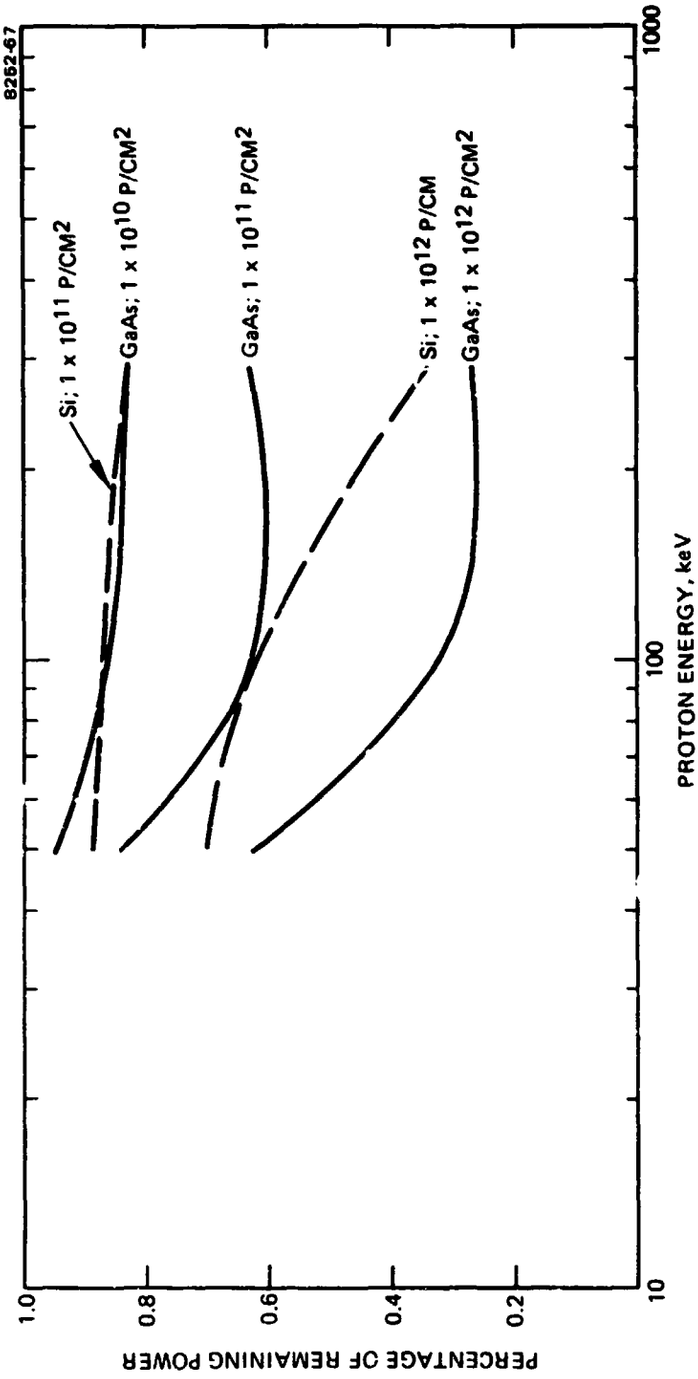

Figure 4. Percentage of remaining solar cell power output versus proton energy.

of low-energy protons. Figure 5 shows the percentage of remaining solar cell power output versus proton energy at both low and high energy proton range. (The high-energy proton irradiation studies were performed under prior NASA Langley contracts.) For comparison, the results obtained with silicon cells irradiated simultaneously with our GaAs cells are also shown in Figure 5. The dotted curve of Figure 5 shows the interpolation for the intermediate proton energy range. The solar cell is usually shielded against low-energy protons by a coverglass (Curve I, Figure 5), while no protection is available against the high-energy protons. In short, Figure 5 shows that at all energies higher than ~5 MeV, GaAs cells show superior radiation hardness as compared with silicon cells. In the regions below 5 MeV where GaAs cells are susceptible to damage, they are effectively shielded by the normal coverglass protection used with the cells in all space missions (Curve 7, Figure 5).

More detailed data and observation on the tests of the (AlGa)As-GaAs and silicon solar cells are given below.

Table 2. Critical Proton Fluence for GaAs and Si Solar Cells

Proton Energy, keV	Critical Fluence, p/cm^2	
	GaAs Solar Cells	Silicon Solar Cells
50	4×10^{11}	5×10^{11}
100	4.2×10^{10}	4×10^{11}
290	3×10^{10}	1.7×10^{11}

6483

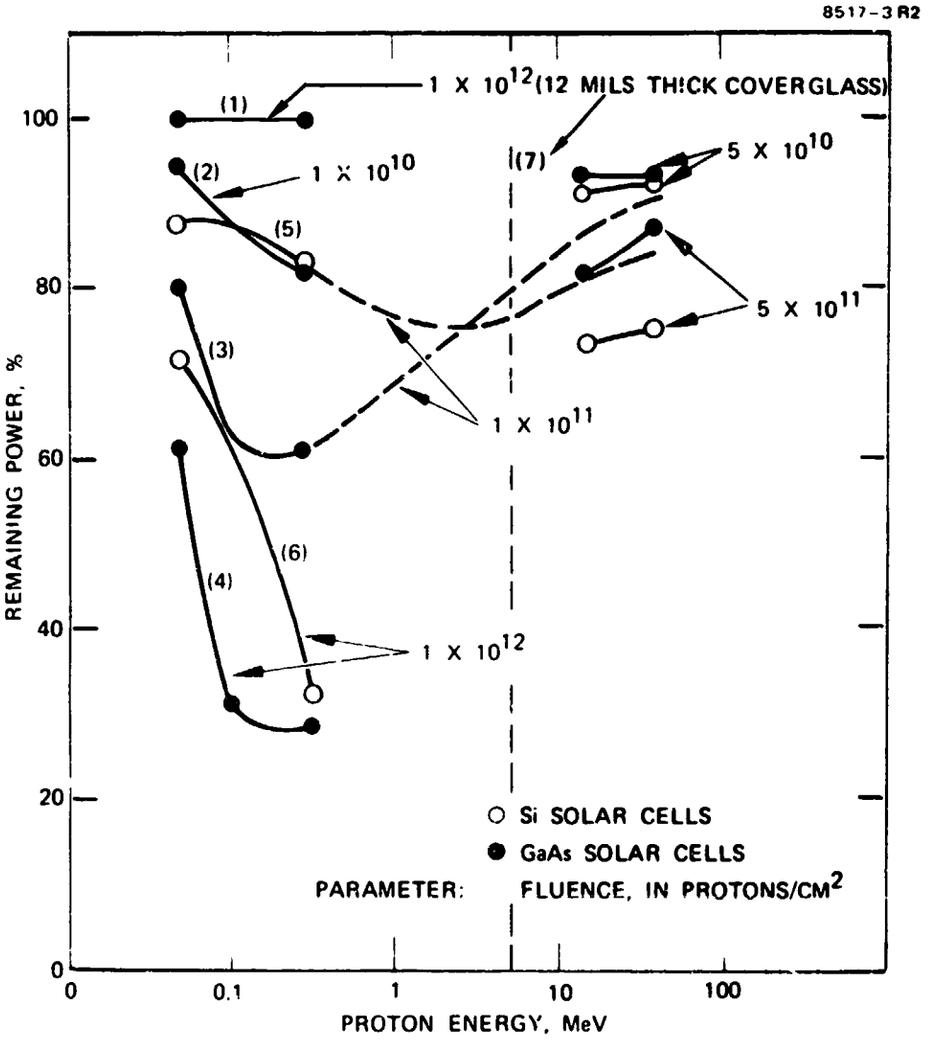

Figure 5. Proton radiation damage: GaAs versus Si solar cells.

SECTION 2

PHOTO I-V CHARACTERISTICS

Figures B-1 through B-24 in Appendix B show the air mass zero (AM0) photo I-V characteristics of GaAs and Si solar cells before and after proton irradiation at 50 keV, 100 keV, and 290 keV. Table 3 has been compiled from these I-V characteristics and gives the following characteristics of the individual cells: I_{sc}; V_{oc}; FF; maximum power output, p_{max}; and power conversion efficiency, η. The (AlGa)As window layer thickness D and the junction depth Xj were measured by a scanning electron microscope (SEM) for each cell and are also shown on Table 3 to assist our understanding of the irradiation results.

Figure 6 shows the percentage of remaining I_{sc} as a function of proton fluences for 50-keV, 100-keV, and 290-keV proton energies. Both the 50-keV and 100-keV protons reduce the I_{sc} less than the 290-keV protons. This is because most of the damage produced by 50-keV and 100-keV protons is close to the junction and only within the p region, whereas the 290-keV protons penetrate deep into the cell, causing damage on both sides of the junction (p and n region). Figure 7 shows the measured V_{oc} as a function of proton energy. For our GaAs solar cell, V_{oc} degrades more with proton irradiation at 100 keV than at 50 keV or at 290 keV. This is explicable because the 100-keV protons are stopped at the p-n junction where they produce most of the damage.

Figures C-1 through C-18 in Appendix C show the photo I-V characteristics of the silicon solar cell before and after proton irradiation; the results are presented in Table 4. The Si solar cell's I_{sc} does not change when the cell is irradiated by 50 keV and 100 keV up to 1×10^{12} cm^{-2} proton fluence. However, it is drastically lower at 290 keV at 1×10^{12} cm^{-2} proton fluence. Also, the silicon solar cell has a shallow junction (less than 0.3 μm) and has no window layer. Therefore, even at the lowest energy, 50 keV, protons penetrate beyond the junction. In this case, the V_{oc} keeps decreasing with increasing proton energies.

PRECEDING PAGE BLANK-NOT FILMED

Table 3(a). (AlGa)As-GaAs Solar Cell Characteristics Before and After Proton Irradiation

Cell Number	Proton Energy, keV	Fluence, p/cm^{-2}	I_{sc}, mA	V_{oc}, V	P_{MAX}, mW	FF	n,%	Junction Depth, xj, μm	(AlGa)As, Thickness, D, μm
2266	0	0	111	1.01	87.7	0.78	16.2	0.5	0.64
	50	1×10^{9}	110	1.00	86.7	0.78	16.0		
	50	1×10^{10}	107	1.00	83.7	0.78	15.5		
2295	0	0	112	1.01	87.6	0.77	16.2	0.54	0.44
	50	1×10^{9}	111	1.00	86.0	0.77	15.9		
	50	1×10^{10}	105	0.99	81.5	0.78	15.1		
2406	0	0	108	1.0	82.9	0.77	15.3	0.50	0.23
	50	1×10^{11}	89	0.96	66.4	0.78	12.3		
2407	0	0	1063	0.99	82.9	0.786	15.3	0.46	0.2
	50	1×10^{11}	85	0.91	61.6	0.797	11.4		
2411	0	0	110	1.01	87.3	0.786	16.1		
	50	1×10^{11}	96	0.975	73.9	0.79	13.7		
2402[a]	0	0	109	1.00	84.2	0.77	15.6	0.52	0.33
	50	1×10^{11}	108	1.00	83.5	0.77	15.4		

[a]Cells with 12-mil-thick cover glass.

6483

Table 3(a). (AlGa)As-GaAs ›lar Cell Characteristics Before and After Proton Irradiation (Continued).

Cell Number	Proton Energy, keV	Fluence, p/cm^{-2}	I_{sc}, mA	V_{oc}, V	P_{MAX}, mW	FF	n, %	Junction Depth, xj, μm	(AlGa)As, Thickness, D, μm
2426	0	0	108	1.01	85.6	0.784	15.8	0.45	0.25
	50	1×10^{12}	72	0.95	53.7	0.785	9.9		
2427	0	0	109	1.0	83.7	0.768	15.5	0.48	0.34
	50	1×10^{12}	76	0.92	44	0.778	8.1		
2428	0	0	109	1.0	83.6	0.767	15.4		
	50	1×10^{12}	76	0.945	55.1	0.767	10.2		
2402[a]	0	0	108	1.00	83.5	0.77	15.4		
	50	1×10^{12}	108	1.00	83.5	0.77	15.4		

[a]Cells with 12-mil-thick cover glass.

6483

Table 3(b). (AlGa)As-GaAs Solar Cell Characteristics Before and After Proton Irradiation

Cell Number	Proton Energy, keV	Fluence, p/cm^{-2}	I_{sc}, mA	V_{oc}, V	P_{MAX}, mW	FF	n, %	Junction Depth, Xj, μm	(AlGa)As, Thickness D, μm
2302	0	0	107	1.0	85.1	0.796	15.7	0.45	0.25
	100	1×10^{9}	105	0.98	81.2	0.796	15.1		
	100	1×10^{10}	104	0.925	75.7	0.786	14.0		
2307	0	0	111	1.01	87.3	0.779	16.1	0.48	0.48
	100	1×10^{9}	111	0.98	84.1	0.773	15.5		
	100	1×10^{10}	108	0.92	75.6	0.76	14.0		
2417	0	0	114	1.01	88	0.764	16.3	0.47	0.3
	100	1×10^{11}	93	0.82	56.4	0.74	10.4		
2419	0	0	115	1.0	89.7	0.78	16.6	0.45	0.25
	100	1×10^{11}	92	0.81	53.6	0.72	9.9		
2420	0	0	114	1.0	88	0.77	16.3	0.45	0.25
	100	1×10^{11}	92	0.82	55.4	0.74	10.2		
2430[a]	0	0	109	0.99	82.6	0.77	15.3		
	100	1×10^{11}	108	0.99	82.5	0.77	15.3		

[a]Cells with 12-mil-thick cover glass.

6483

Table 3(b). (AlGa)As-GaAs Solar Cell Characteristics Before and After Proton Irradiation (Continued).

Cell Number	Proton Energy, keV	Fluence, p/cm^{-2}	I_{sc}, mA	V_{oc}, V	P_{MAX}, mW	FF	n, %	Junction Depth, Xj, μm	Window Thickness, D, μm
2429	0	0	107	1.0	83.4	0.78	15.4	0.52	0.26
	100	1×10^{12}	54	0.66	24	0.674	4.4		
2432	0	0	108	1.0	83.3	0.77	15.4	0.45	0.16
	100	1×10^{12}	56	0.68	26.6	0.698	4.9		
2456[a]	0	0	113	1.02	88.6	0.768	16.4	0.57	0.76
	100	1×10^{12}	71	0.935	51.2	0.771	9.5		
2430[b]	0	0	108	0.99	82.5	0.77	15.3		
	100	1×10^{12}	108	0.99	82.5	0.77	15.3		

[a]Cell number 2456 shows less degradation than cells 2429 and 2432 because it has a thicker window layer (0.76 μm), which prevents the 100 keV protons from penetrating to the p-n junction.

[b]Cells with 12-mil-thick cover glass.

6483

Table 3(. (AlGa)As-GaAs Solar Cell Characteristics Before and After Proton Irradiation

Cell Number	Proton Energy, keV	Fluence, p/cm^{-2}	I_{sc}, mA	V_{oc}, V	P_{MAX}, mW	FF	n, %	Junction Depth, Xj, μm	Window Thickness, D, μm
2370	0	0	110	1.0	85.4	0.78	15.9	0.5	0.34
	290	1×10^{9}	107	0.98	81.7	0.78	15.0		
	290	1×10^{10}	96	0.94	70.4	0.78	13.0		
2375	0	0	108	1.0	84.6	0.783	15.6	0.53	0.53
	290	1×10^{9}	106	0.98	81.3	0.783	15.0		
	290	1×10^{10}	94	0.94	69.1	0.782	12.8		
2421	0	0	115	1.0	89.3	0.776	16.5	0.45	0.25
	290	1×10^{11}	80	0.85	50.8	0.746	9.4		
2422	0	0	114	1.0	86.8	0.762	16.0	0.45	0.25
	290	1×10^{11}	82	0.86	53.3	0.755	9.84		
2424	0	0	108	1.01	84.2	0.77	15.6	0.48	0.48
	290	1×10^{11}	80	0.865	52.9	0.765	9.8		
2446[a]	0	0	105.5	1.00	82.5	0.78	15.2		
	290	1×10^{11}	104	1.0	82.0	0.78	15.1		
2457	0	o	114	1.01	90.5	0.786	16.7	0.62	0.62
	290	1×10^{12}	48	0.725	25	0.716	4.6		

[a]Cells with 12-mil-thick cover glass.

6483

Table 3(c). (AlGa)As-GaAs Solar Cell Characteristics Before and After Proton Irradiation (Continued)

Cell Number	Proton Energy, keV	Fluence, p/cm^{-2}	I_{sc}, mA	V_{oc}, V	P_{MAX}, mW	FF	n, %	Junction Depth, Xj, μm	Window Thickness, D, μm
2477	0	0	110	1.0	83.2	0.756	15.4		
	290	1×10^{12}	51	0.78	26	0.70	4.8		
2311	0	0	109	1.01	82.6	0.75	15.3		
	290	1×10^{12}	45	0.71	21.7	0.68	4.0		
2446[a]	0	0	104	1.0	82.0	0.78	15.1		
	290	1×10^{12}	104	1.0	82.0	0.78	15.1		

[a]Cells with 12-mil-thick cover glass.

6483

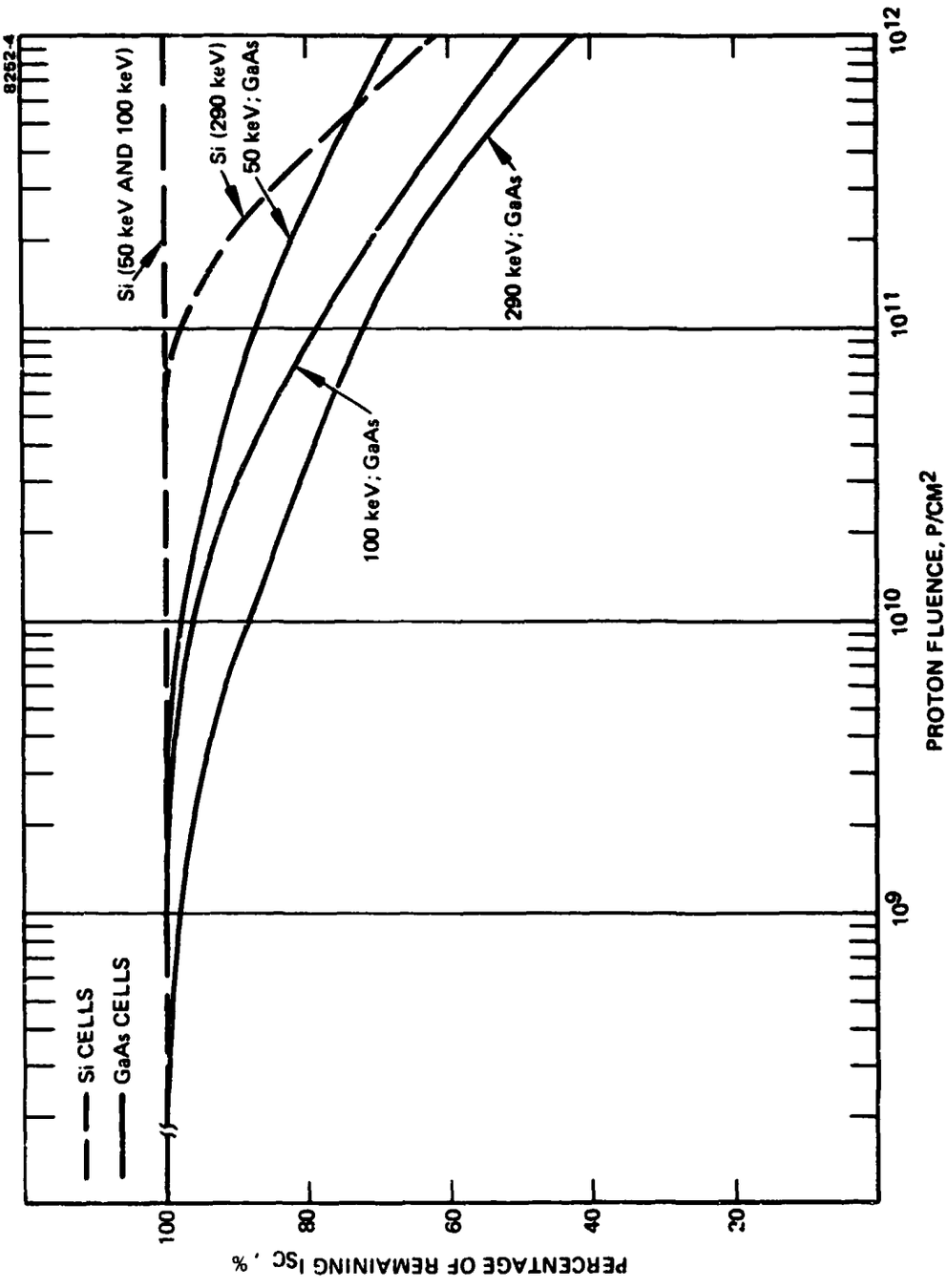

Figure 6. Short circuit current versus proton irradiation fluence.

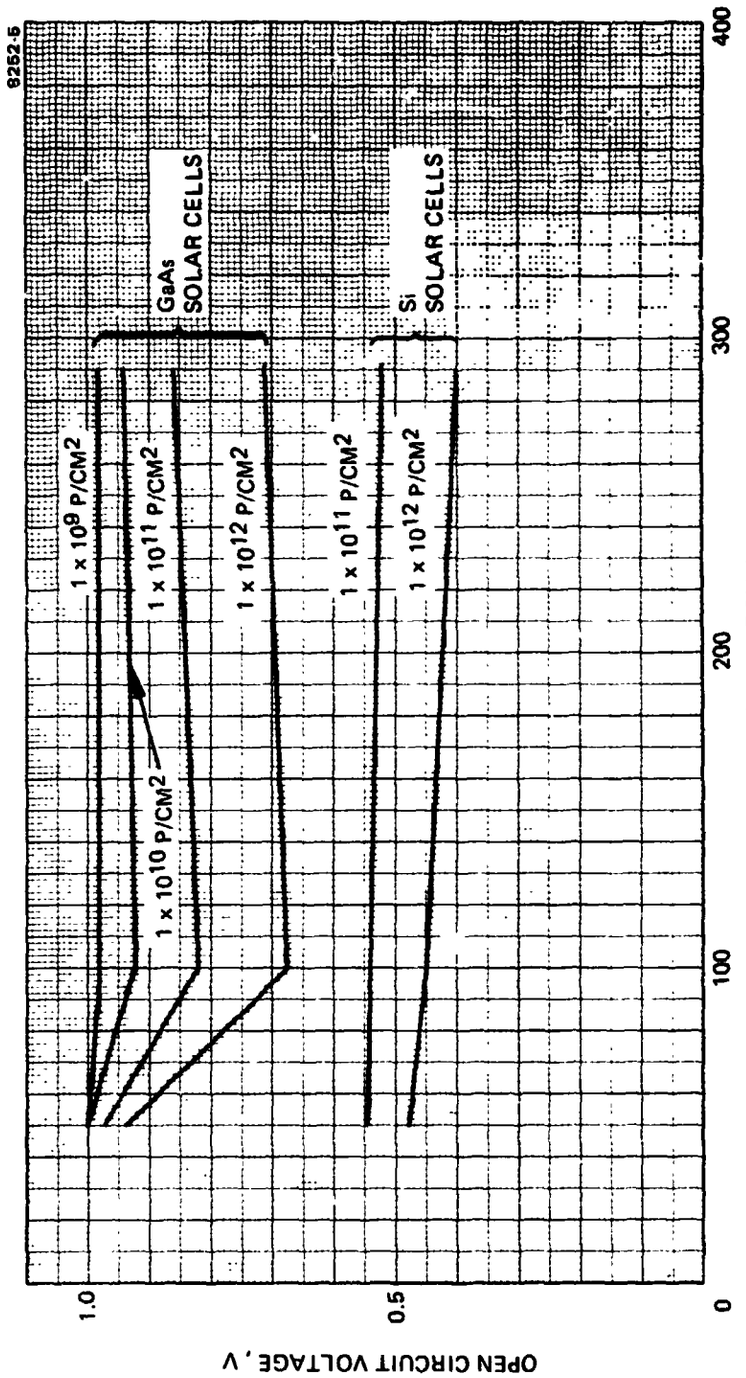

Figure 7. Open circuit voltage versus proton energy.

Table 4. Silicon Solar Cell Characteristics Before and After Proton Irradiation

Cell Number	Energy, keV	Fluence, ρ/cm^{-2}	I_{sc}, mA	V_{oc}, V	P_{MAX}, mA	FF	n, %
3	0	0	168	0.595	73	0.73	12
	50	1×10^{11}	169	0.54	65.1	0.71	10.9
6	0	0	171	0.59	75.2	0.72	12.6
	50	1×10^{11}	170	0.54	65.5	0.713	11.0
9	0	0	168	0.59	72.9	0.735	12.2
	50	1×10^{11}	167	0.54	63.8	0.708	10.7
10	0	0	170.8	0.6	76.2	0.74	12.8
	50	1×10^{12}	168.5	0.48	54.4	0.672	4.12
11	0	0	170	0.60	76	0.745	12.8
	50	1×10^{12}	169	0.475	54	0.673	9.1
12	0	0	169.5	0.6	76	0.747	12.8
	50	1×10^{12}	169	0.475	54	0.673	9.1
2	0	0	172	0.60	75.7	0.733	12.7
	100	1×10^{11}	172	0.54	66.4	0.714	11.1
5	0	0	174	0.595	76.1	0.734	12.8
	100	1×10^{11}	174	0.54	68	0.723	11.4
8	0	0	169	0.59	73	0.73	12.3
	100	1×10^{11}	168	0.54	63.6	0.70	11.8
13	0	0	171.5	0.6	77	0.748	13.0
	100	1×10^{12}	168	0.45	48.9	0.65	8.2
14	0	0	171.5	0.6	77.6	0.754	13.0
	100	1×10^{12}	169	0.445	48.5	0.645	8.15
15	0	0	172	0.6	76.1	0.738	12.8
	100	1×10^{12}	169	0.45	48.7	0.64	8.2

6483

Table 4. Silicon Solar Cell Characteristics Before and After Proton Irradiation (Continued)

Cell Number	Energy, keV	Fluence, p/cm^{-2}	I_{sc}, mA	V_{oc}, V	P_{MAX}, mA	FF	n, %
4	0	0	173	0.59	76.1	0.75	12.8
	290	1×10^{11}	169	0.52	63.9	0.727	10.7
7	0	0	165	0.585	71.7	0.743	12.0
	290	1×10^{11}	164	0.52	60.3	0.707	10.1
1	0	0	173	0.6	76.5	0.737	12.8
	290	1×10^{11}	166	0.52	61.5	0.712	10.3
16	0	0	172	0.59	76	0.749	12.8
	290	1×10^{12}	103	0.39	24	0.60	4.0
17	0	0	172	0.60	76.1	0.737	12.8
	290	1×10^{12}	114	0.39	26.5	0.60	4.46
18	0	0	172	0.59	68.2	0.67	11.5
	290	1×10^{12}	104	0.40	23.2	0.56	3.9

6483

SECTION 3

SPECTRAL RESPONSE

Figures 8 through 10 show the average spectral response of the (AlGa)As-GaAs solar cell before and after proton irradiation with proton energies at 50 keV, 100 keV, 290 keV, respectively. At 50 keV and 100 keV, the short wavelength region of the spectral response shows more degradation than does the long wavelength region. At 290 keV, both the long- and short-wavelength regions of the spectral response show degradation. This is consistent with the fact that the lower energy protons, as does the shorter wavelength light, penetrate less deeply into the GaAs than do the higher energy protons. Thus, the lower energy protons produce most damage where the shorter wavelength light generates most of the electron-hole pairs. The lower energy protons therefore produce most damage in that part of the solar cell where the short wavelength light generates most of the current. This means, as observed above, that lower energy protons should affect mostly the spectral response on the shorter wavelength side. Conversely, the higher energy protons penetrate more deeply into the GaAs, as does the longer wavelength light. The higher energy protons will therefore also affect the long wavelength part of the spectral response. These observations show that the spectral response is strongly affected by proton energy as well as by the proton fluence, in agreement with our physical model of the GaAs solar cell.

Figures 11 through 13 show the average spectral response of the silicon solar cells before and after proton irradiation. There is no change in silicon solar cell spectral response after 50-keV or 100-keV proton irradiation. However, a drastic reduction occurs, as expected, in the long wavelength region after irradiation with the higher energy 290 keV protons.

The change in the spectral response of the GaAs solar cells is in good agreement with the change in I_{sc} after irradiation Furthermore, as indicated above, the change in the spectral response of the cells after irradiation agrees with our model of the performance of these cells.

PRECEDING PAGE BLANK NOT FILMED

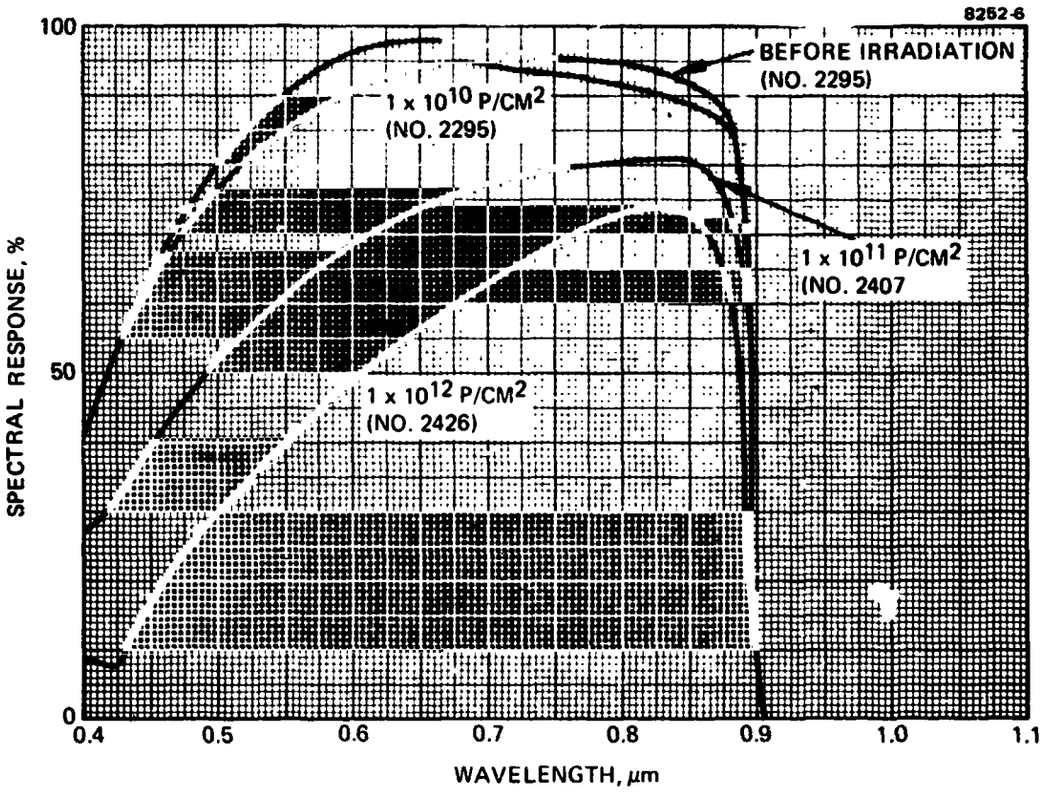

Figure 8. (AlGa)As-GaAs solar cell spectral response before and after proton irradiation (proton energy = 50 keV).

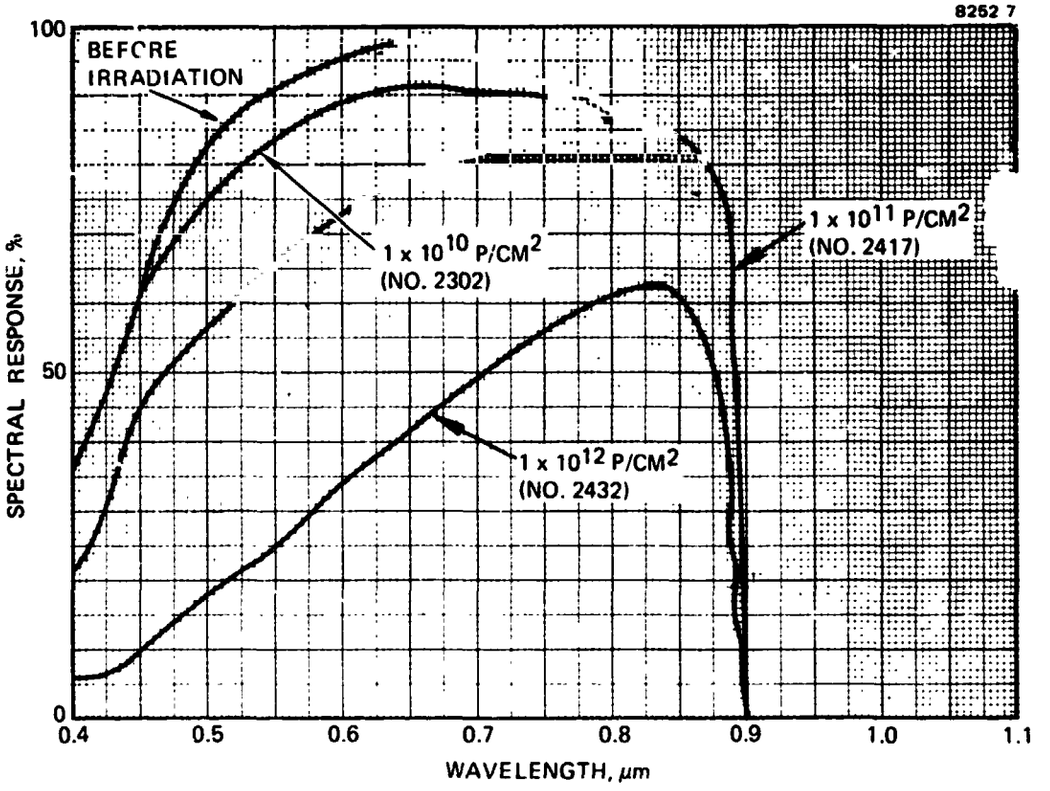

Figure 9. (AlGa)As-GaAs solar cell spectral response before and after proton irradiation (proton energy = 100 keV).

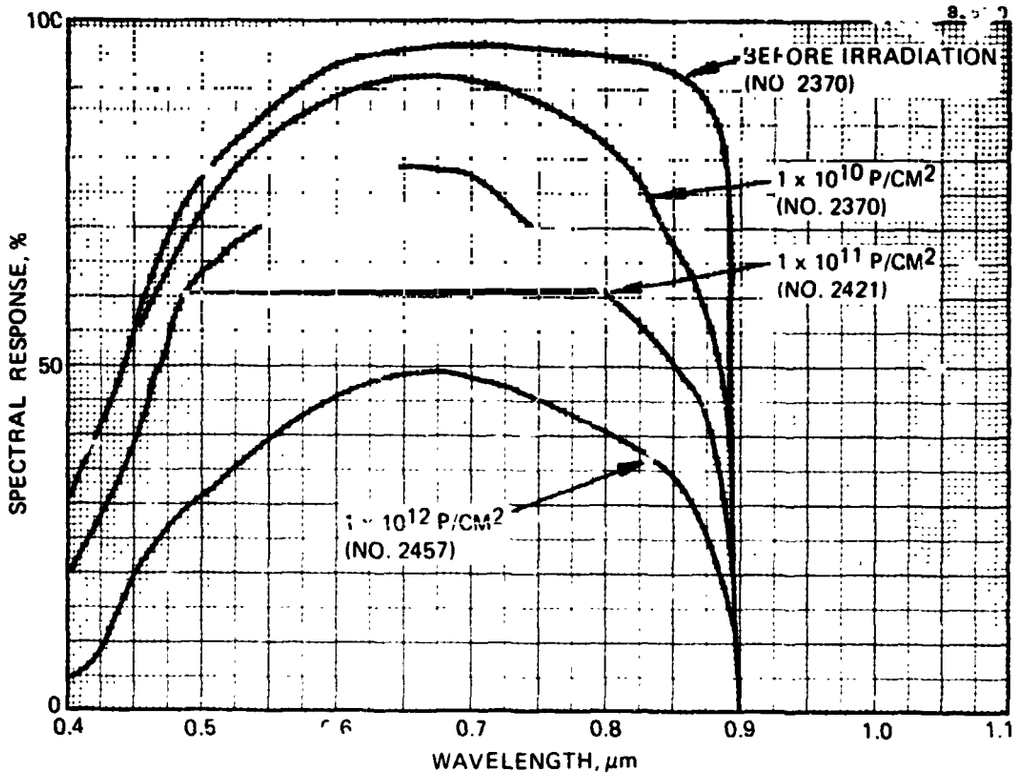

Figure 10. (AlGa)As-GaAs solar cell spectral response before and after proton irradiation (proton energy = 290 keV).

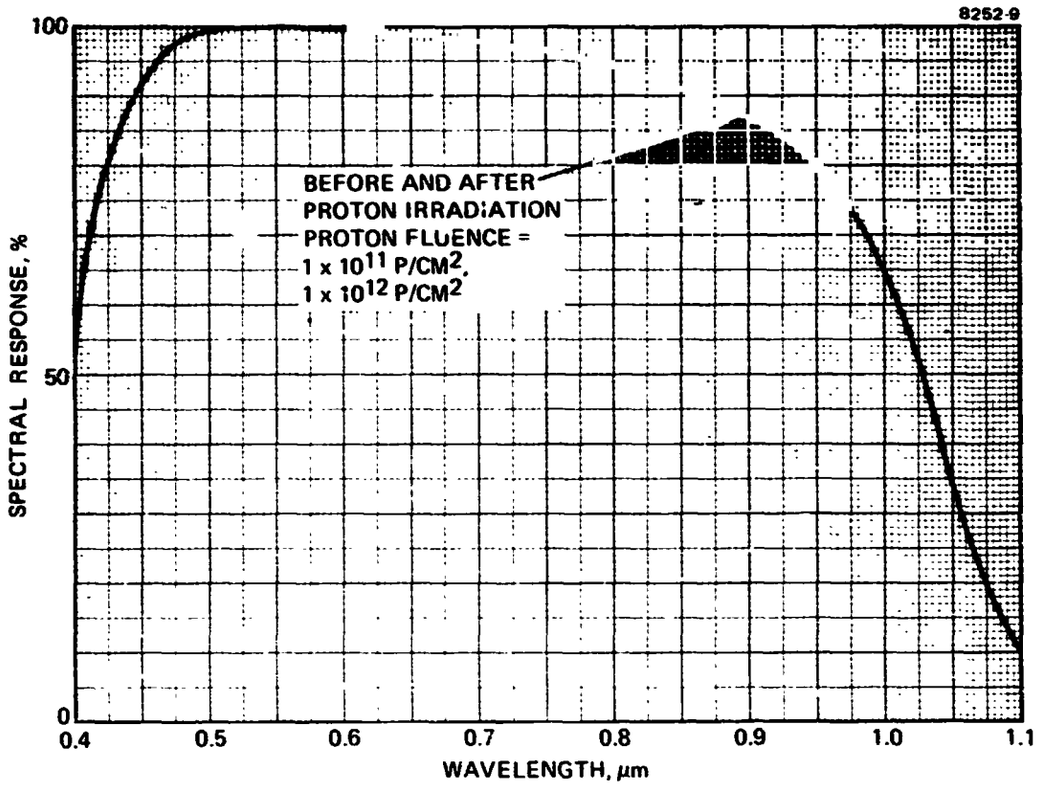

Figure 11. Spectral response of Si solar cells before and after proton irradiation (proton energy = 50 keV).

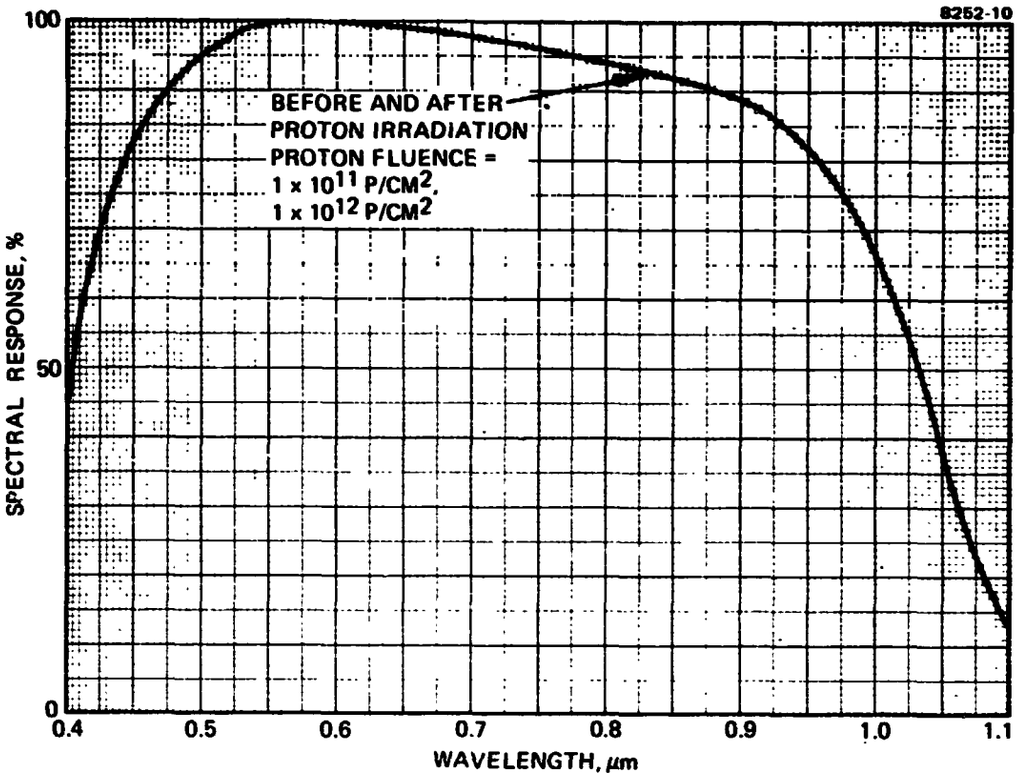

Figure 12. Spectral response of Si solar cells before and after proton irradiation (proton energy = 100 keV).

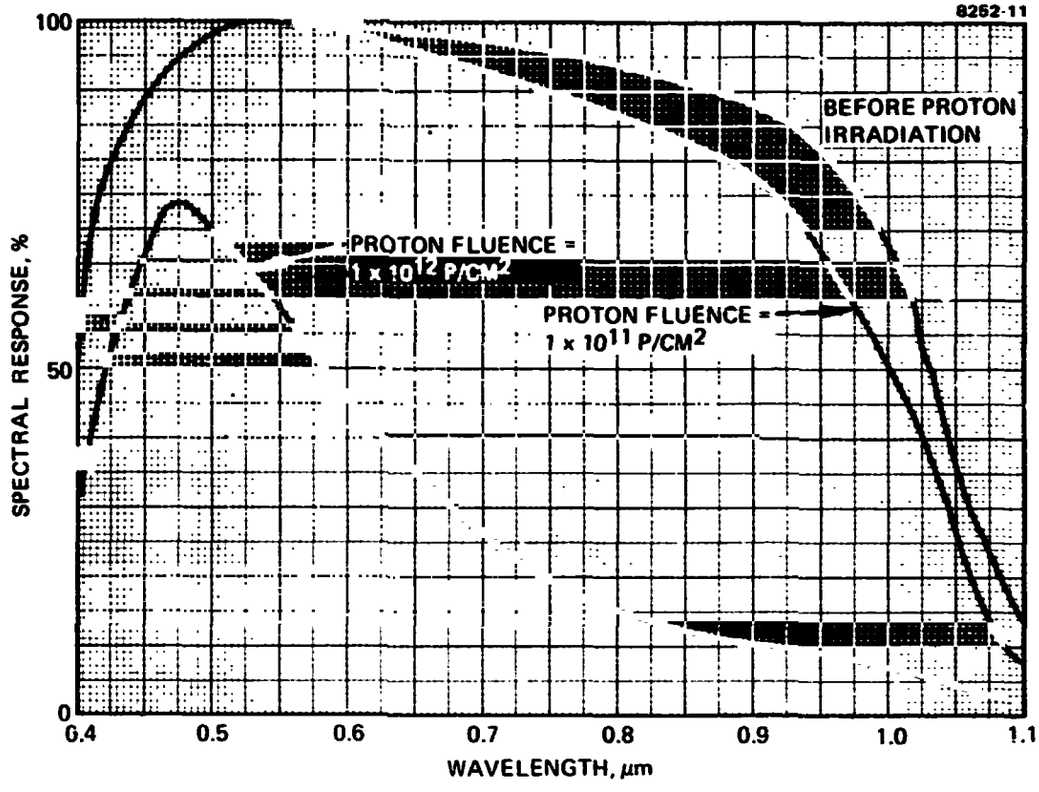

Figure 13. Spectral response of Si solar cells before and after proton irradiation (proton energy = 290 keV).

SECTION 4

DARK I-V CHARACTERISTICS

The dark I-V characteristics are an important measure of solar cell performance because they affect the cell's fill factor and open-circuit voltage. The dark I-V characteristics are determined by the combined effect of the current transport mechanisms: diffusion and recombination currents. The total forward current voltage relationship is the sum of these two current components:

$$I = I_o\left(e^{\frac{qV}{nkT}} - 1\right) ,$$

where I_o is the diode leakage current, and n is the junction quality factor, which varies between 1 and 2. The lower limit of n(n=1) implies that the diode is diffusion limited. In this case, the upper value n=2 corresponds to the limiting case controlled by the generation-recombination mechanism. Values of n greater than 2 are also possible if the space-charge recombination process involves more than one intermediate energy level.

Figures 14 through 22 show the dark I-V characteristics before and after proton irradiation for our GaAs cells. Before irradiation, the slope of log I-V characteristics of these cells has an n factor between 2.0 and 2.4. Thus, the current transport mechanism is dominated by more than one energy level at the junction. After irradiation, the slope of log I-V characteristics is lower, and the n factor is between 1.8 and 1.9. This indicates that the transport mechanism is dominated by a new recombination center introduced during irradiation. Also, the dark I-V characteristics after irradiation (Figure 23) show that 100-keV protons damage the junction more than do 290-keV protons. This agrees well with our previous observation in the V_{oc} measurements.

The dark I-V characteristics for silicon solar cells were also measured before and after irradiation, as shown on Figures 24 through 26.

PRECEDING PAGE BLANK NOT FILMED

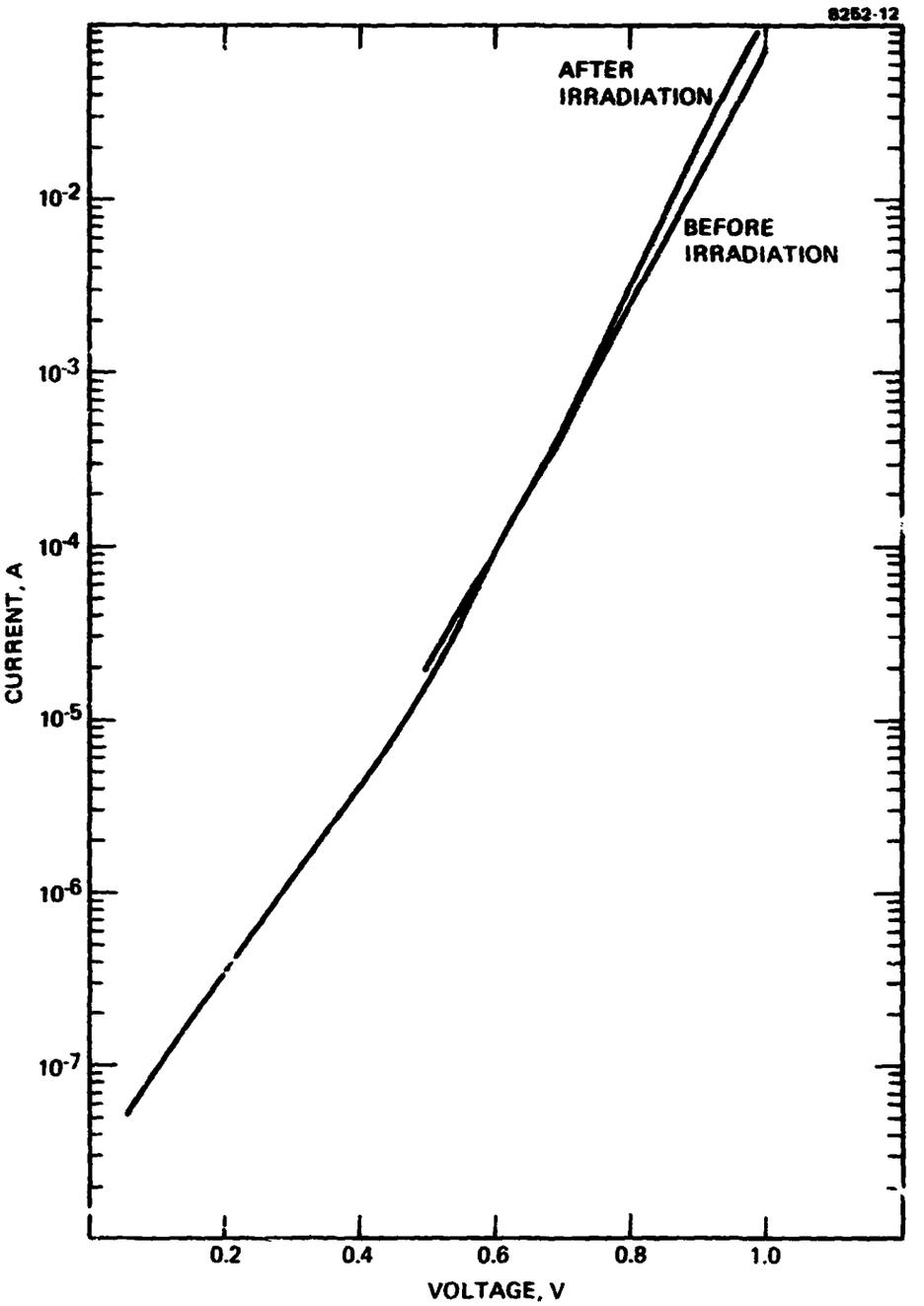

Figure 14. (AlGa)As-GaAs solar cell dark I-V characteristics before and after proton irradiation (cell 2295). Proton energy = 50 keV; proton fluence = 1×10^{10} p/cm^2.

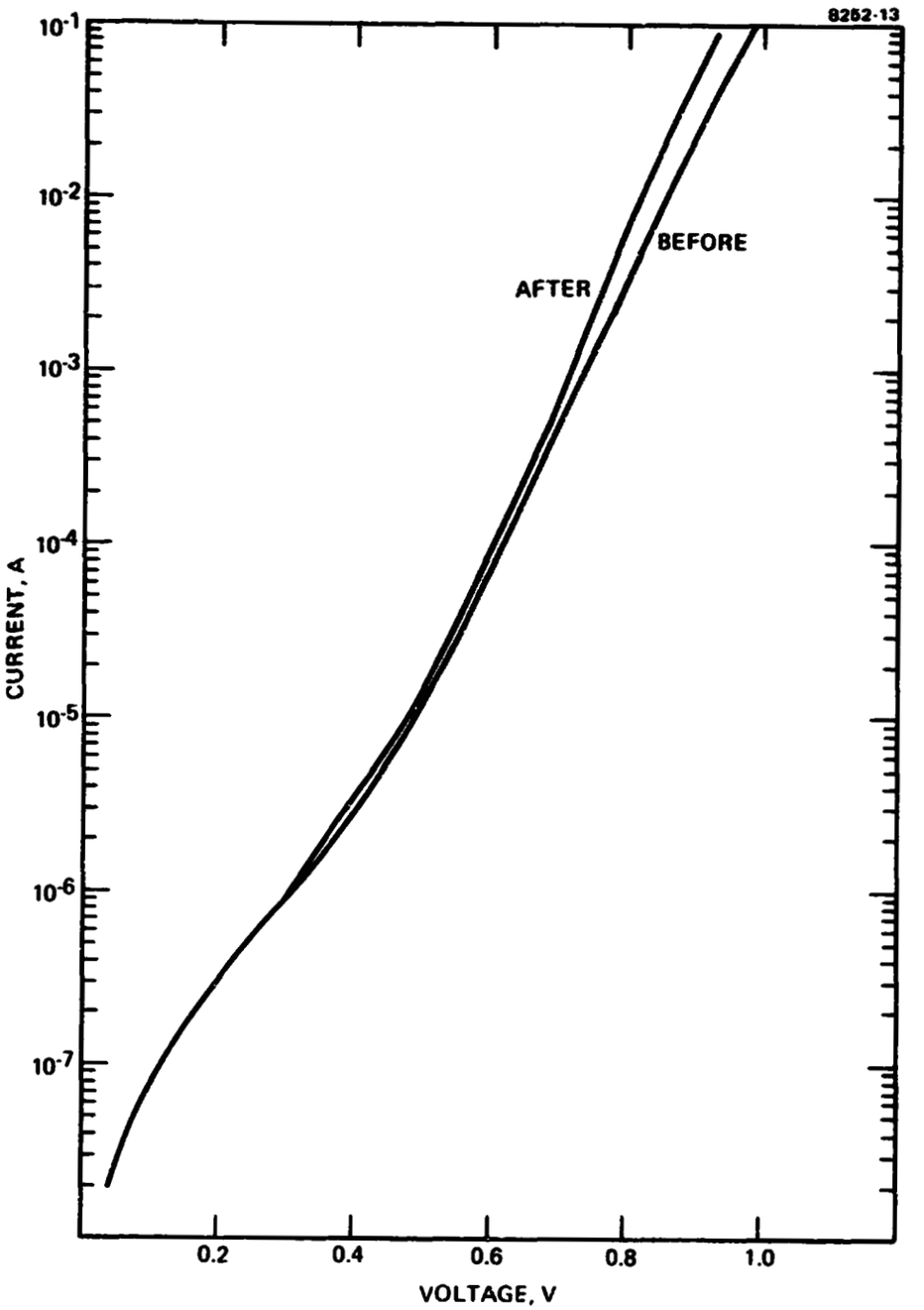

Figure 15. (AlGa)As-GaAs solar cell dark I-V characteristics before and after proton irradiation (cell 2407). Proton energy = 50 keV; proton fluence = 1×10^{11} p/cm^2.

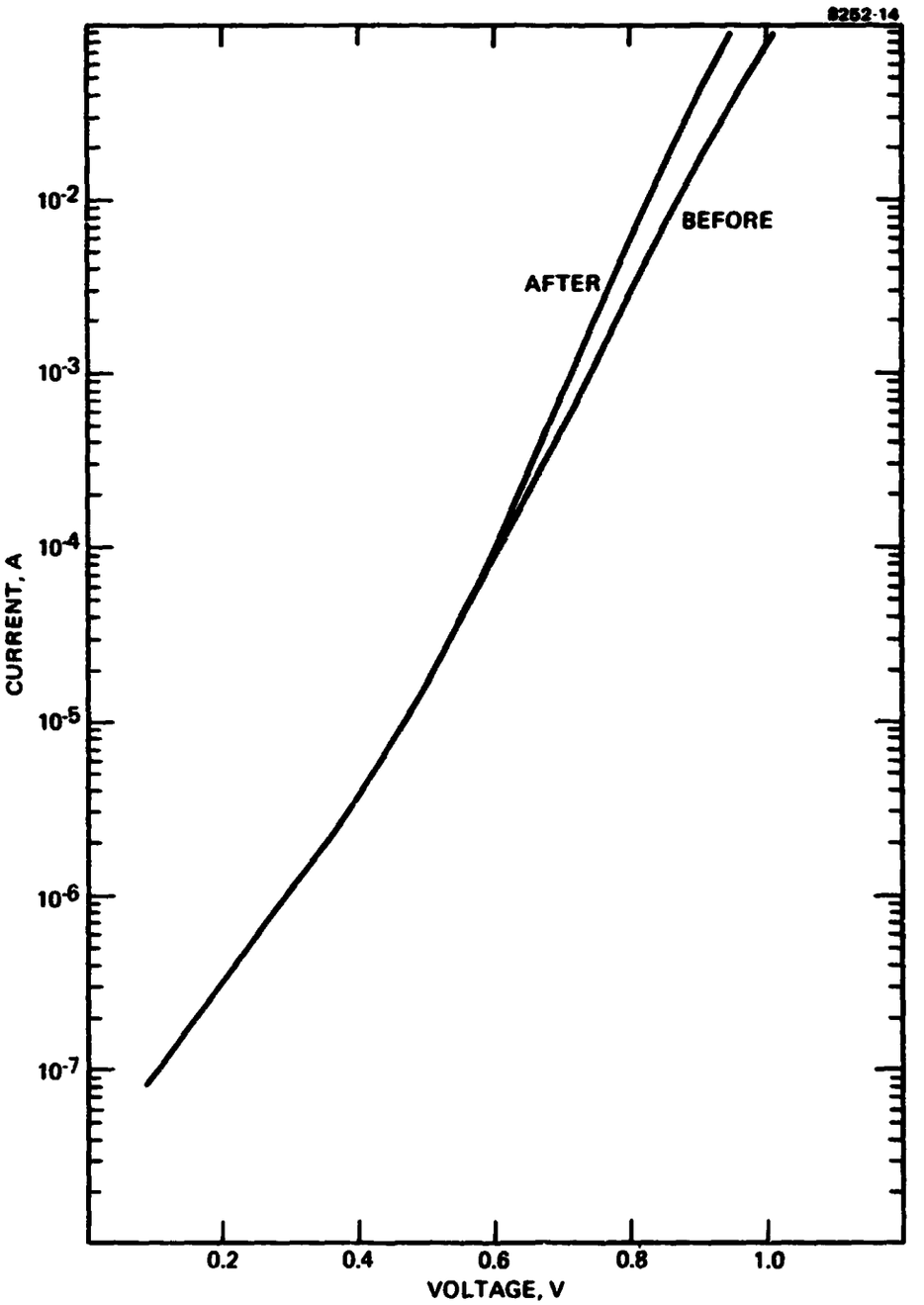

Figure 16. (AlGa)As-GaAs solar cell dark I-V characteristics before and after proton irradiation (cell 2427). Proton energy = 50 keV; proton fluence = 1 x 10^{12} P/cm^2.

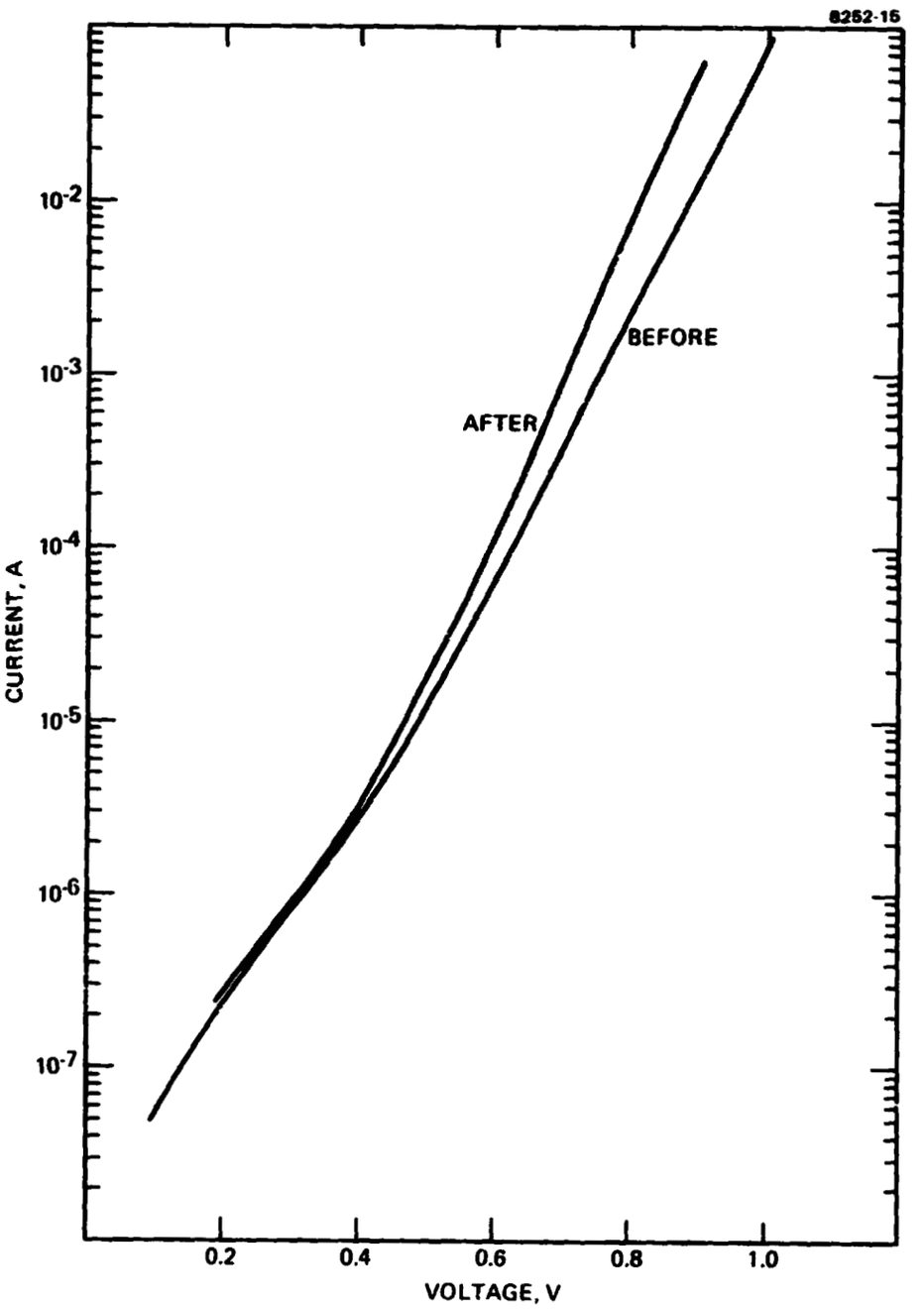

Figure 17. (AlGa)As-GaAs solar cell dark I-V characteristics before and after proton irradiation (cell 2302). Proton energy = 100 keV/ proton fluence = 1×10^{10} p/cm^2.

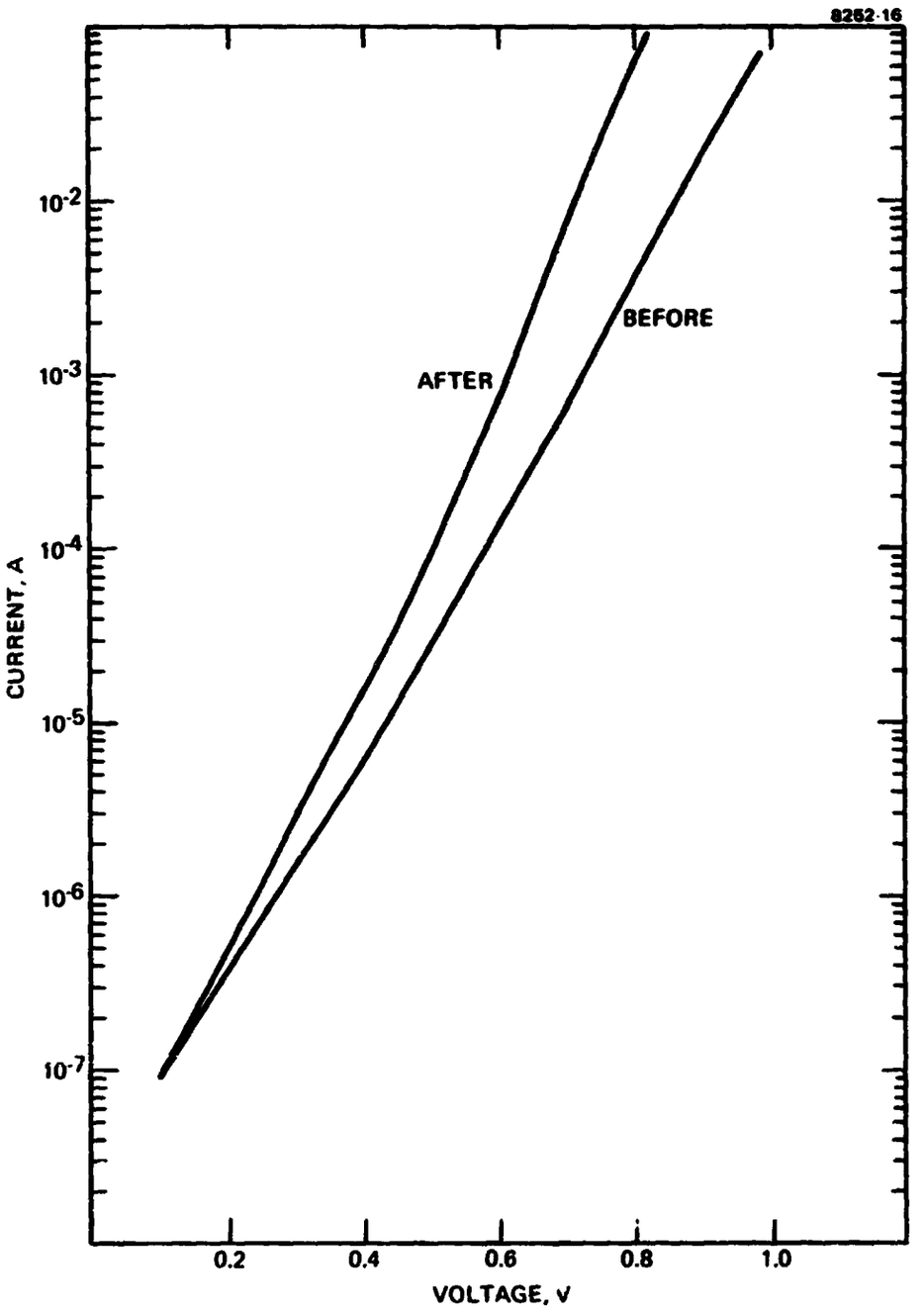

Figure 18. (AlGa)As-GaAs solar cell dark I-V characteristics before and after proton irradiation (cell 2420). Proton energy = 100 keV; proton fluence = 1×10^{11} p/cm^2.

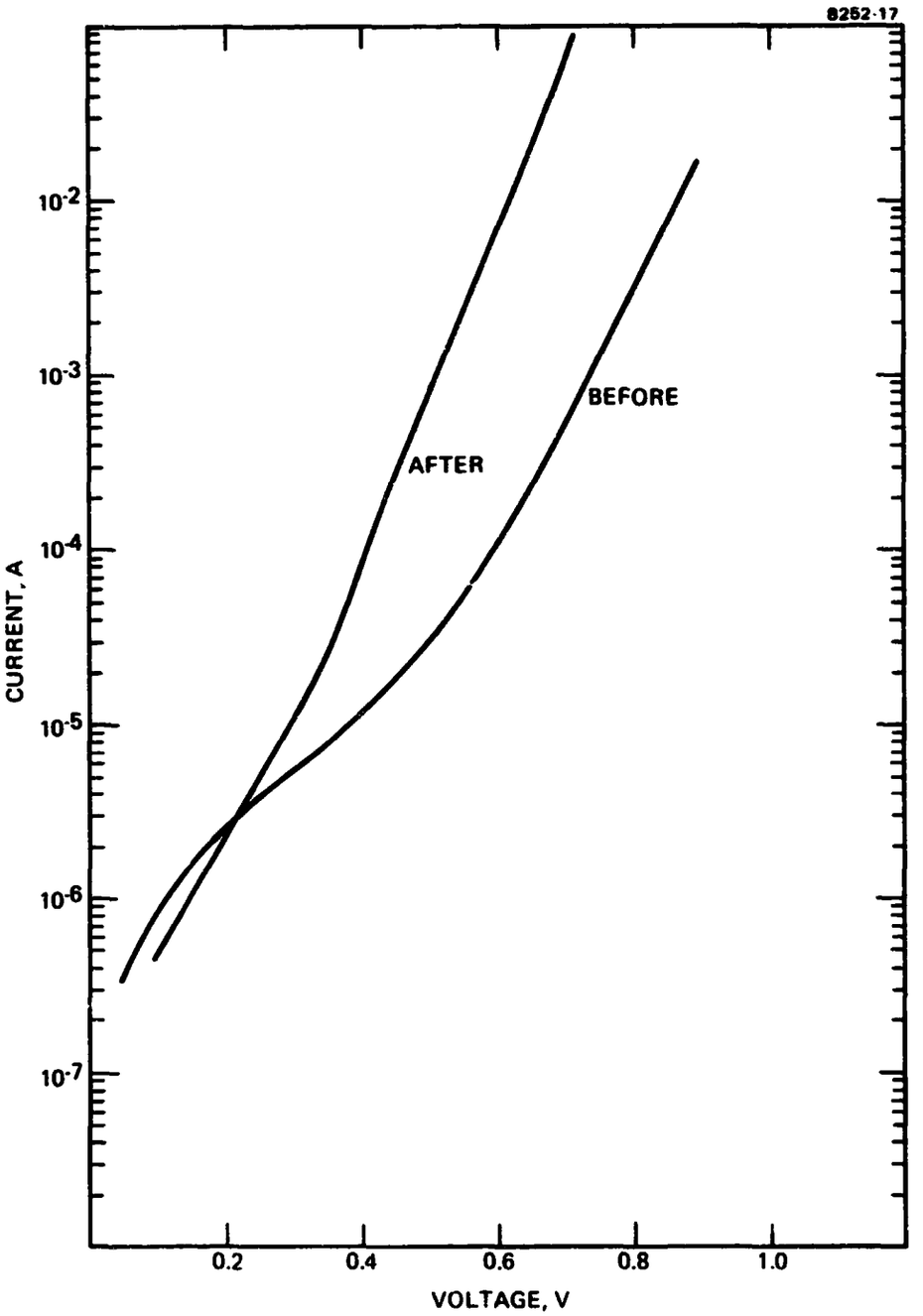

Figure 19. (AlGa)As-GaAs solar cell dark I-V characteristics before and after proton irradiation (cell 2432). Proton energy = 100 keV; proton fluence = 1×10^{12} p/cm^2.

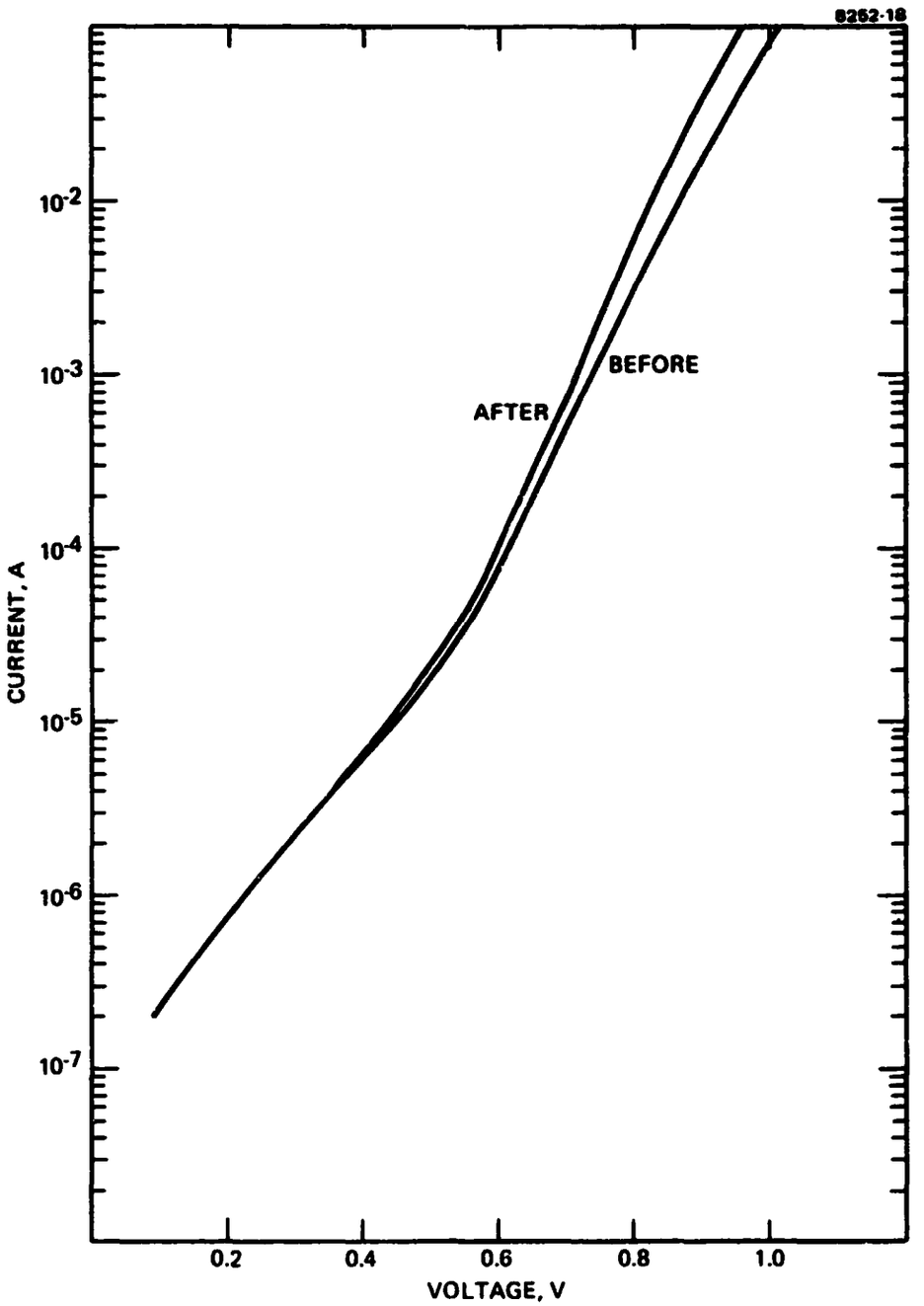

Figure 20. (AlGa)As-GaAs solar cell dark I-V characteristics before and after proton irradiation (cell 2375). Proton energy = 290 keV; proton fluence = 1×10^{10} p/cm^2.

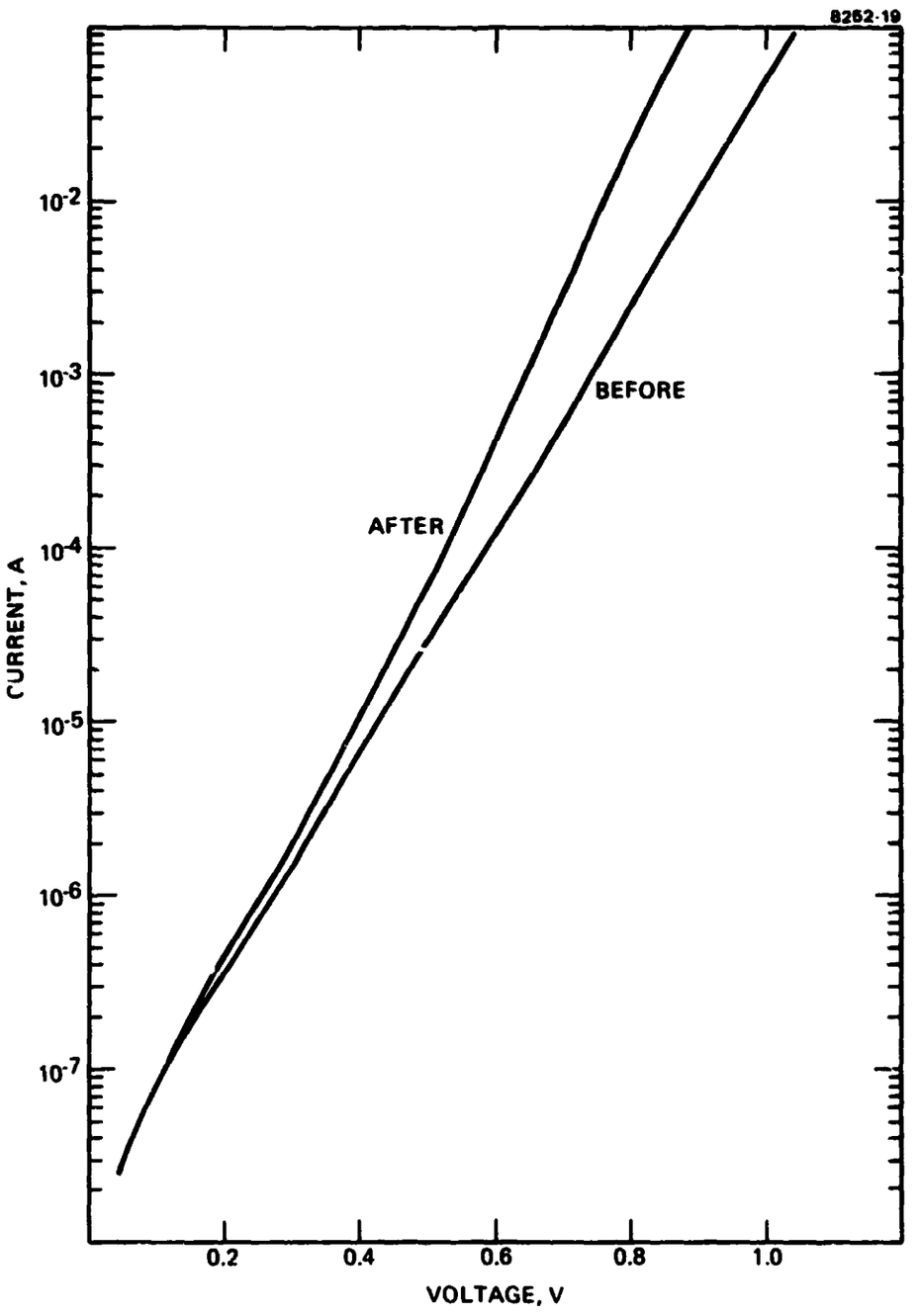

Figure 21. (AlGa)As-GaAs solar cell dark I-V characteristics before and after proton irradiation (cell 2424). Proton energy = 290 keV; proton fluence = 1×10^{11} p/cm^2.

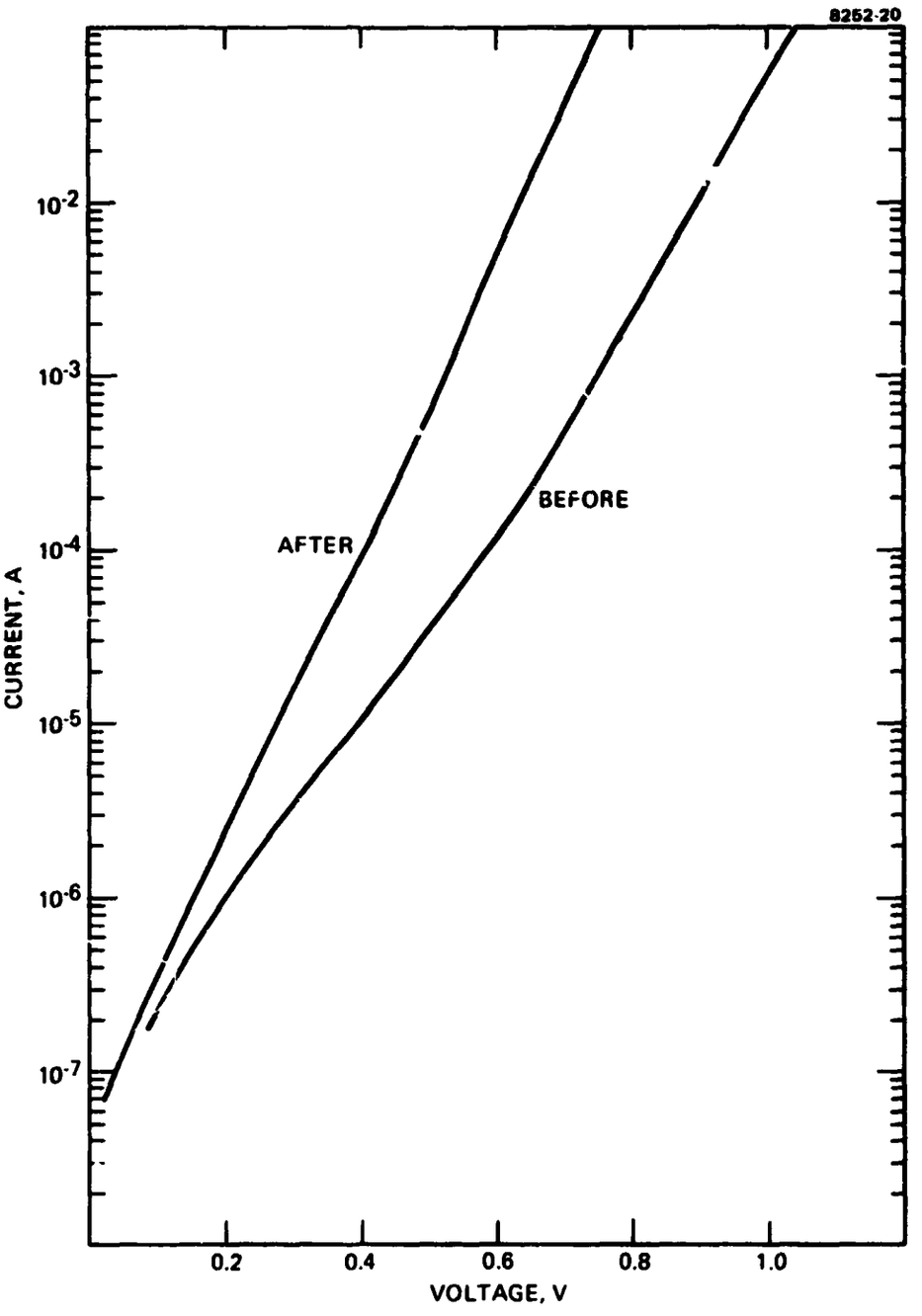

Figure 22. (AlGa)As-GaAs solar cell dark I-V characteristics (cell 2311). Proton energy = 290 keV; proton fluence = 1 x 10^{12} p/cm^2.

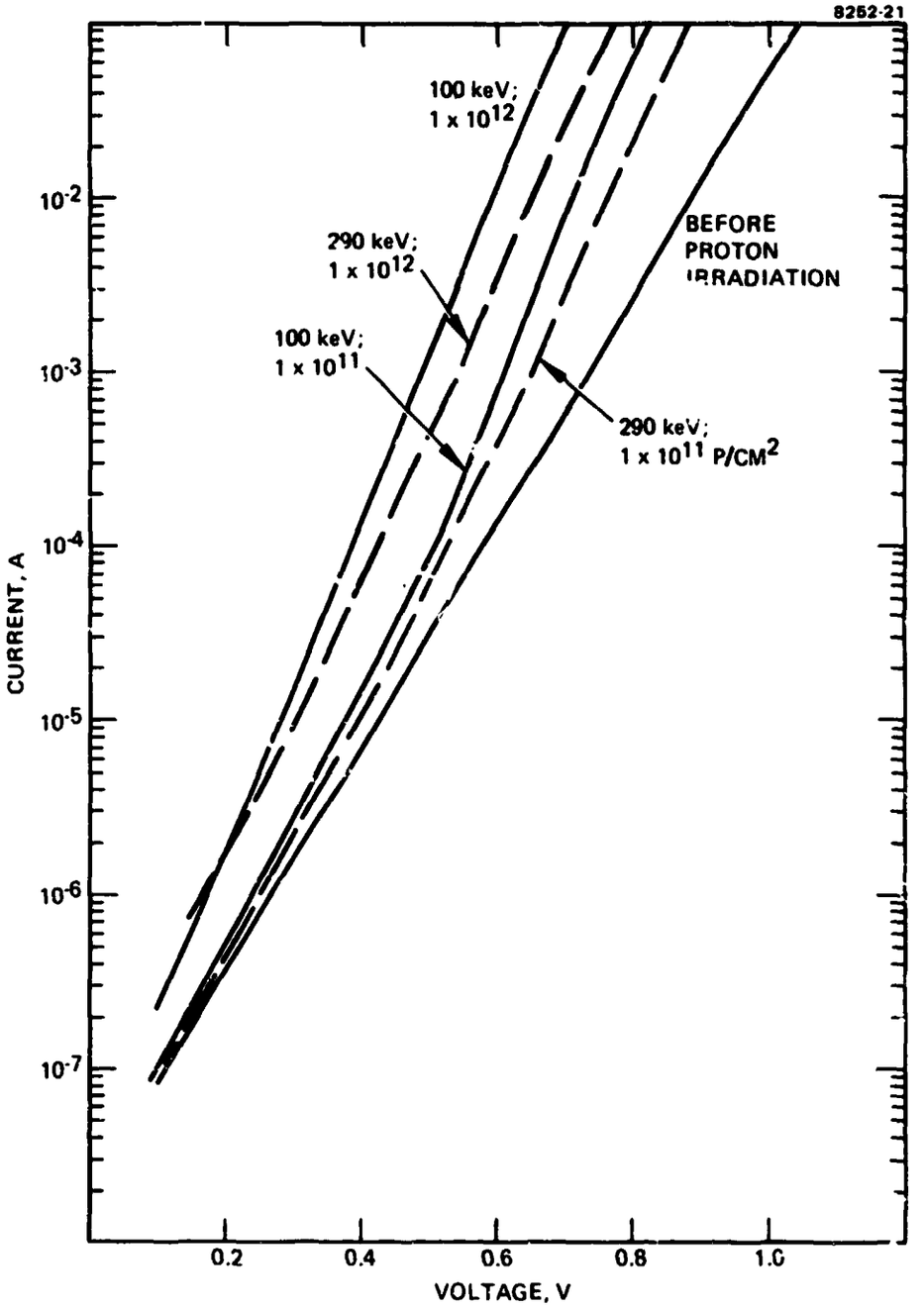

Figure 23. (AlGa)As-GaAs solar cell dark I-V characteristics.

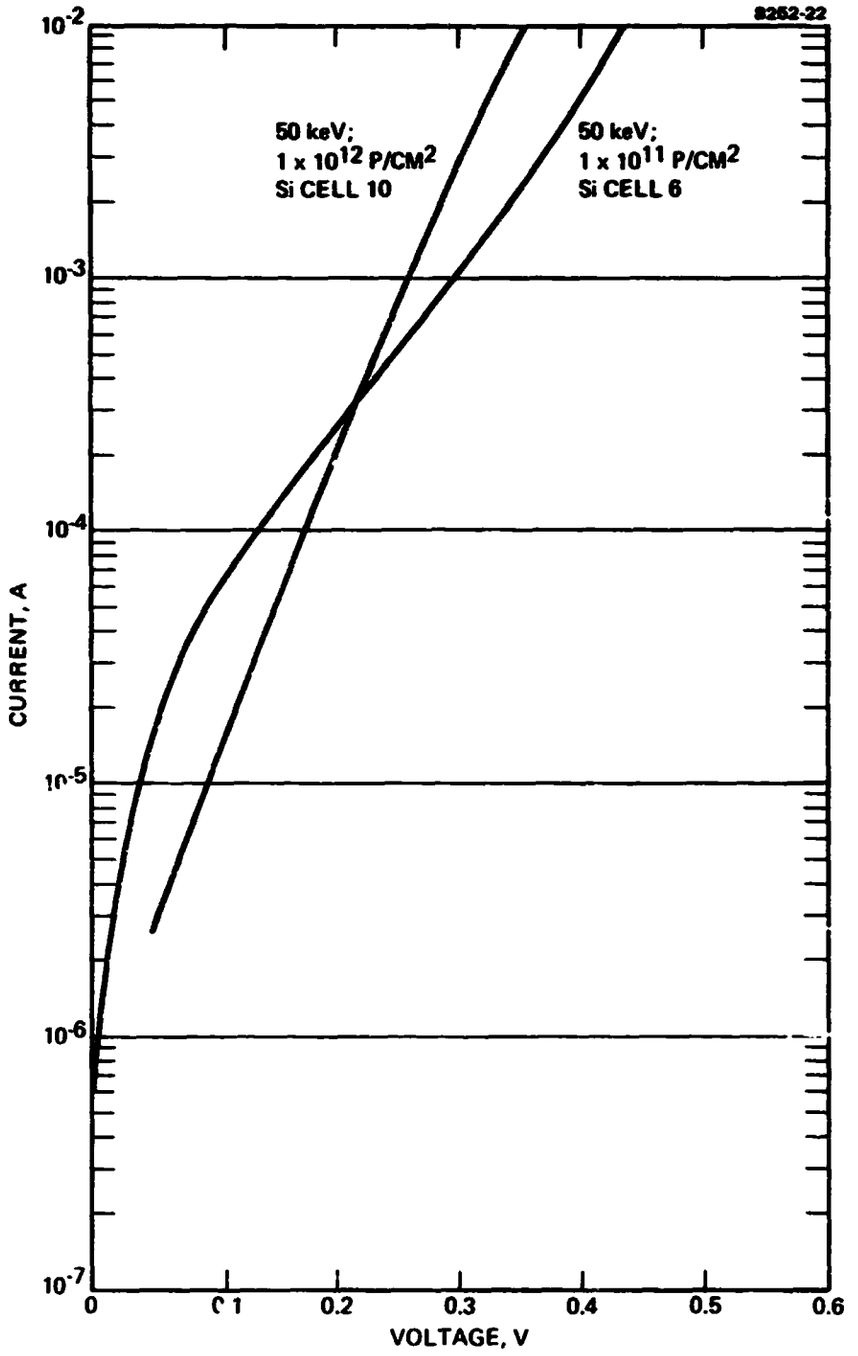

Figure 24. Si solar cell dark I-V characteristics after irradiation.

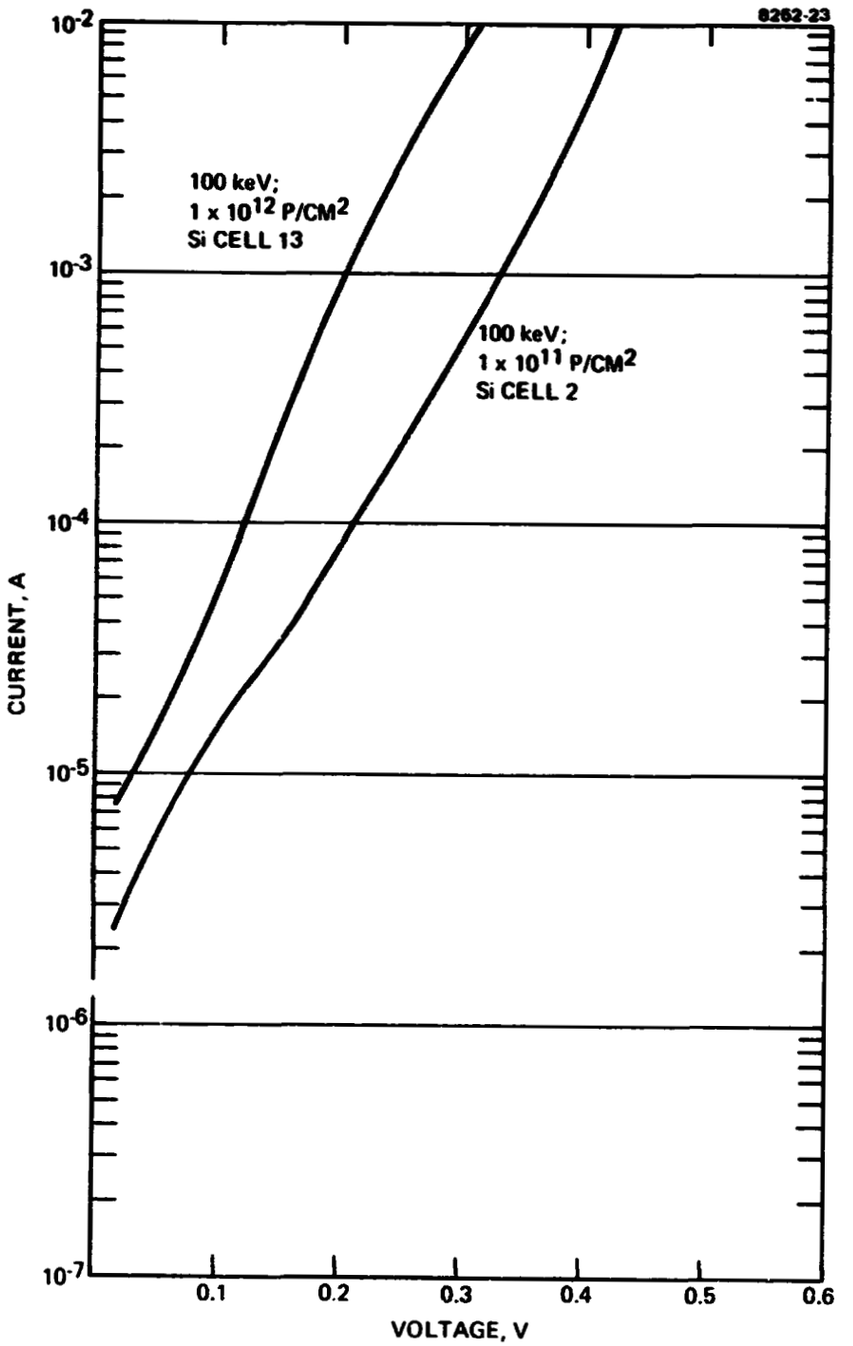

Figure 25. Si solar cell dark I-V characteristics after irradiation (proton energy = 100 keV).

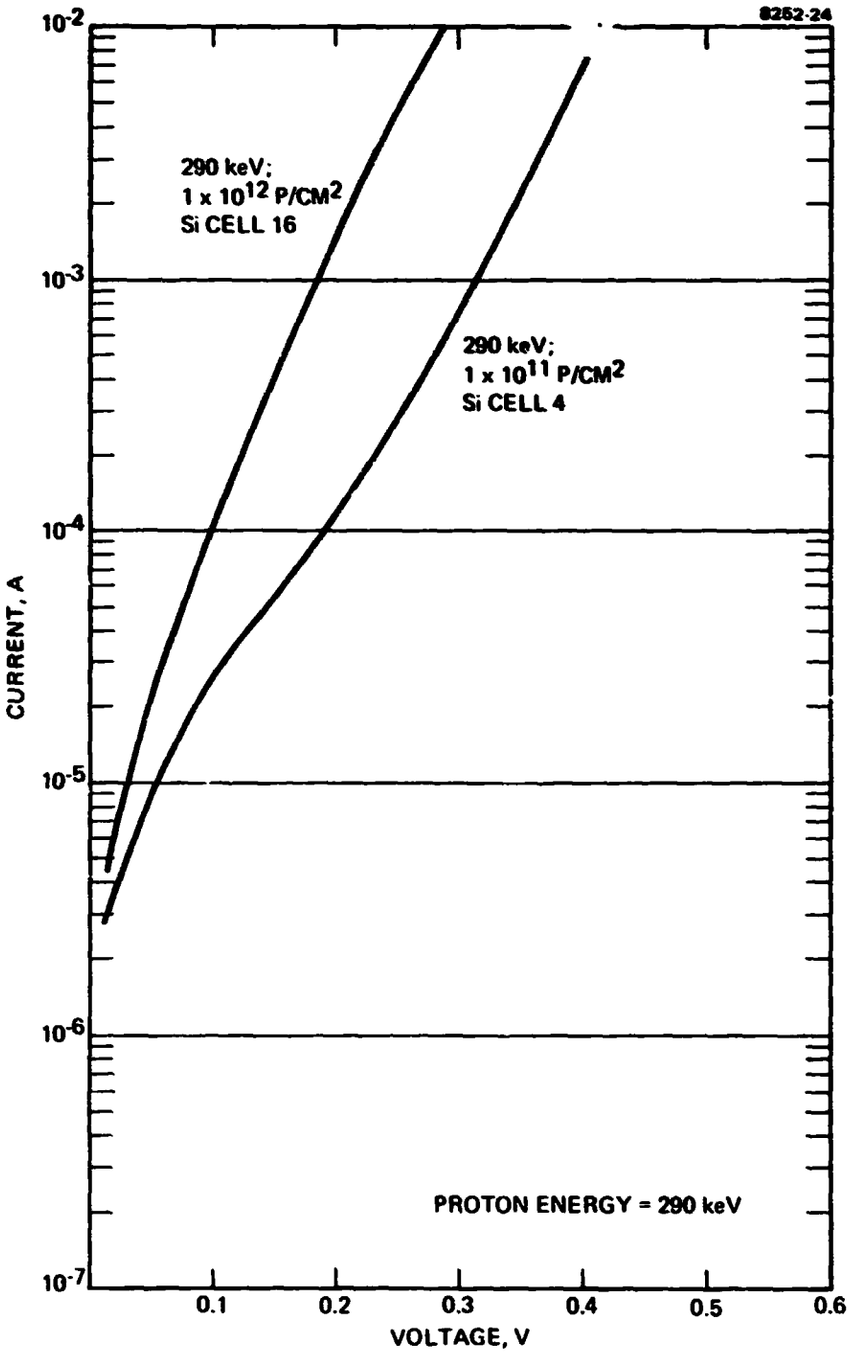

Figure 26. Si solar cell dark I-V characteristics after irradiation (proton energy = 290 keV).

In the case of the silicon cells, although they became more leaky after irradiation, the basic transport mechanism did not change. This conclusion resulted from our observation that the two I-V curves before and after irradiation stayed parallel to each other at the higher currents. The increased leakage current after irradiation probably resulted from an increase in the number of recombination centers at the junction, without the generation of new types of recombination centers. In summary, the change in the cells dark I-V characteristics after proton irradiation is in good agreement with the change in V_{oc} for each proton energy and fluence. In addition, the change in the log I-V slope after irradiation gives us further insight into the effects of proton irradiation on the current transport mechanism in these cells.

SECTION 5

CONCLUSION

This investigation has given us a more detailed understanding of the effect of the non-uniform damage produced by low-energy protons in both GaAs and Si solar cells. The damage in the solar cell's short-circuit current, open-circuit voltage, spectral response, and dark I-V characteristics are explained by the proton penetration pattern into the solar cell. In GaAs solar cells, the 50-keV protons are stopped at the front surface of the cell and have little effect on the solar cell's performance. The 100-keV protons are stopped close to the junction, thus reducing the open-circuit voltage by degrading the junction quality. The 290-keV protons penetrate deep into the cell, creating heavy damage in the base n region, thus greatly reducing the short-circuit current and causing greater power loss.

The 50-keV, 100-keV, and 290-keV protons penetrate beyond the junction in the silicon cells (x_j = 0.2 to 0.3 μm). The power loss in the silicon cell after low-energy proton irradiation is mostly reflected in the change in the open-circuit voltage and fill factor. There was no loss in short-circuit current in these silicon cells until they were bombarded by 290-keV protons at a 1×10^{12} p/cm^2 fluence level. The change in the open-circuit voltage, short-circuit current, spectral response, and dark I-V characteristics after irradiation at each proton energy and fluence were found to be consistent with our explanation of the effect of protons. Also, the GaAs cells' dark I-V characteristics show that a new recombination center dominates the current transport mechanism after irradiation.

The GaAs cells are more affected by low-energy protons than is the silicon cell because the low-energy protons are stopped within the short active region of the GaAs cell and produce a high amount of effective damage. However, these cells can be effectively shielded by the cover glass, as demonstrated in Figure 3.

To complete our proton damage studies on GaAs cells as a function of proton energy and fluence, it is important to study the damage at

intermediate proton energies (from 50 keV to 15 MeV). This information will improve understanding of proton damage characteristics in GaAs cells and provide the data required for determining the optimum cover glass protection that can be provided for these solar cells in specific space missions, with given proton energy spectra and fluences. It will also be instructive, as another future study, to study the annealing characteristics of the various damage centers produced by protons of different energies and fluences. A detailed understanding of these annealing characteristics could provide additional means for increasing the life of GaAs solar cells in space missions.

APPENDIX A

This paper was presented to the 13th Photovoltaic Specialists Conference, June 1978 at Washington, D.C.

APPENDIX A

ELECTRON AND PROTON DEGRADATION IN (AlGa)As-GaAs SOLAR CELLS

R. Loo, L. Goldhammer,* B. Anspaugh,** R.C. Knechtli and G.S. Kamath

Hughes Research Laboratories
Malibu, California 90265

ABSTRACT

Results on radiation damage in (AlGa)As-GaAs solar cells by 1 MeV electron fluences up to 1×10^{16} e/cm^{-2} and by 15, 20, 30 and 40 MeV proton fluences up to 5×10^{11} P cm^{-2} are presented. The damage is compared with data on state-of-the-art silicon cells which were irradiated along with the gallium arsenide cells. We verified experimentally our theoretical expectation that the junction depth has to be kept relatively shallow, to minimize radiation damage. The damage to the GaAs cells as a function of irradiation, is correlated with the change in their spectral response and dark I-V characteristics. The effect of thermal annealing on the (AlGa)As-GaAs solar cells was also investigated. This data is used to predict further avenues of optimization of the GaAs cells.

INTRODUCTION

The behavior of solar cells under radiation environment is of great importance for space application. Previous studies have shown that the (AlGa)As-GaAs solar cells have achieved an efficiency of 18.5% AMO (1) with a radiation resistance equal to or better than that observed in violet silicon cells (2). In this paper, we report the radiation effect on large-area (2 cm x 2 cm) (AlGa)As-GaAs solar cells fabricated at Hughes Research Laboratories (HRL) using the infinite melt liquid phase epitaxial (LPE) growth system. Our best cell to date has an AMO efficiency of 18%, and our improved shallow-junction cells show more radiation resistance than silicon cells.

GaAs has a large optical absorption constant and a short diffusion length; essentially, all the photovoltaic response is close to the GaAs surface. The radiation damage beyond this active region has a negligible effect on cell performance. Consequently, the reduction in the required minority carrier diffusion length and the relative shallowness of the active region are the key factors that can be exploited to make GaAs solar cells more radiation resistant. Data consistent with these observations is presented below.

EXPERIMENTAL

Figure 1 shows the (AlGa)As-GaAs solar cell structure. The n^+ concentration for the substrate is fixed at > 5×10^{17} cm^{-3} with Te as the dopant. The n buffer layer concentration is 1×10^{17} cm^{-3}. (At this doping level, the open-circuit voltage is 1 V.) The thickness of this layer was fixed at 10 μm or more because results indicated that the substrate visibility is minimized at a buffer layer thickness of 10 μm. A thickness less than this is not always sufficient to remove the effect of the substrate on cell performance.

7545-6

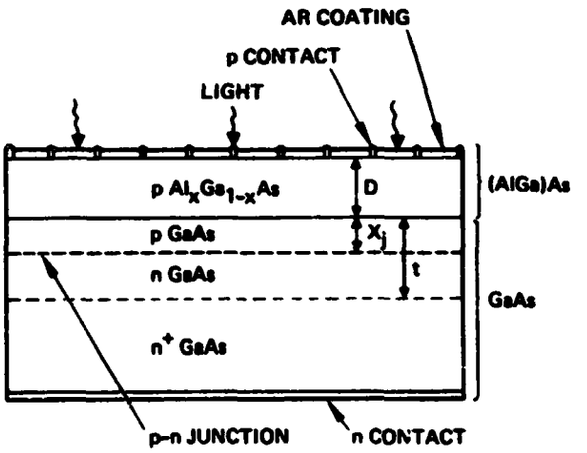

NUMBER OF FINGERS = 24
p CONTACT: Au-Zn-Ag
n CONTACT: Au-Ge-Ni-Ag
AR COATING: Ta_2O_5
p $Al_xGa_{1-x}As$: $X \geq 0.95$
CELL SIZE = 2 x 2 CM^2

Figure 1. The (AlGa)As-GaAs solar cell

*Hughes Aircraft Company, El Segundo, California
**J.P.L., Pasadena, California

The window layer of $(Al_xGa_{1-x})As$ is grown by LPE on GaAs. Our layer has $x > 0.90$, making the bandgap and hence the optical transmission as high as possible. The dopant is beryllium (Be). The concentration is 1×10^{18} cm^{-3}. During (AlGa)As window layer growth, a p-n homojunction is formed by Be diffusion from the (AlGa)As layer into the n buffer layer. The carrier concentration of the p-diffused region is also 1×10^{18} cm^{-3}.

The remaining parts of the baseline structure are self-explanatory. The Au-Zn contacts are about 3000 to 4000 Å with a silver overlay about 4 µm thick, and the n contact is AuGeNi (~ 5000 Å) with an Ag overlay. The AR coating is Ta_2O_5.

The Dynamitron particle accelerator at JPL was used as the electron source for high-energy electron irradiation; the irradiations were performed in vacuum at room temperature. The uniformity over the test plane was ± 4% with no areas of discontinuity. Fluxes and fluences were measured with a Faraday cup the current of which was integrated to establish electron fluences and to automatically stop the irradiation at the desired fluence levels.

High-energy proton irradiation was performed at the Crocker Nuclear Laboratory at the University of California at Davis. This cyclotron can produce a primary proton beam at energies between approximately 8 and 68 MeV. The solar cells were mounted with small pieces of double-face masking tape to aluminum plates. Each plate was irradiated separately in air at specific proton energies and fluences.* The fluence over the target plane was uniform within ±5%. The cell temperature during irradiation was kept at 30°C.

The full matrix of tests performed on the (AlGa)As-GaAs solar cells and on several representative silicon solar cells are given in Tables 1 and 2.

Table 1. Electron Irradiation Experiments

7545-4

ELECTRON ENERGY MeV	ELECTRON FLUENCE E/CM^2	TYPE AND NUMBER OF CELLS		
		(AlGa)As-GaAs	Si CONVENTIONAL	Si HIGH EFFICIENCY
1.0	1×10^{13}	3	3	3
	4×10^{14}	3	3	3
	1×10^{15}	3	3	3
	5×10^{15}	3	3	3
	1×10^{16}	3	3	3
0.7	1×10^{15}	2		
1.9	1×10^{15}	2		

Table 2. High-Energy Proton Irradiation Experiments

7545-5

PROTON ENERGY MeV	PROTON FLUENCE E/CM^2	TYPE AND NUMBER OF CELLS		
		(AlGa)As-GaAs	Si HIGH EFFICIENCY	Si CONVENTIONAL
15.4	5×10^{10}	3	5	4
15.4	5×10^{11}	3	4	4
22	5×10^{10}	3	2	3
22	5×10^{11}	3	2	3
30	5×10^{10}	3	2	3
30	5×10^{11}	3	2	3
40	5×10^{10}	3	2	3
40	5×10^{11}	3	2	3

RESULTS AND DISCUSSION

Electron Damage

A group of cells were fabricated early in the program for electron radiation tests. These cells were designed to have high efficiency with no attempt at optimizing the design parameters to increase radiation hardness. Figure 2 shows the maximum power obtained from the cells plotted against 1 MeV electron radiation fluence. These results were then compared with those for two types of silicon cells as shown in Table 1. This showed the need to improve these early cells for better resistance to electron radiation damage at fluences in excess of 4×10^{14}/cm^2.

Figure 3 shows the spectral response before and after electron irradiation. The results show that in these cells the spectral response in the short wavelength region shows greater damage compared to the longwavelength region. Since the optical absorption coefficient is greater for short wave lengths, most of the absorption in this region will be close to the surface of the cell. The photo generated carriers, therefore, must travel farther to reach the junction than do those generated by longer wavelengths. We suspected from the spectral response of the damaged cells that their junctions had to be relativily deep compared to the minority carrier diffusion length in the damaged layer. Our suspicion was confirmed by the measured junction depth of ≥ 1 µm. These observation led us to examine the influence of the junction depth on radiation damage more carefully.

*By comparing the results from previous solar cells irradiated both in air and in vacuum, we found that the ionized gases in air surrounding the cell during irradiation have no effect on the cells.

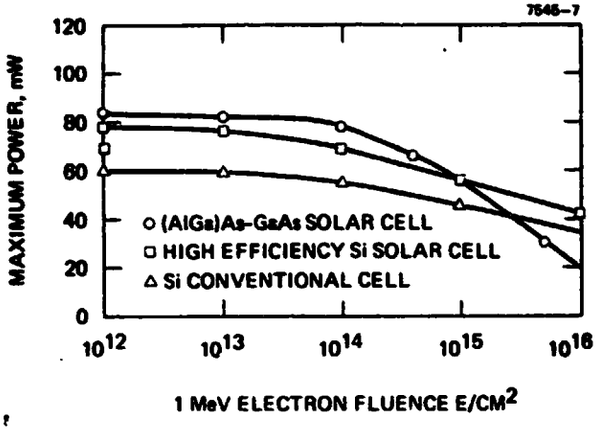

Figure 2. Maximum power as a function of 1 MeV electron fluence

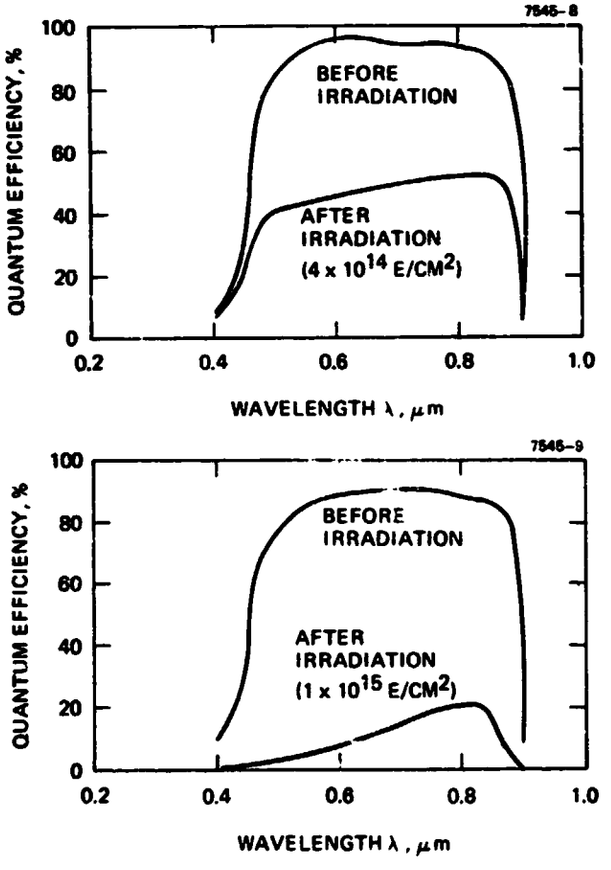

Figure 3. (AlGa)As-GaAs solar cell spectral response before and after 1 MeV electron irradiation

To correlate theory and experiments, Figure 4 shows the (AlGa)As-GaAs solar cell short circuit current density as a function of 1 MeV electron radiation fluence. The continuous curve represents the normalized experimental values. The dotted

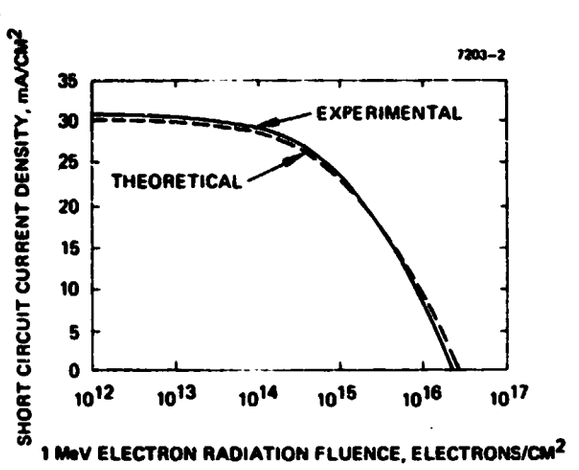

Figure 4. Short circuit current density versus 1 MeV electron radiation fluence, electrons/cm^2

line is the theoretical curve. Both curves correspond to an (AlGa)As layer thickness of 1 μm and a junction depth of 1 μm. For calculating the theoretical curve, the minority carrier diffusion length L was related to the fluence ϕ by the usual relation:

$$\frac{1}{L^2} = \frac{1}{L_o^2} + K_L \phi \quad . \qquad (1)$$

The initial diffusion lengths for holes (L_{po}) and electrons (L_{no}) were assumed to be 2 and 5 μm, respectively in these calculations. The damage constant K_L for the diffusion length used for both p- and n-type GaAs was deduced by matching the theoretical curve to the experimental curve as shown in Figure 4. It was found to be $K_L = 7 \times 10^{-8}$, assuming the same value of K_L for the n- and p-doped GaAs.

Using this value for K_L, the short-circuit density was calculated for several junction depths as a function of a 1 MeV electron fluence. The results, shown in Figure 5, show that radiation damage decreases as junction depth decreases.

Based on this analysis, we proceeded to fabricate a second-generation of (AlGa)As-GaAs solar cells with the goal of decreased sensitivity to the radiation environment. The window layer thickness was made at 0.5 μm while the junction depth was decreased to ∿ 0.5 μm by readjusting the LPE layer growth parameters.

Figure 6 shows the measured short-circuit current of these shallower junction cells versus 1 MeV electron fluence. The experimentally observed improved radiation resistance is in good agreement

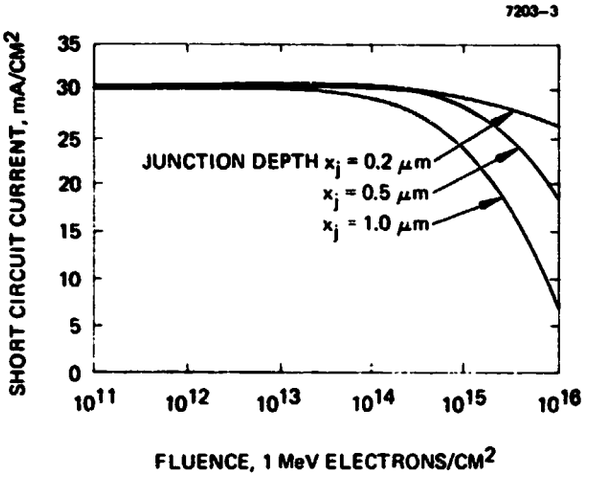

Figure 5 Predicted (AlGa)As-GaAs solar cell short circuit current density versus 1 MeV electron radiation fluence ((AlGa)As layer thickness = 1.0 μm, initial diffusion length L_{po} = 2 μm, L_{no} = 5 μm, and diffusion length damage constant $K_L = 7 \times 10^{-8}$)

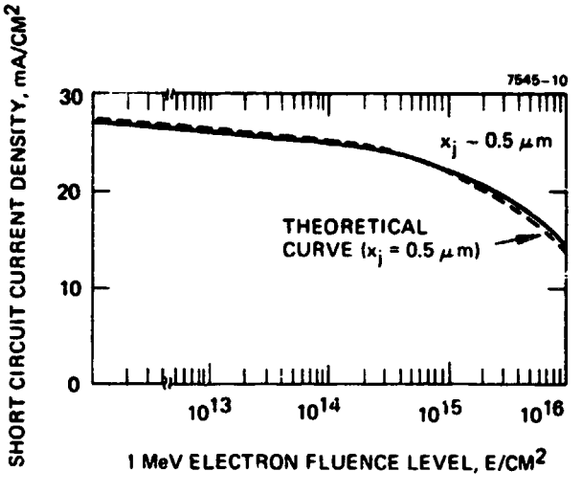

Figure 6. Short circuit current versus electron fluence level (1 MeV)

with the predictions of the theory. Figure 7 shows the experimental results for both (AlGa)As-GaAs solar cells and newly developed high-efficiency Si solar cells as a function of 1 MeV electron irradiation. Also shown for reference are the results of our previous set of irradiated (AlGa)As-GaAs deep-junction solar cells.

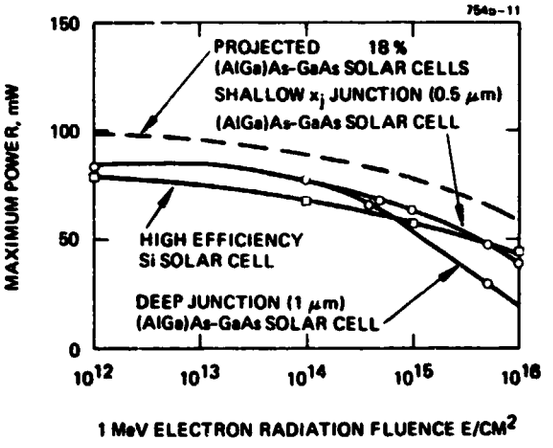

Figure 7. Maximum output power versus 1 MeV electron fluence

The spectral response of the deep-junction and shallower junction cells, both before and after irradiation, are given in Figure 8(a and b). The figure shows that the radiation damage in the deeper junction cells is concentrated in the short-wavelength region, whereas the shallower junction causes the damage to shift to the longer wavelength. This is consistent with our observation that the collection of minority carriers in the p region is not much affected up to the fluence at which the electron diffusion length is reduced to less than the p layer thickness.

Figure 8(c) shows the spectral response of the shallower junction solar cells irradiated at fluences 1×10^{15} e/cm^2 with electron energies varying from 0.7 MeV to 1.9 MeV. As expected at higher energies, these cells show more degradation, probably because K_L increases with increasing electron energy. Figure 9 shows typical dark current-voltage (I-V) characteristics before and after electron irradiation. Although solar cells become more leaky after irradiation, the basic transport mechanism remains the same (as shown by the I-V curves, which remain parallel to each other). This increased leakage current probably results from an increase in the number of recombination centers at the junction.

High Energy Proton Damage

Twenty-four (AlGa)As-GaAs solar cells and several representative silicon cells were irradiated with 15.4 MeV to 40 MeV protons at fluences of 5×10^{10} and 5×10^{11} p/cm^2 (Table 2).

The baseline structure of the solar cell used for proton irradiation was the same as that of the shallow-junction solar cells used for electron

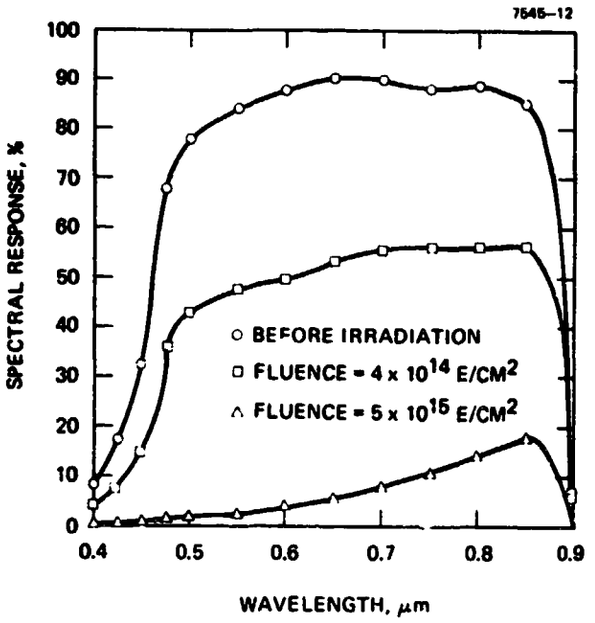

Figure 8(a). (AlGa)As-GaAs solar cell spectral response versus 1 MeV electron radiation fluences

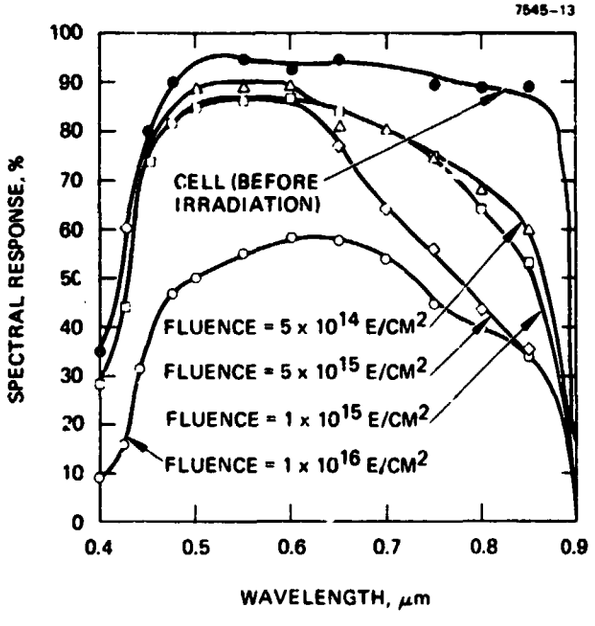

Figure 8(b). (AlGa)As-GaAs solar cell spectral response versus 1 MeV electron radiation fluence

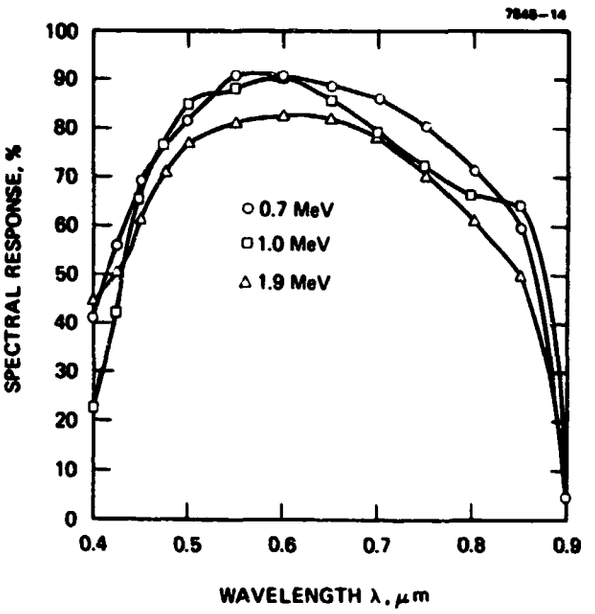

Figure 8(c). (AlGa)As-GaAs solar cell spectral response for several electron energies

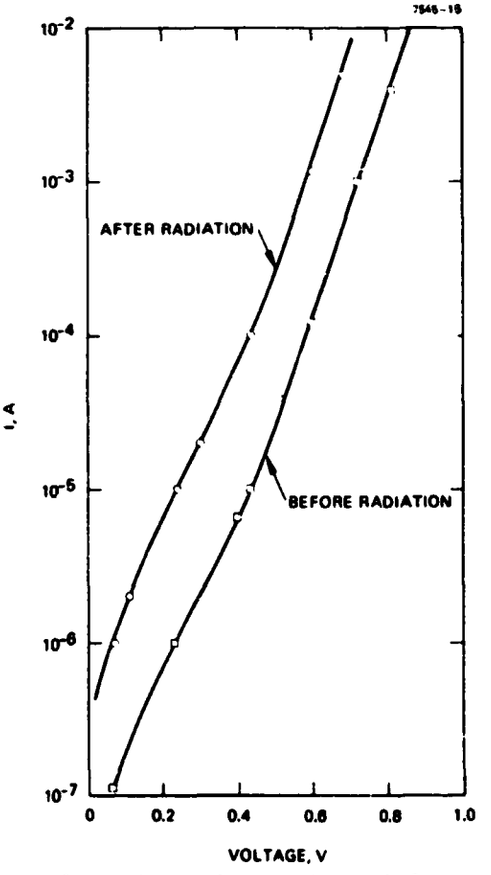

Figure 9. Dark I-V characteristics before and and after electron irradiation

irradiation, except that no cover glass was applied to these cells.

The results of these proton irradiation tests are summarized in Figure 10 (a and b), which shows the maximum solar cell output power versus proton irradiation fluence for the three types of cells specified in Table 2. The (AlGA)As-GaAs solar cells are more resistant to high-energy proton radiation damage than the silicon cells. The dotted lines plotted in Figure 10 are extrapolations of our test results; these show the effect expected from proton fluence on an improved (AlGa)As-GaAs solar cell with a beginning-of-life AMO power-conversion efficiency of 18%. This extrapolation is pertinent since the feasibility of an 18% efficiency has already been demonstrated for this type of cell.

Figures 11 and 12 show the average spectral response of the (AlGa)As-GaAs solar cells before and after proton irradiation with proton energies of 15.4 MeV and 40 MeV, respectively. The spectral response in the short wavelength region of these shallow-junction solar cells is almost insensitive to the proton irradiation. A slight decrease in the solar cell spectral response occurs only in the long wavelength region.

Figure 13 shows the dark I-V characteristic before and after irradiation. Again, just as in the case of electron irradiation, the solar cell junction becomes slightly leaky due to the increasing number of recombination centers produced by proton irradiation although the basic transport mechanism remains unchanged.

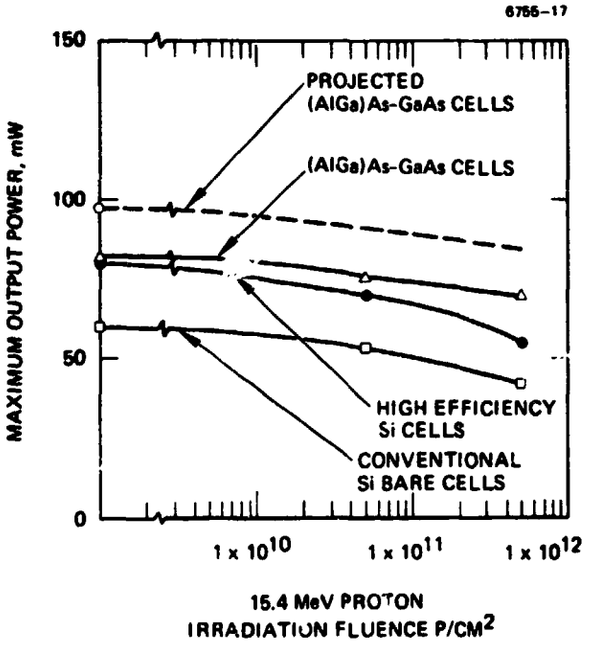

Figure 10(a). Solar cell maximum output power versus 15.4 MeV proton irradiation fluence.

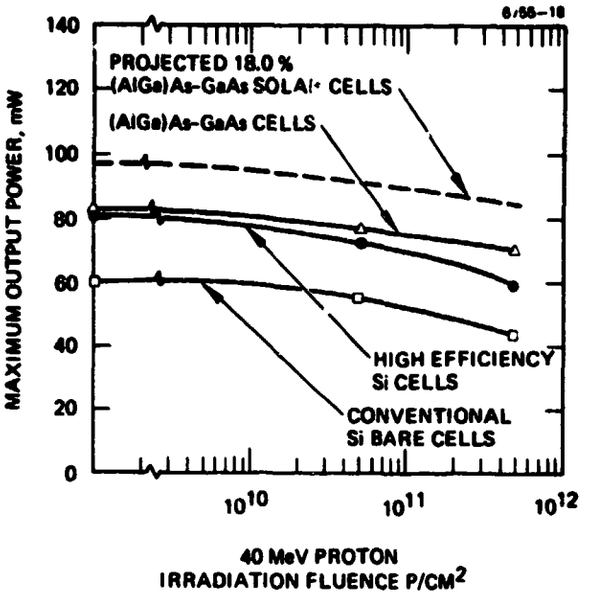

Figure 10(b). Solar cell maximum output power versus 40 MeV proton irradiation fluence

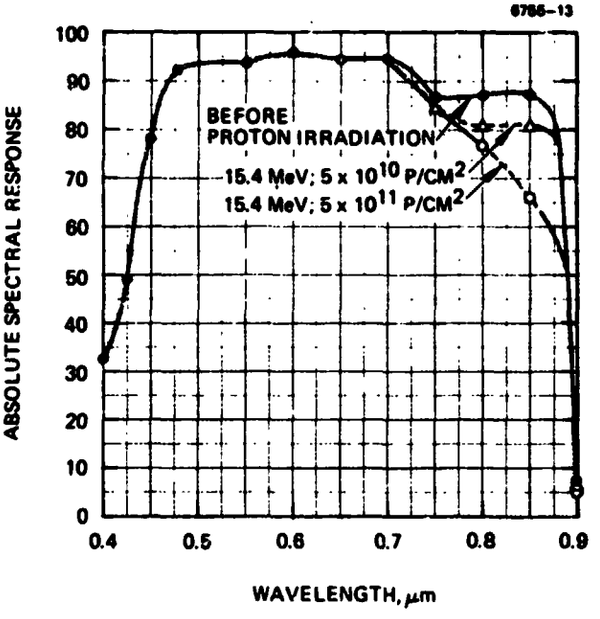

Figure 11. (AlGa)As-GaAs solar cell spectral response before and after 15.4 MeV proton irradiation

Radiation Annealing Studies

GaAs solar cells damaged by radiation recover their efficiency when annealed at low temperatures

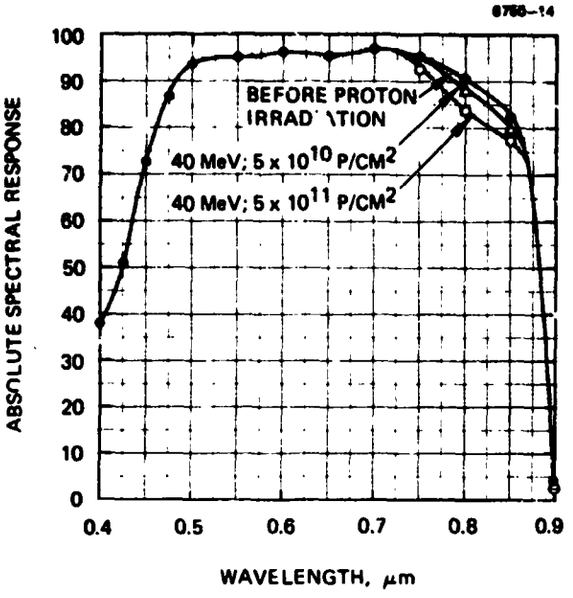

Figure 12. (AlGa)As-GaAs solar cell spectral response before and after 40 MeV proton irradiation

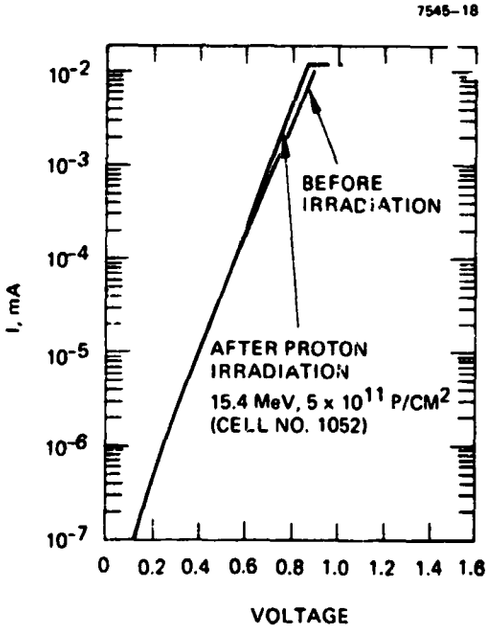

Figure 13. Dark I-V characteristics before and after proton irradiation

Figure 13. Dark I-V characteristics before and after proton irradiation

on the order of 200°C to 300°C (3,4). Some preliminary thermal annealing experiments on the radiation-damaged (AlGa)As-GaAs solar cells were performed in our laboratory. The cells were irradiated at fluences of 1 x 10^{15}/cm^2 with electron energies varying from 0.7 MeV through 1.0 MeV to 1.9 MeV. Subsequently, they were annealed in vacuum at temperatures of over 200°C. Figure 14 shows the effect of annealing as a function of annealing time and temperatures.

Figure 15 compares the spectral response of these cells after the annealing step with the spectral response before and after electron irradiation. The long wavelength region shows significant recovery. This suggests that the annealing leads to a significant recovery in the minority carrier diffusion length in GaAs after radiation damage.

Figure 16 shows the dark I-V characteristics of these cells. These cells show leaky p-n junctions after irradiation; however, they almost completely recover to their pre-irradiation condition after annealing at 210°C. These results indicate that (AlGa)As-GaAs solar cells can be annealed at practical temperatures to remove radiation damage. This could be exploited for longer space missions.

CONCLUSION AND SUMMARY

Several 2 cm x 2 cm (AlGa)As-GaAs cells were subjected to radiation damage studies using both electrons and protons. The results show that:

- (AlGa)As-GaAs solar cells can be made more resistant to radiation damage than can silicon cells for both electron and proton irradiation.
- The junction depth is a sensitive parameter in determining radiation resistance.
- The (AlGa)As-GaAs solar cells suffer only a moderate amount of degradation at proton energies above 15.4 MeV.
- The efficiencies of electron-radiation-damaged (AlGa)As-GaAs solar cells recover when annealed at temperatures as low as 200°C to 300°C.

ACKNOWLEDGMENTS

The radiation damage studies reported here were supported in part by contracts from NASA Langley, Contract NAS 1-14727

REFERENCES

1. J.M. Woodall and H.J. Hovel, "An Isothermal Etchback - Regrowth Method for High Efficiency GaAlAs-GaAs Solar Cells," Appl. Phys Lett. 30, 492 (1977).
2. R.I. Moon, et al., "Performance of (AlGa)As-GaAs Solar Cells in the Space Environment," 12th IEEE Photovoltaic Specialists Conference, 255 (1975).
3. R.S. Miller and J.S. Harris, "Gallium Arsenide Concentration System," presented at the AIAA Conference on the Future of Aerospace Power System, March 1977.
4. G.H. Walker and E.J. Conway, "Annealing of GaAs Solar Cells Damaged by Electron Irradiation," J. of Electrochemical Chemical Society, Vol. 125, No. 4, p. 76, 1978.

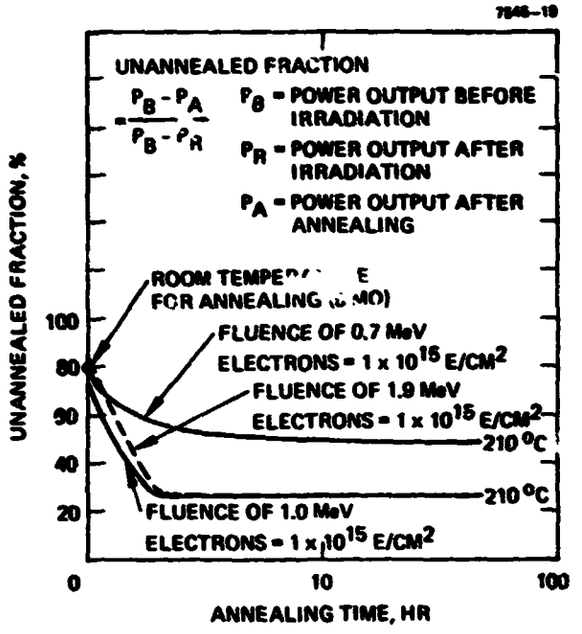

Figure 14. Unannealed fraction versus annealing time

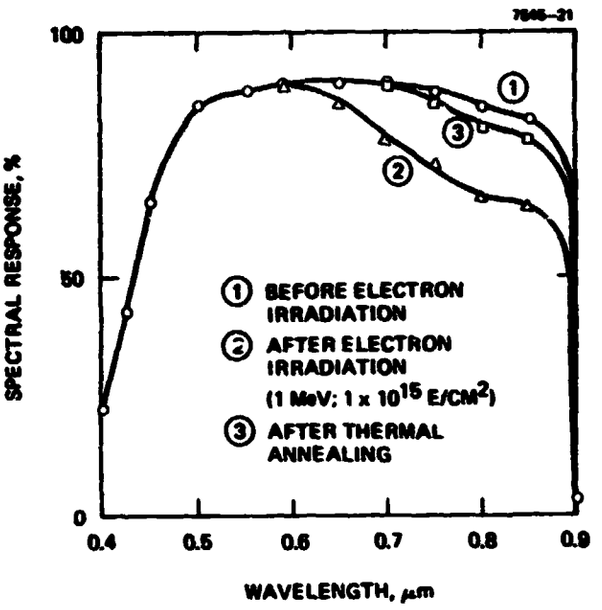

Figure 15(b). Spectral response before and after thermal annealing cell #1008

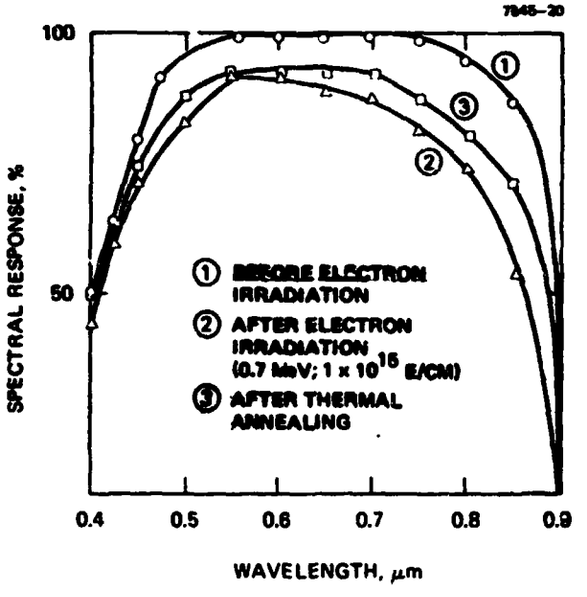

Figure 15(a). Spectral response before and after thermal annealing Cell #1222

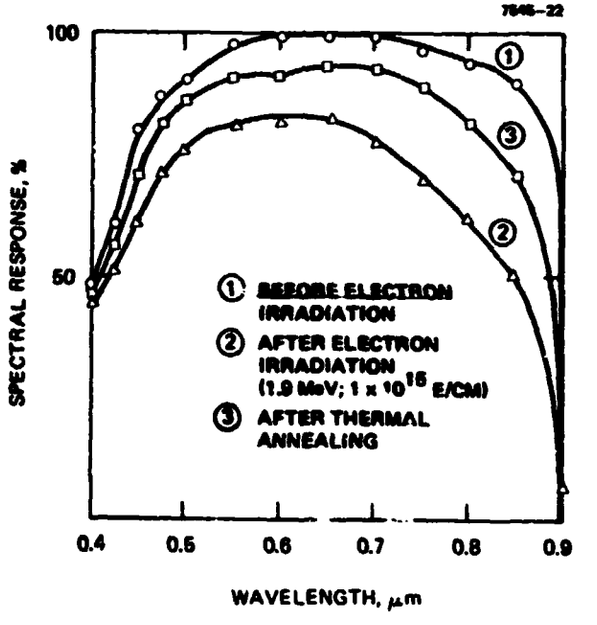

Figure 15(c). Spectral response before and after irradiation and after annealing cell #1278

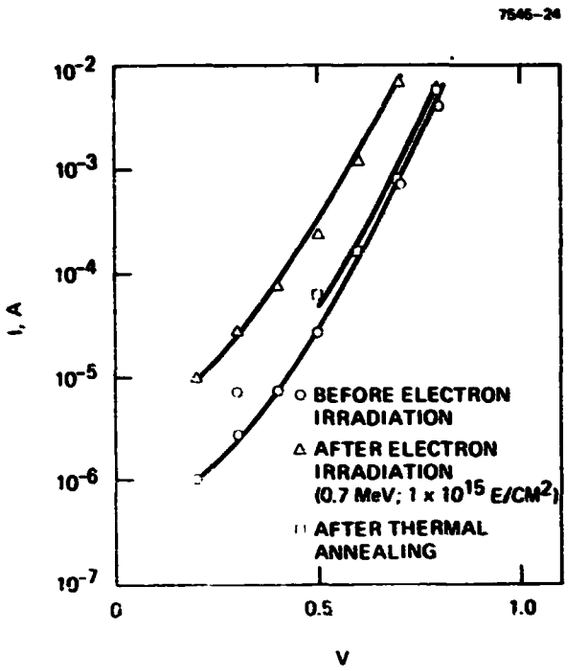

Figure 16(a). Dark I-V characteristic before and after thermal annealing cell #1222

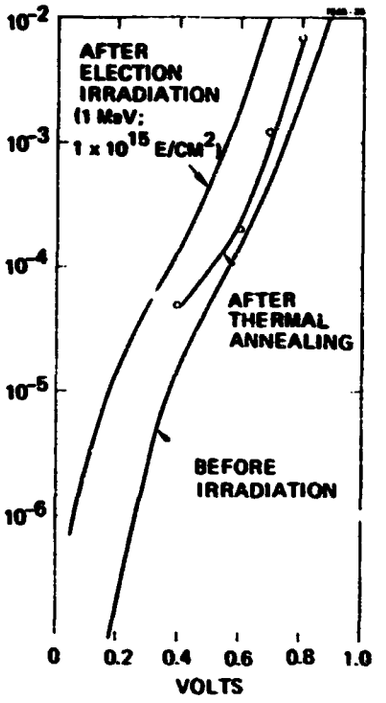

Figure 16(b). Dark I-V characteristic before and after thermal annealing cell #1008

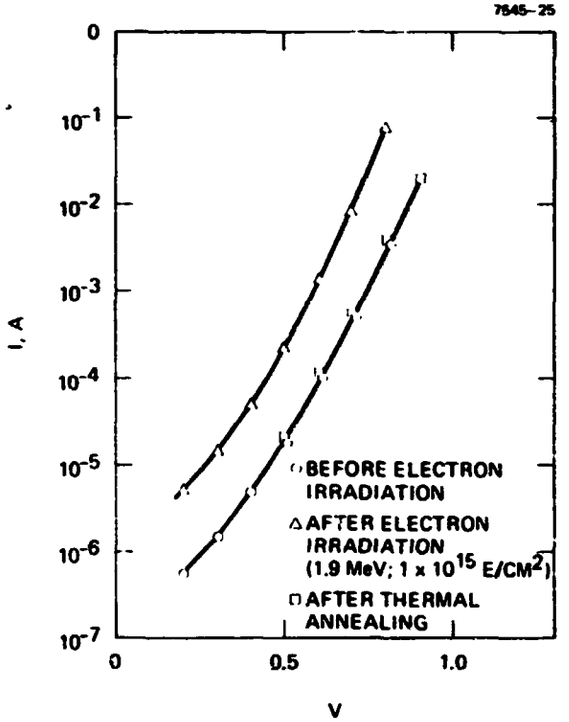

Figure 16(c). Dark I-V characteristic before and after thermal annealing cell #1278

APPENDIX B

PHOTO I-V CHARACTERISTICS OF (AlGa)As-GaAs SOLAR CELL BEFORE AND AFTER PROTON IRRADIATION

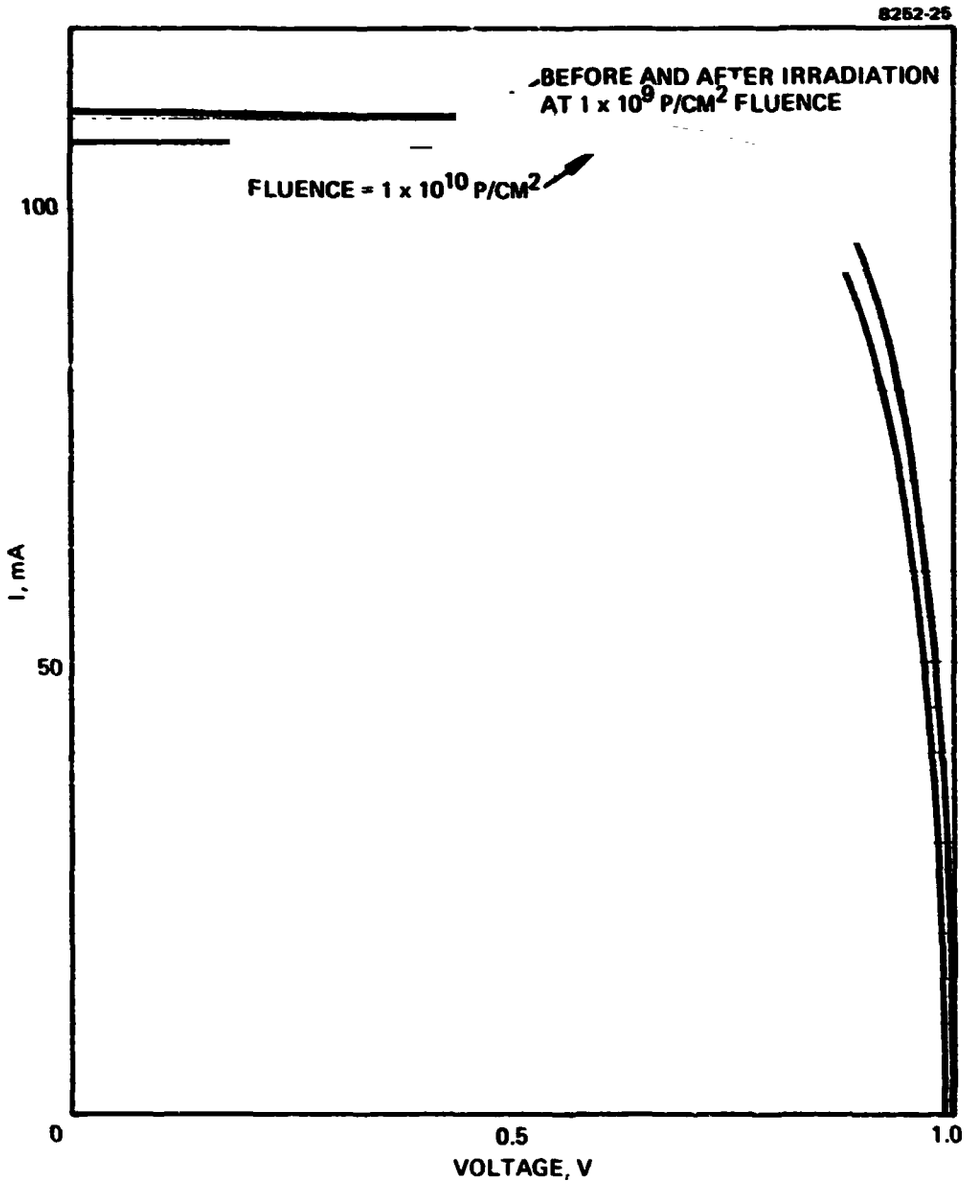

Figure B-1. Photo I-V characteristics before and after proton irradiation. Proton energy = 50 keV (cell 2266).

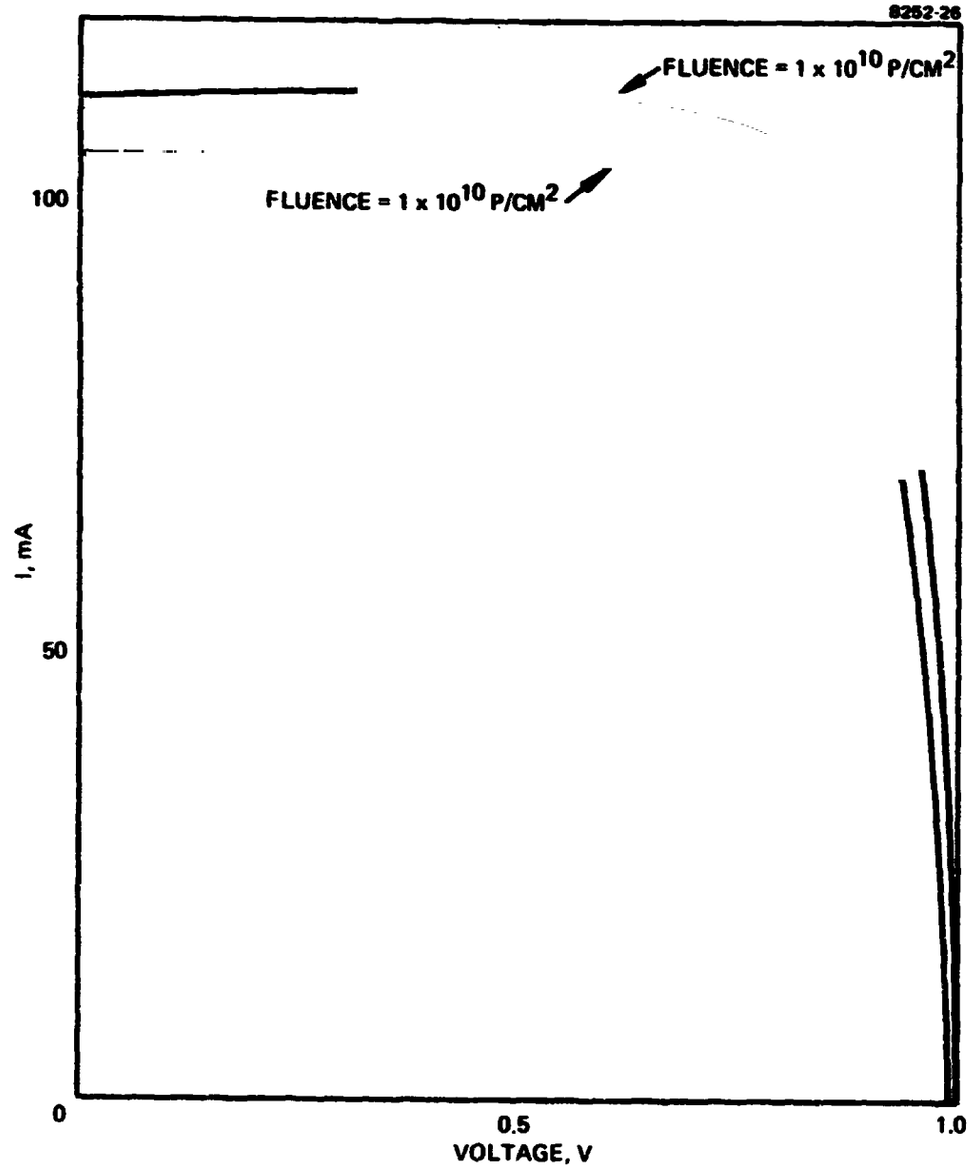

Figure B-2. Photo I-V characteristics before and after proton irradiation; proton energy = 50 keV (cell 2295).

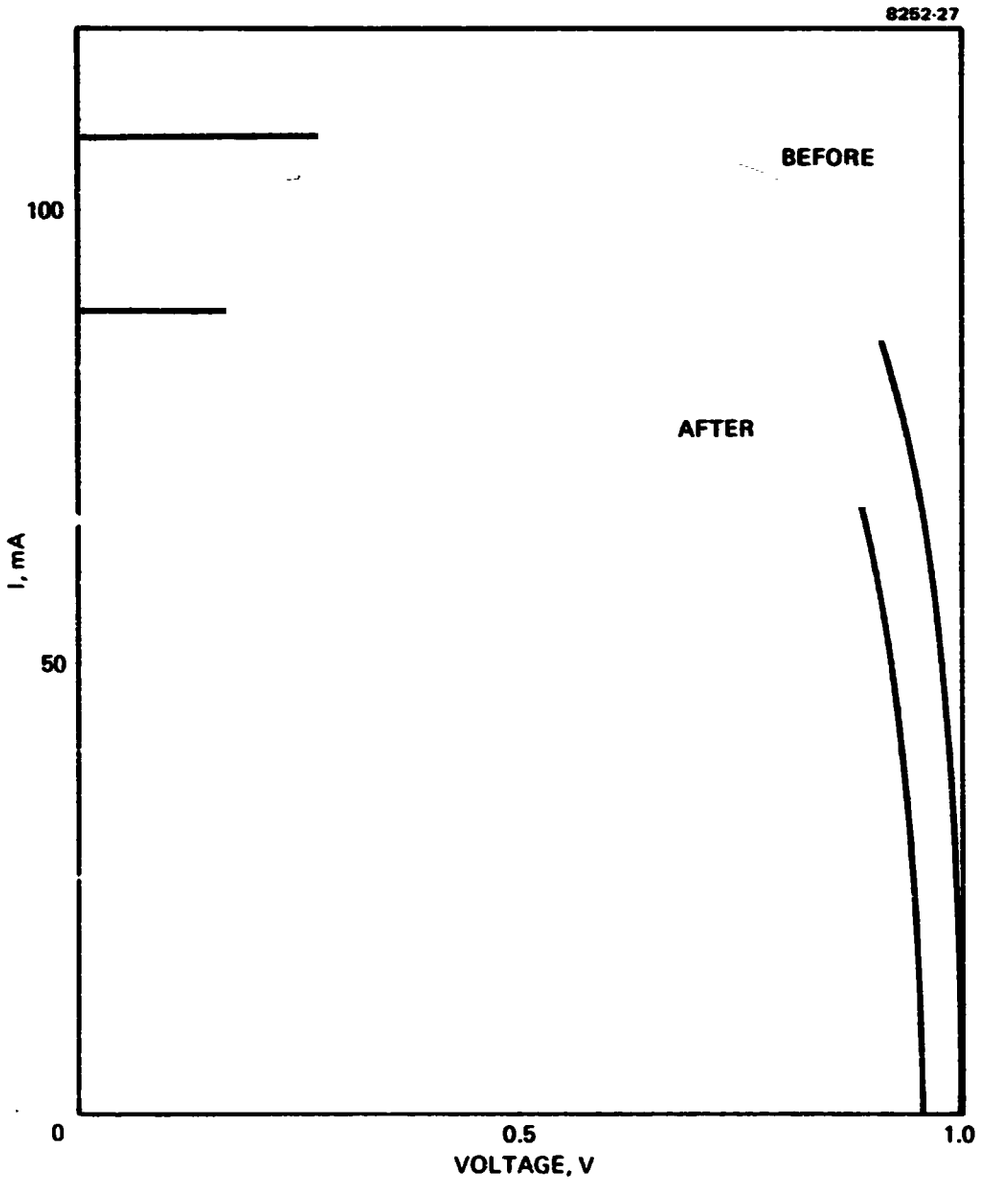

Figure B-3. Photo I-V characteristics before and after proton irradiation; proton energy = 50 keV; 1 x 10^{11} P/cm^2 (cell 2406).

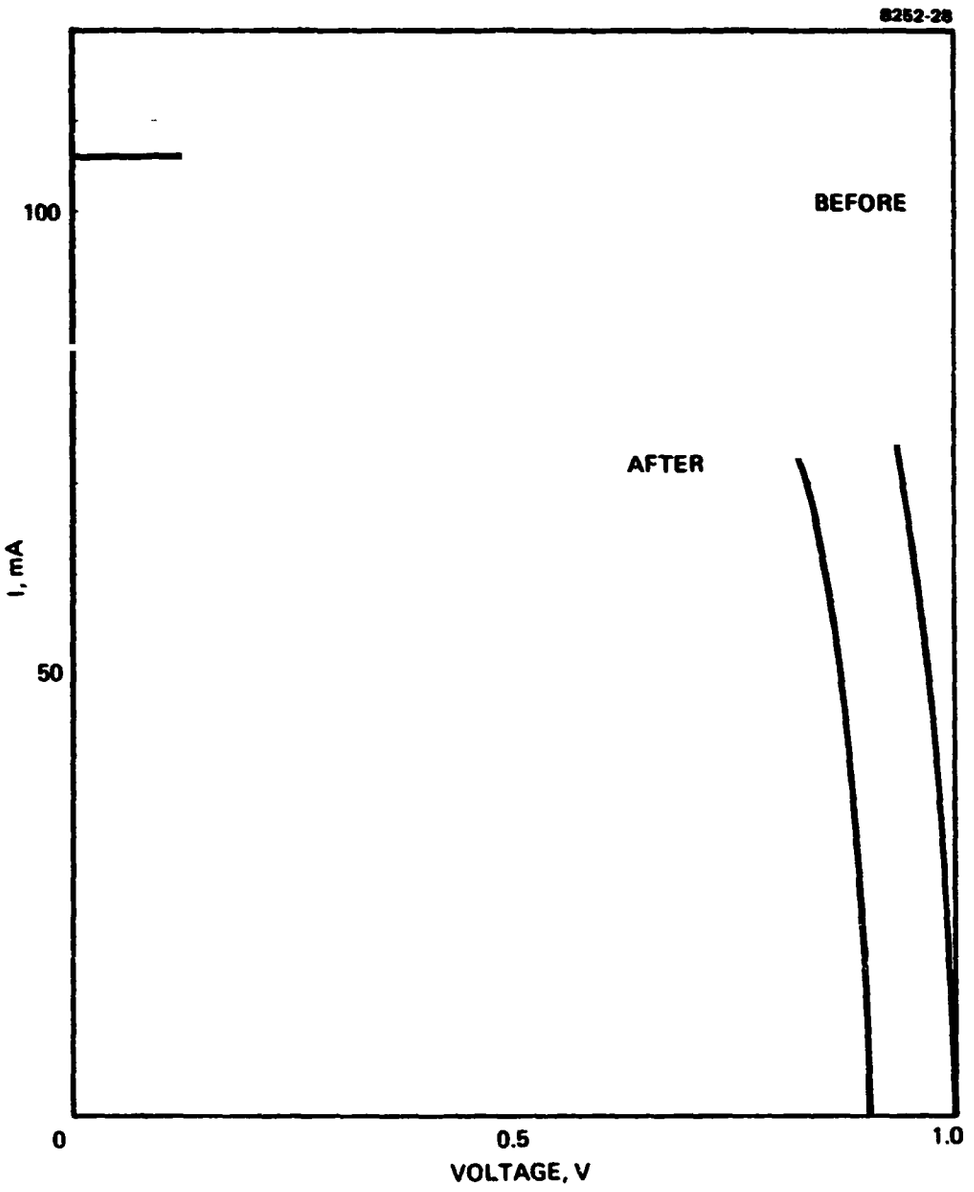

Figure B-4. Photo I-V characteristics before and after proton irradiation; proton energy = 50 keV; 1 x 10^{11} P/cm^2 (cell 2407).

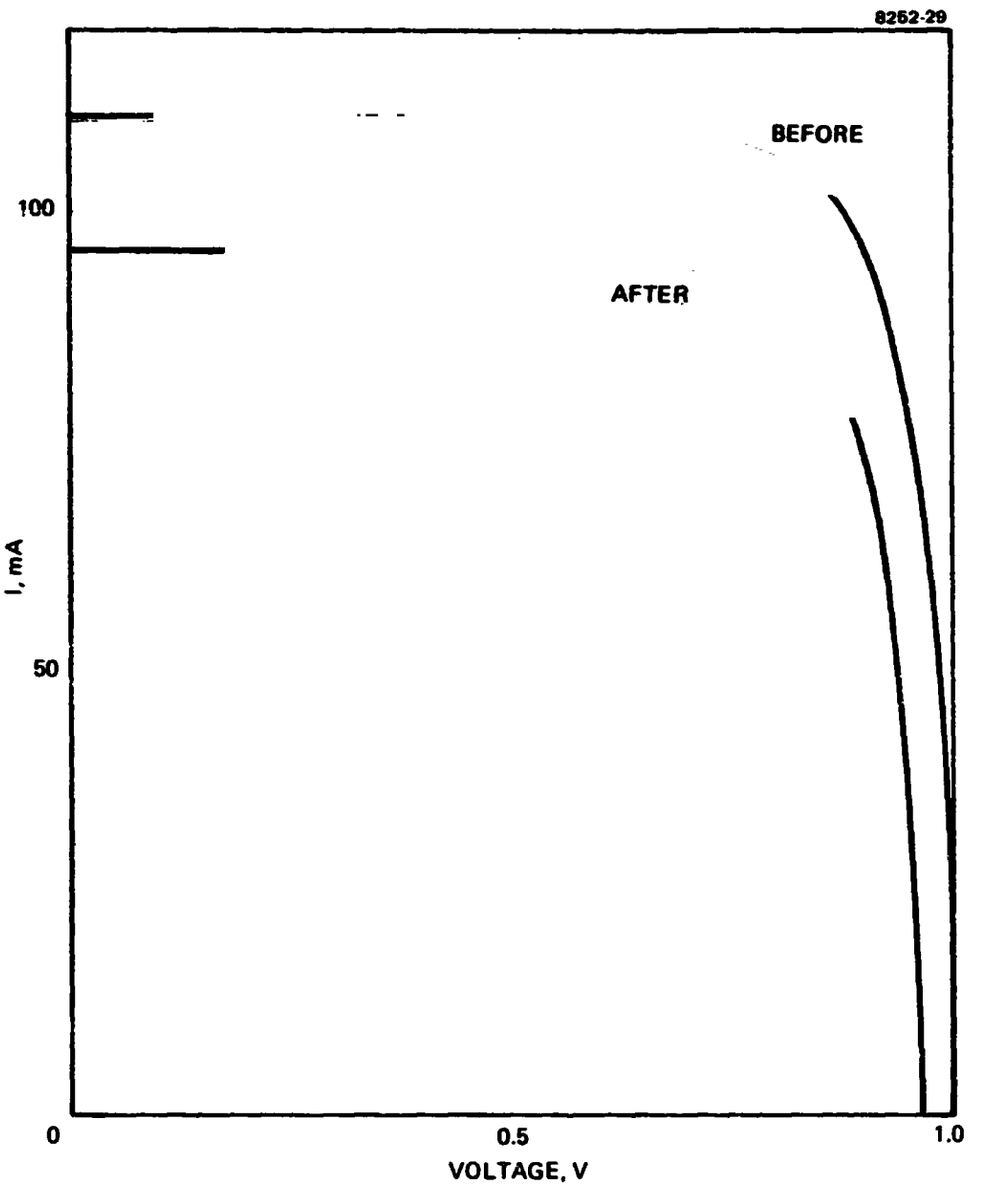

Figure B-5. Photo I-V characteristics before and after proton irradiation; proton energy = 50 keV; 1 x 10^{11} P/cm^2 (cell 2411).

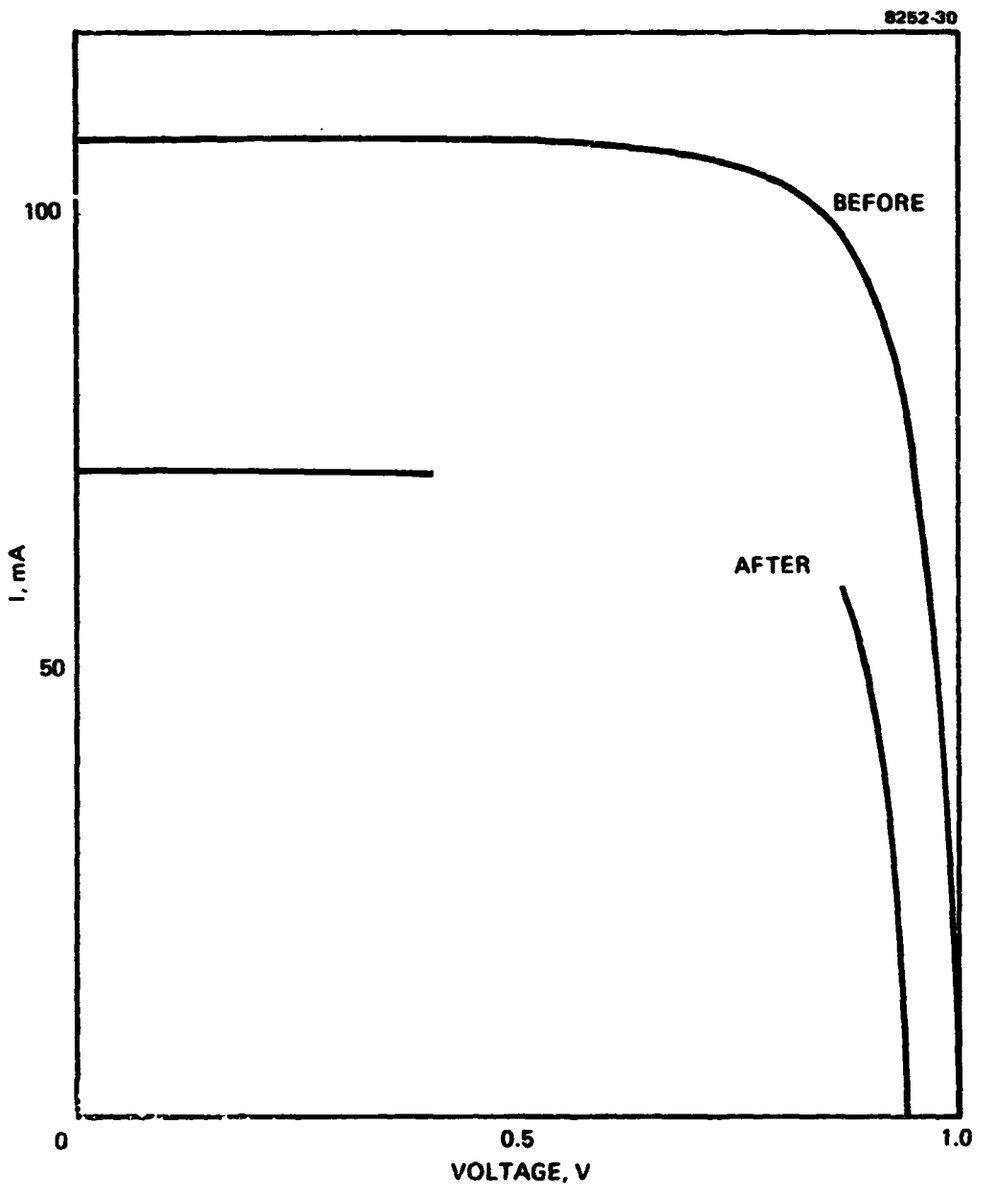

Figure B-6. Photo I-V characteristics before and after proton irradiation; proton energy = 50 keV; 1 x 10^{12} P/cm^2 (cell 2426).

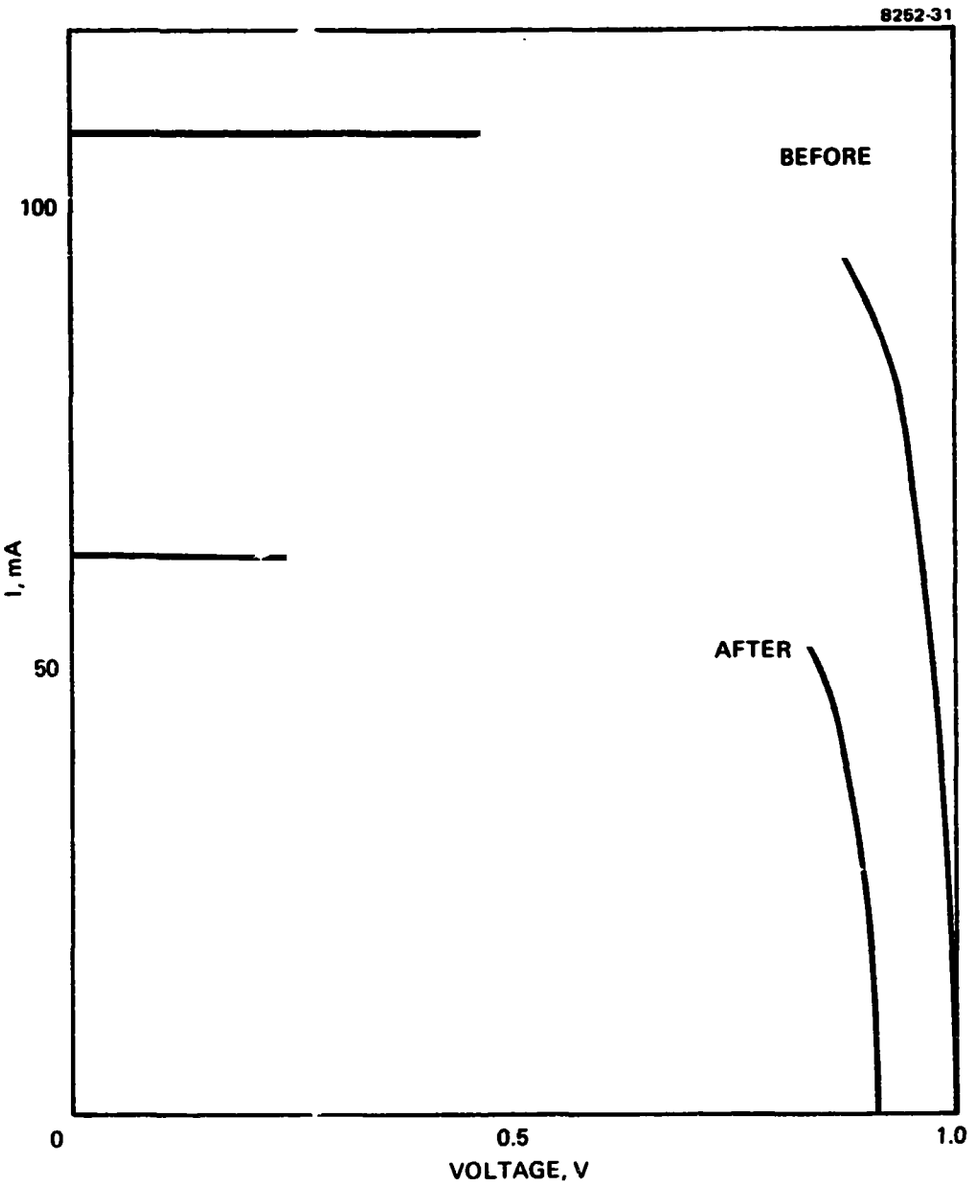

Figure B-7. Photo I-V characteristics before and after proton irradiation; proton energy = 50 keV; 1 x 10^{12} P/cm^2 (cell 2427).

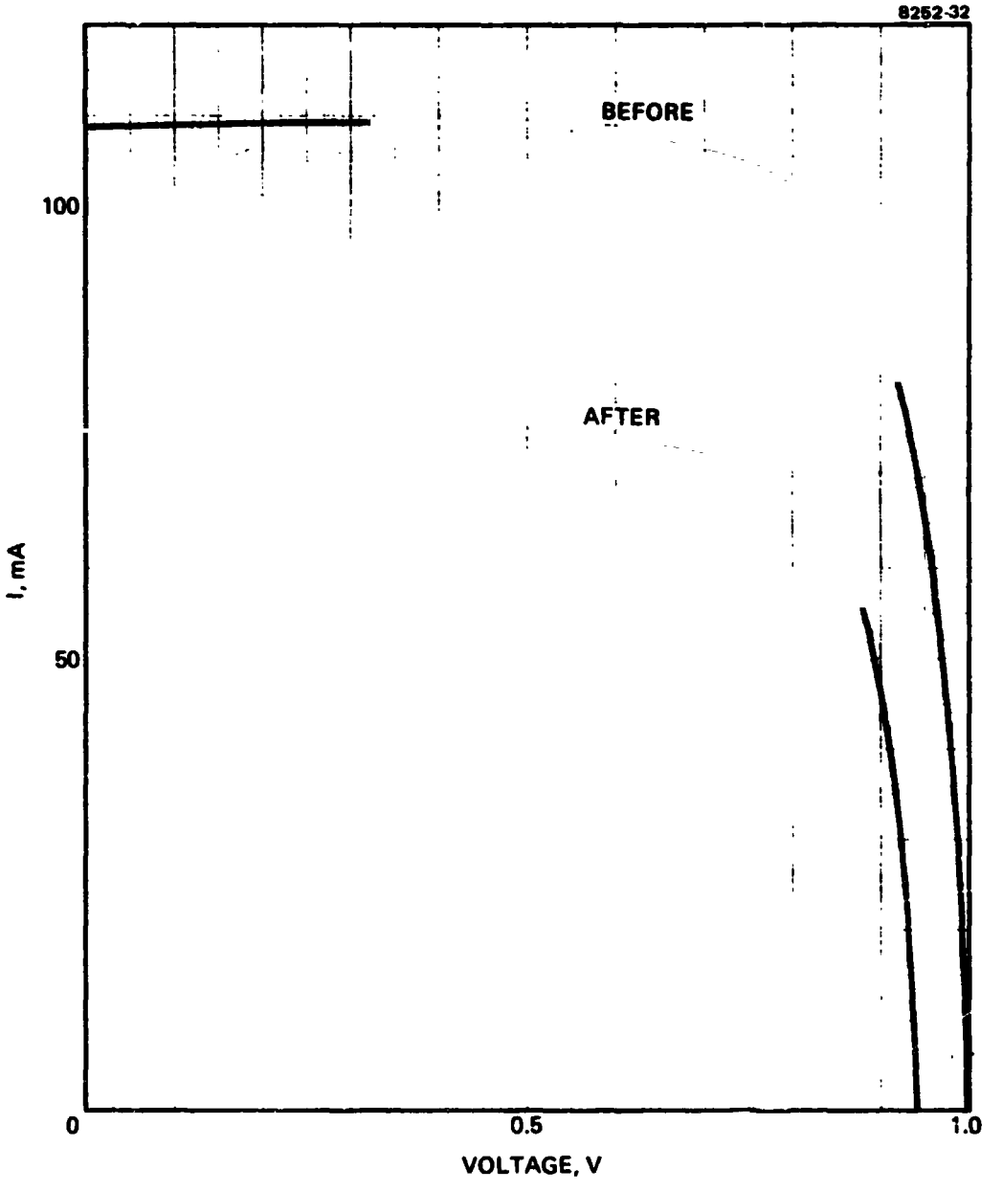

Figure B-8. Photo I-V characteristics before and after proton irradiation; proton energy = 50 keV; 1 x 10^{12} P/cm^2 (cell 2428).

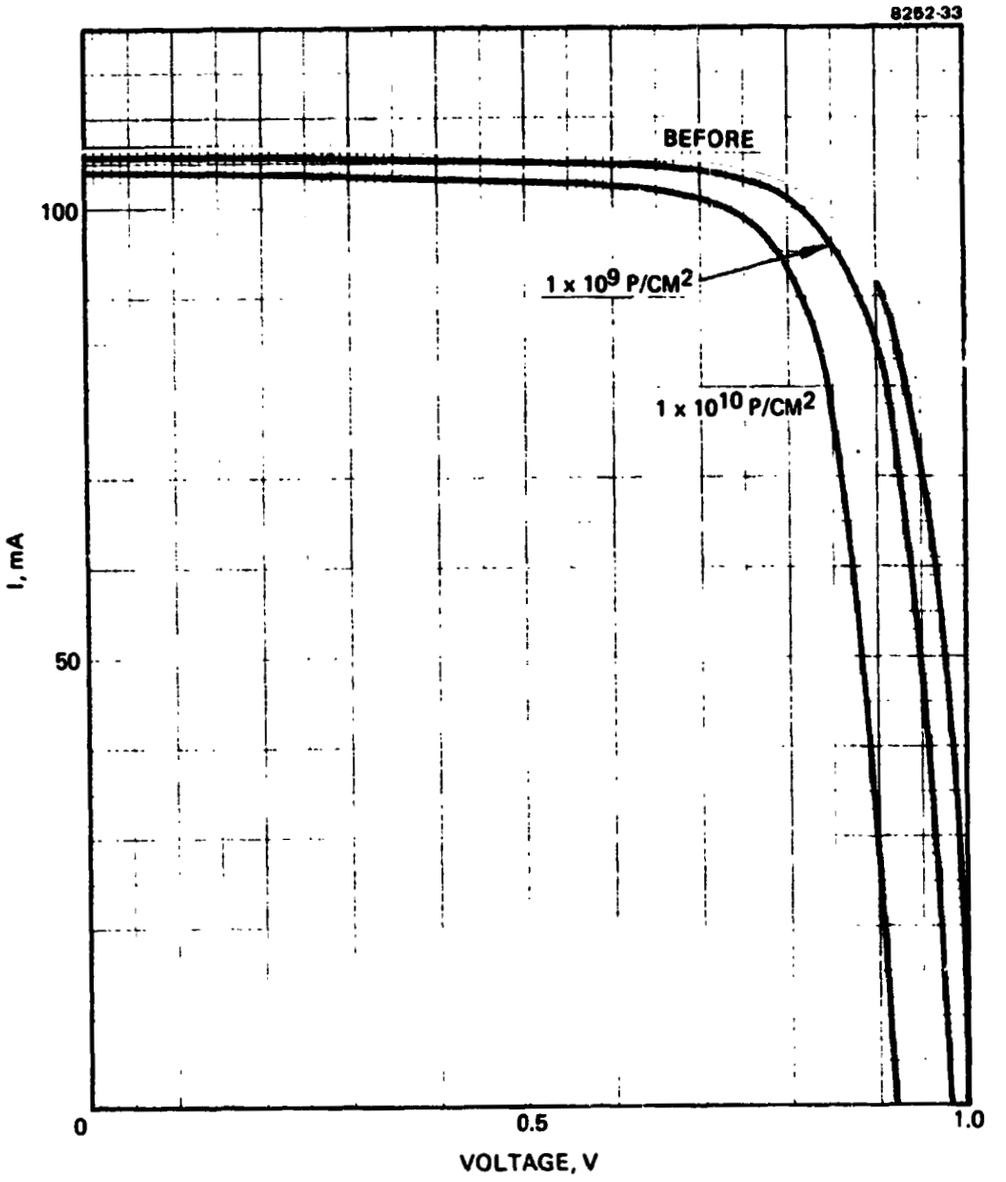

Figure B-9. Photo I-V characteristics before and after proton irradiation; proton energy = 100 keV (cell 2302).

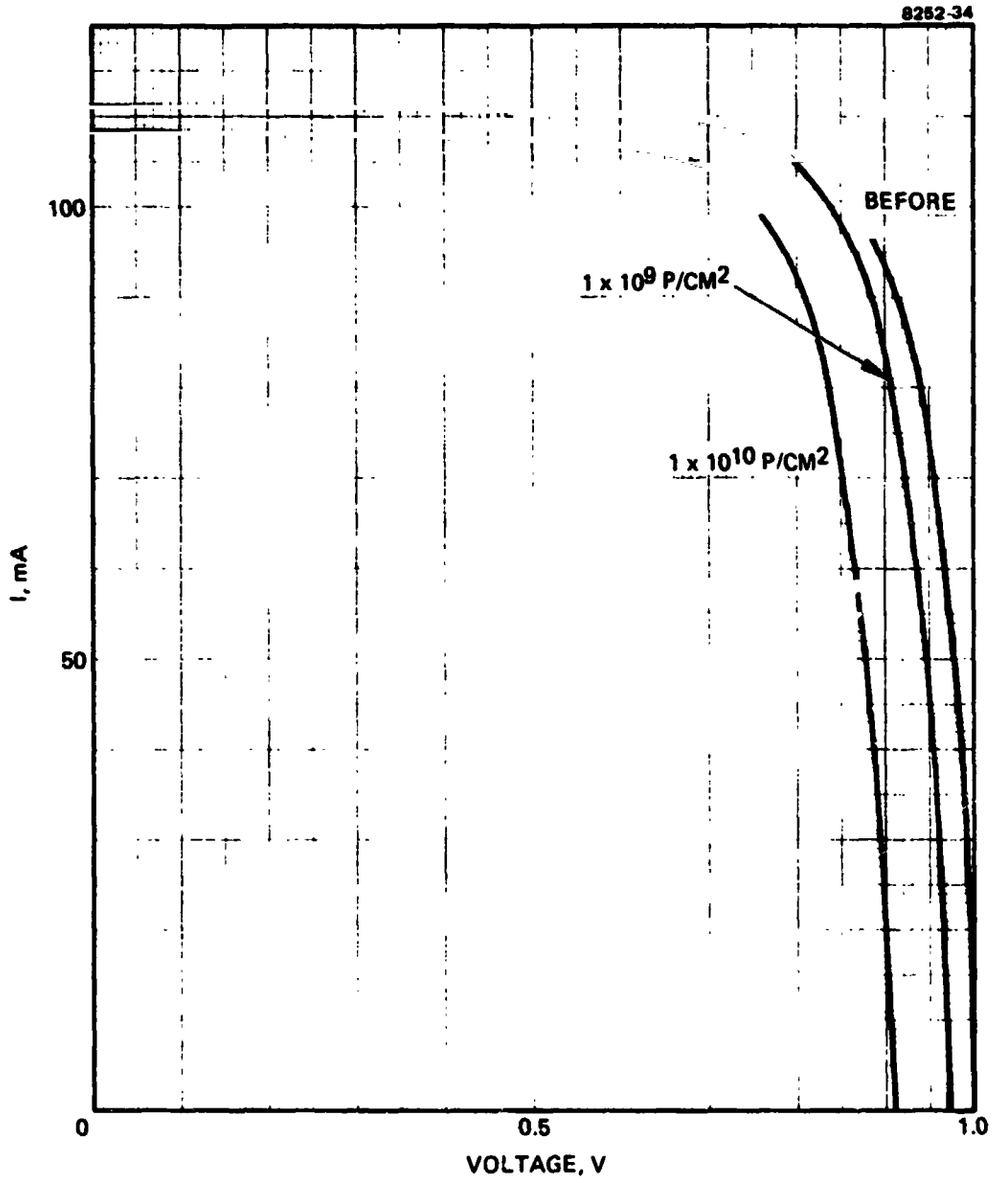

Figure B-10. Photo I-V characteristics before and after proton irradiation; proton energy = 100 keV (cell 2307).

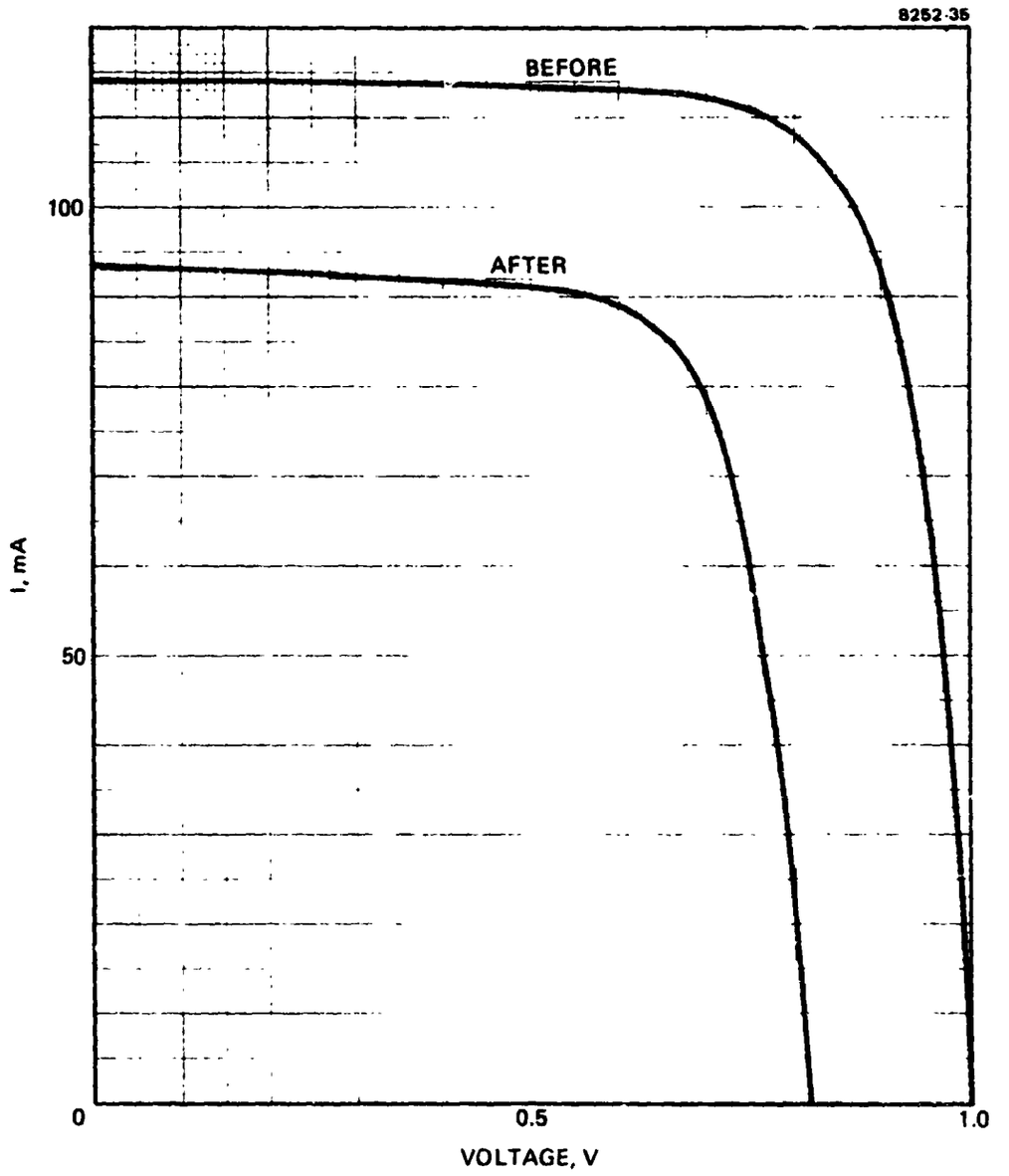

Figure B-11. Photo I-V characteristics before and after proton irradiation; proton energy = 100 keV; 1 x 10^{11} P/cm^2 (cell 2417).

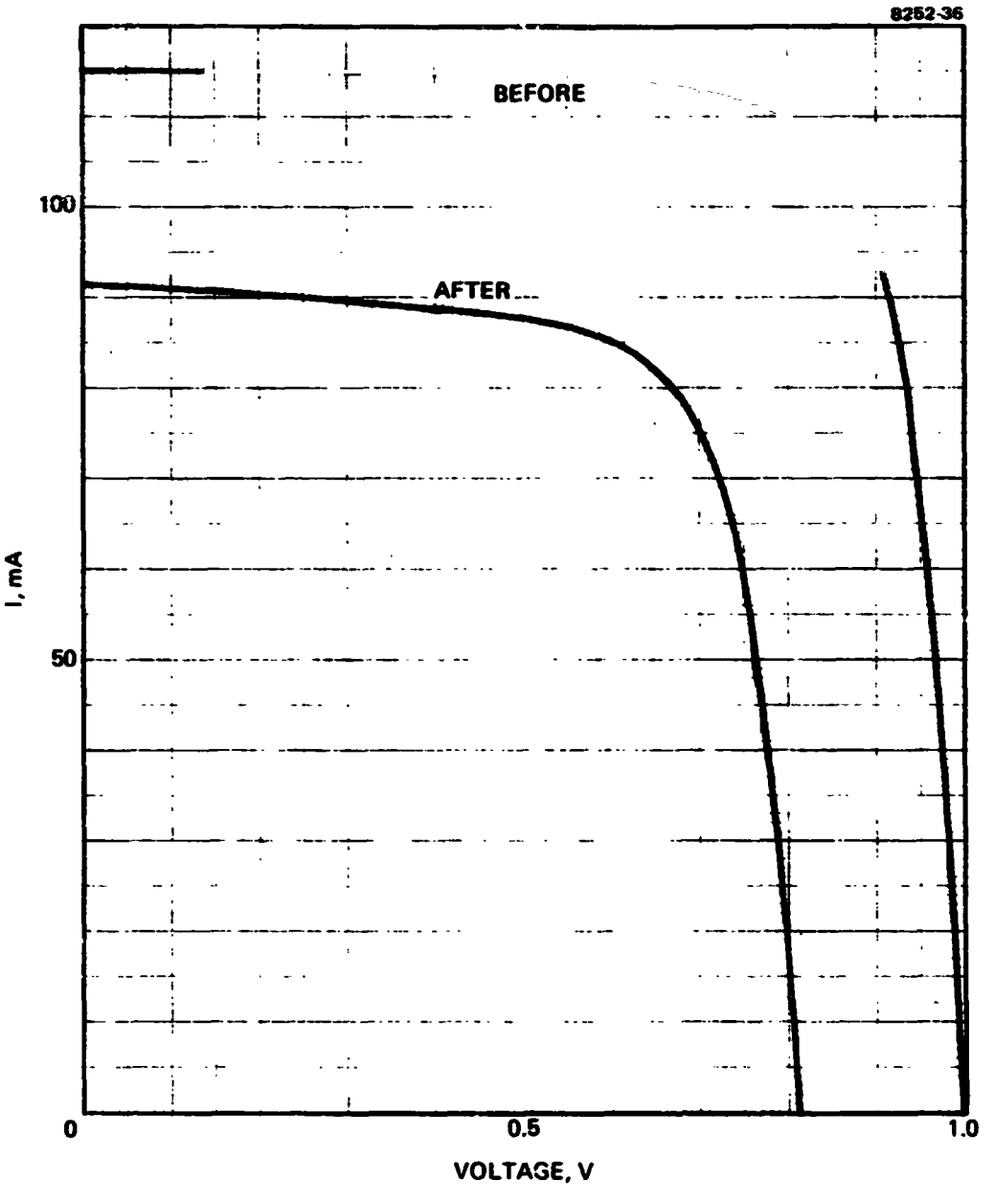

Figure B-12. Photo I-V characteristics before and after proton irradiation; proton energy = 100 keV; 1 x 10^{11} P/cm^2 (cell 2419).

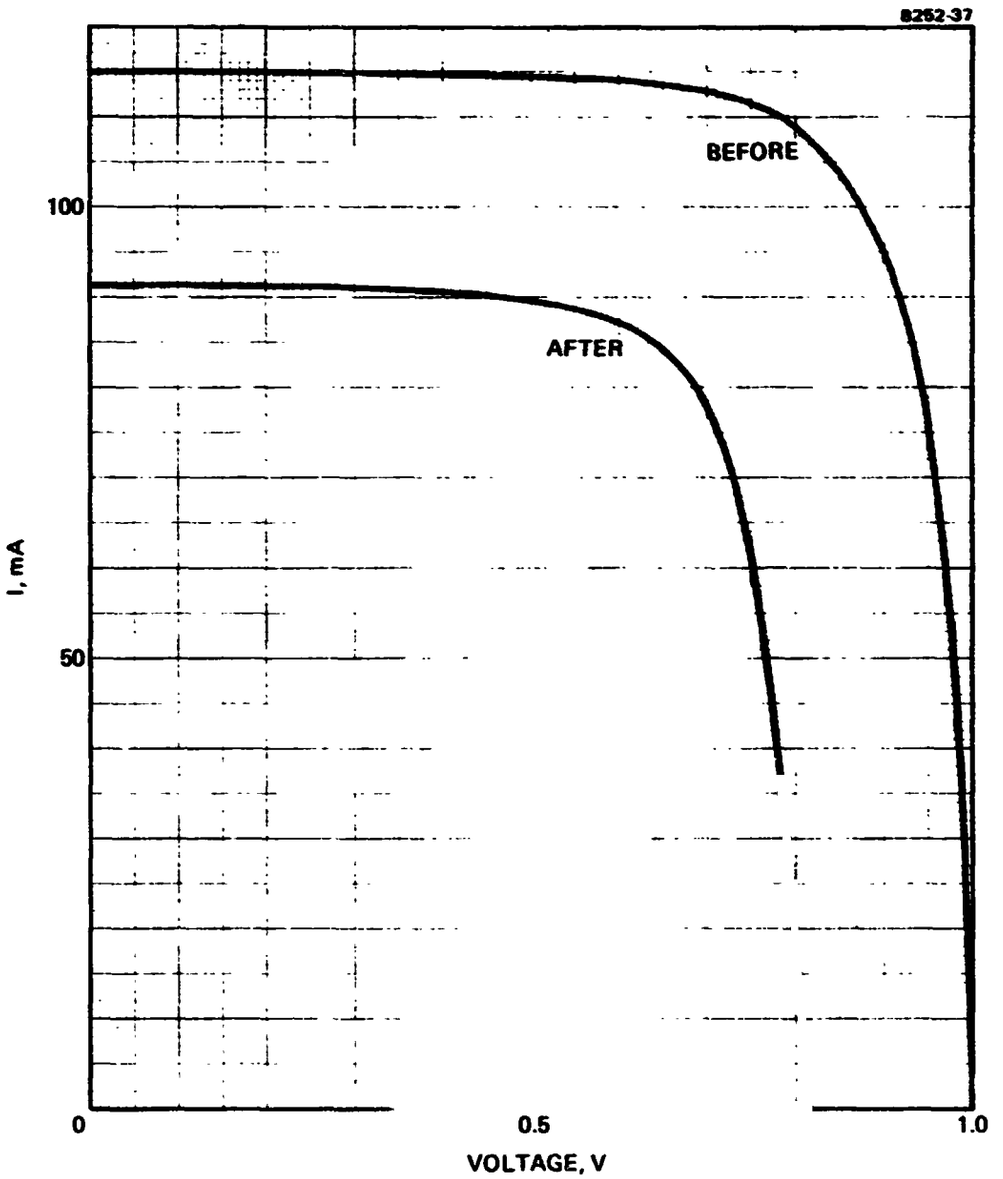

Figure B-13. Photo I-V characteristics before and after proton irradiation; proton energy = 100 keV; 1 x 10^{11} P/cm^2 (cell 2420).

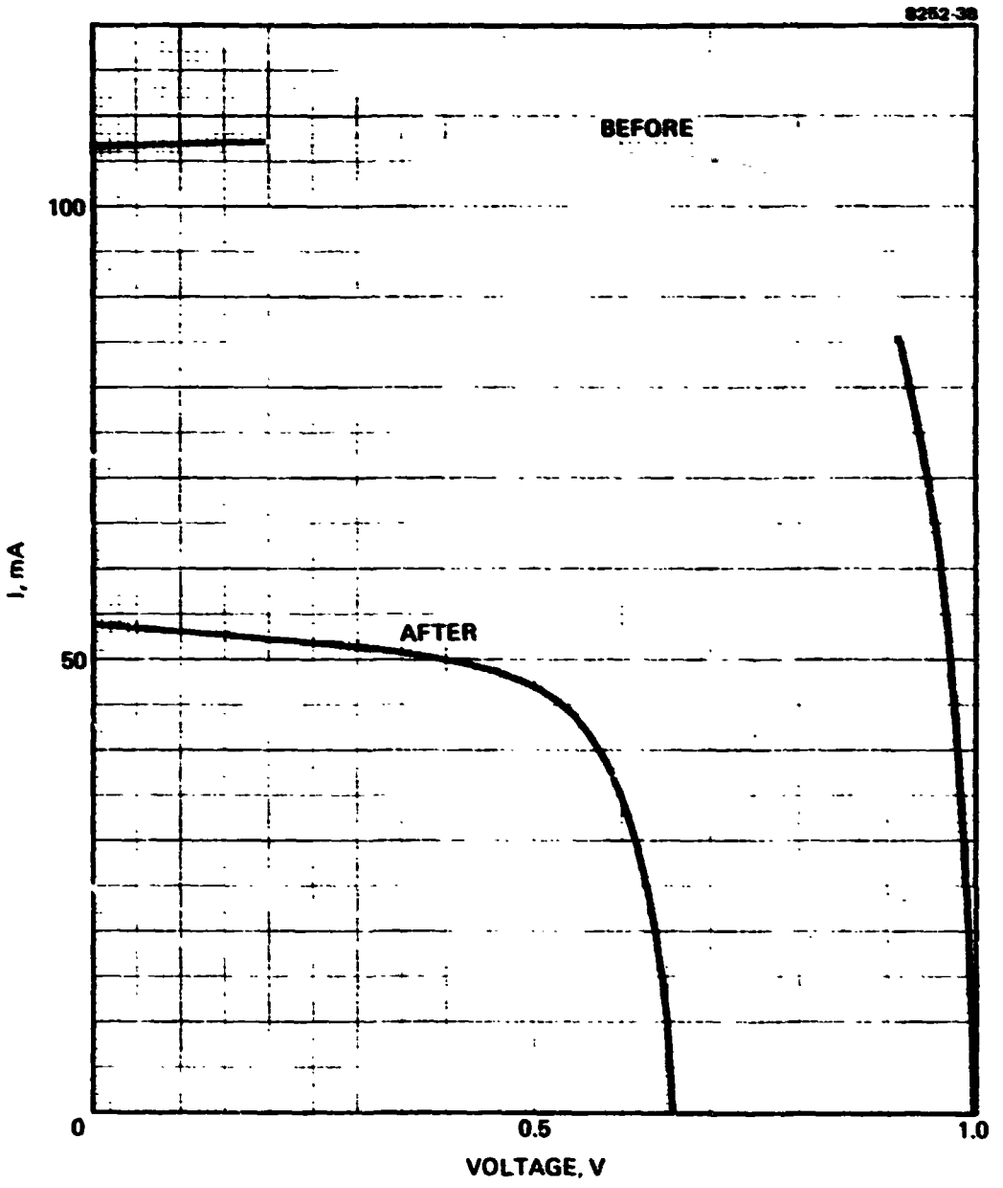

Figure B-14. Photo I-V characteristics before and after proton irradiation; proton energy = 100 keV; 1 x 10^{12} P/cm^2 (cell 2429).

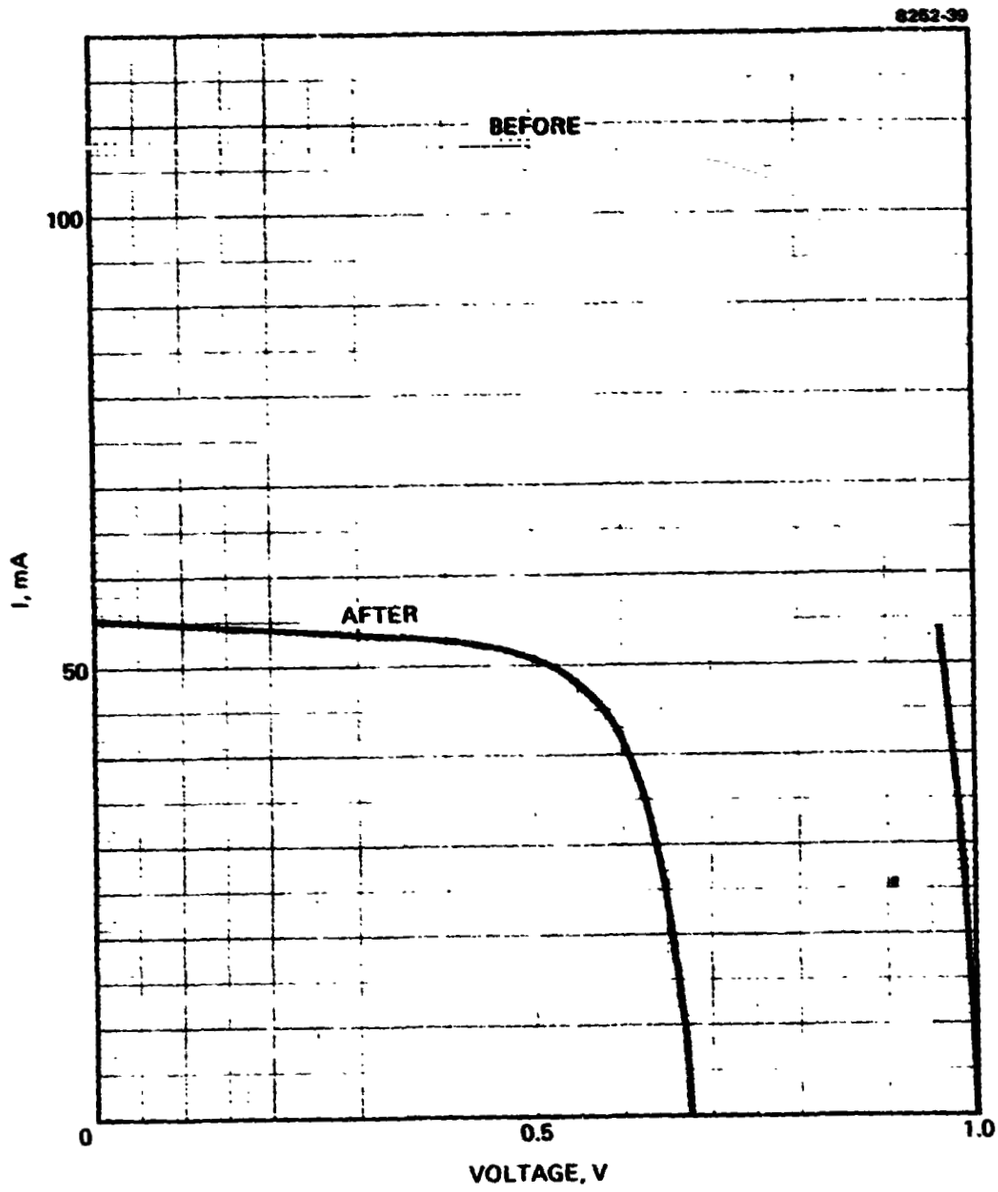

Figure B-15. Photo I-V characteristics before and after proton irradiation; proton energy = 100 keV; 1 x 10^{12} P/cm^2 (cell 2432).

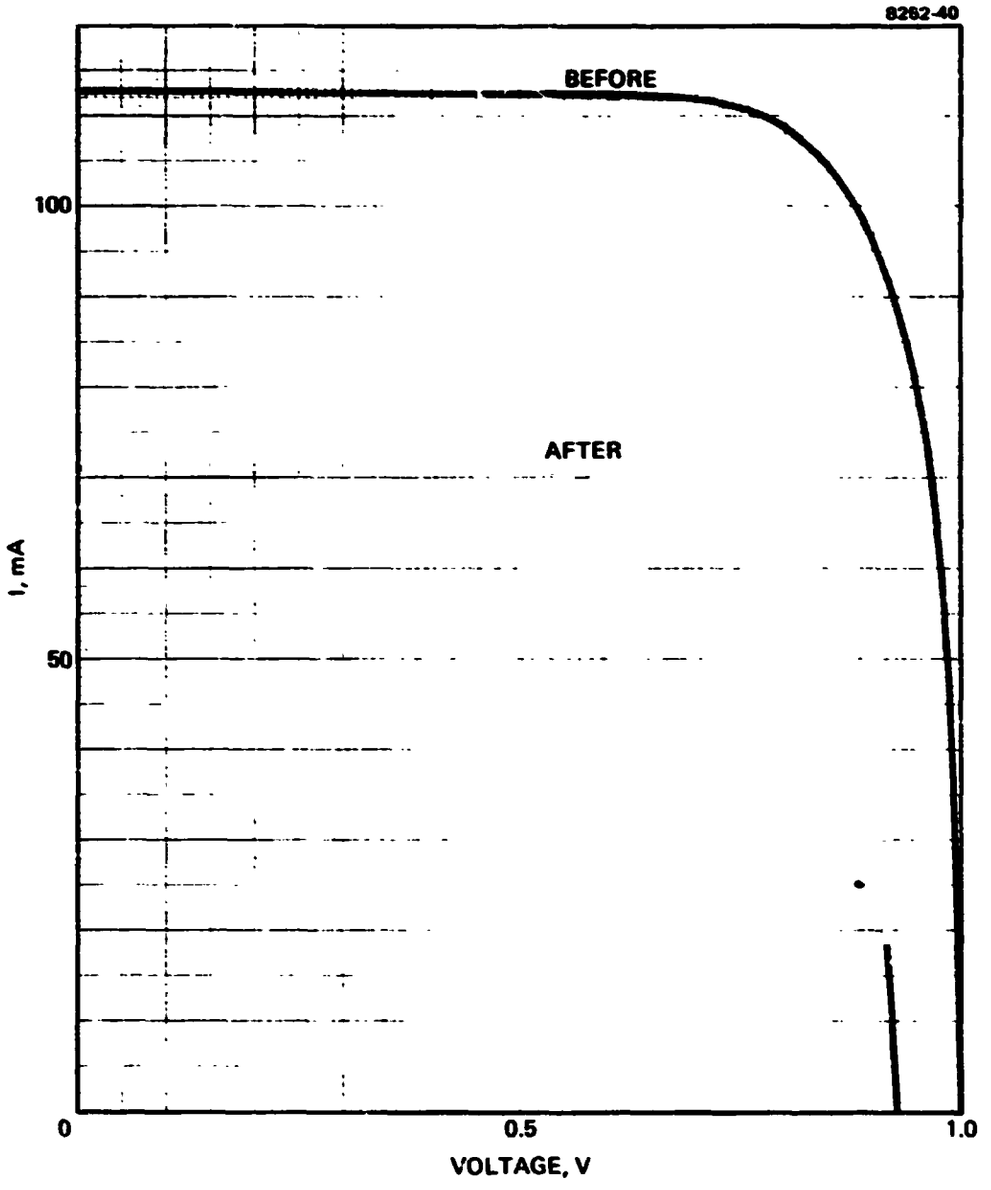

Figure B-16. Photo I-V characteristics before and after proton irradiation; proton energy = 100 keV; 1 x 10^{12} P/cm^2 (cell 2456).

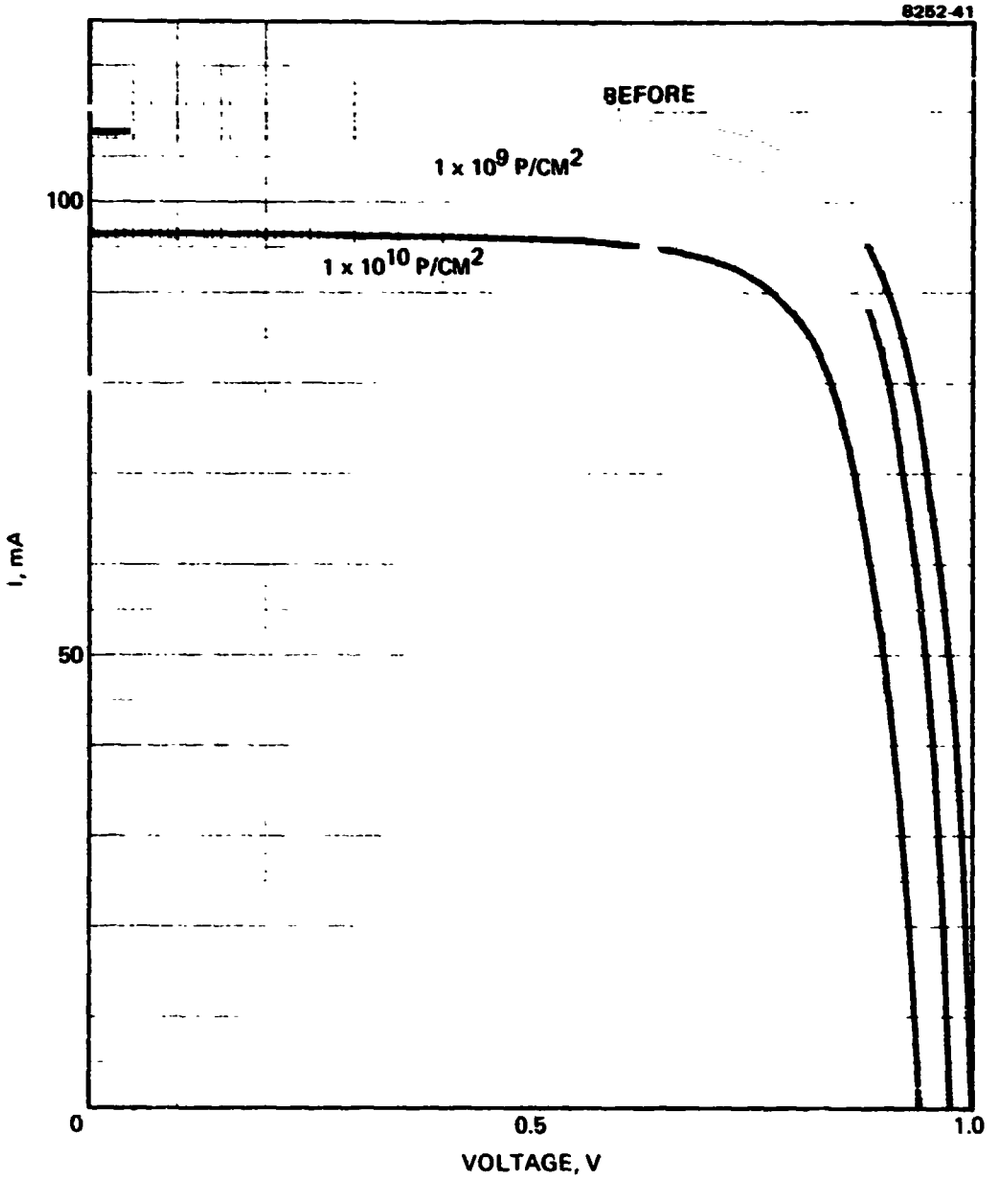

Figure B-17. Photo I-V characteristics before and after proton irradiation; proton energy = 290 keV (cell 2370).

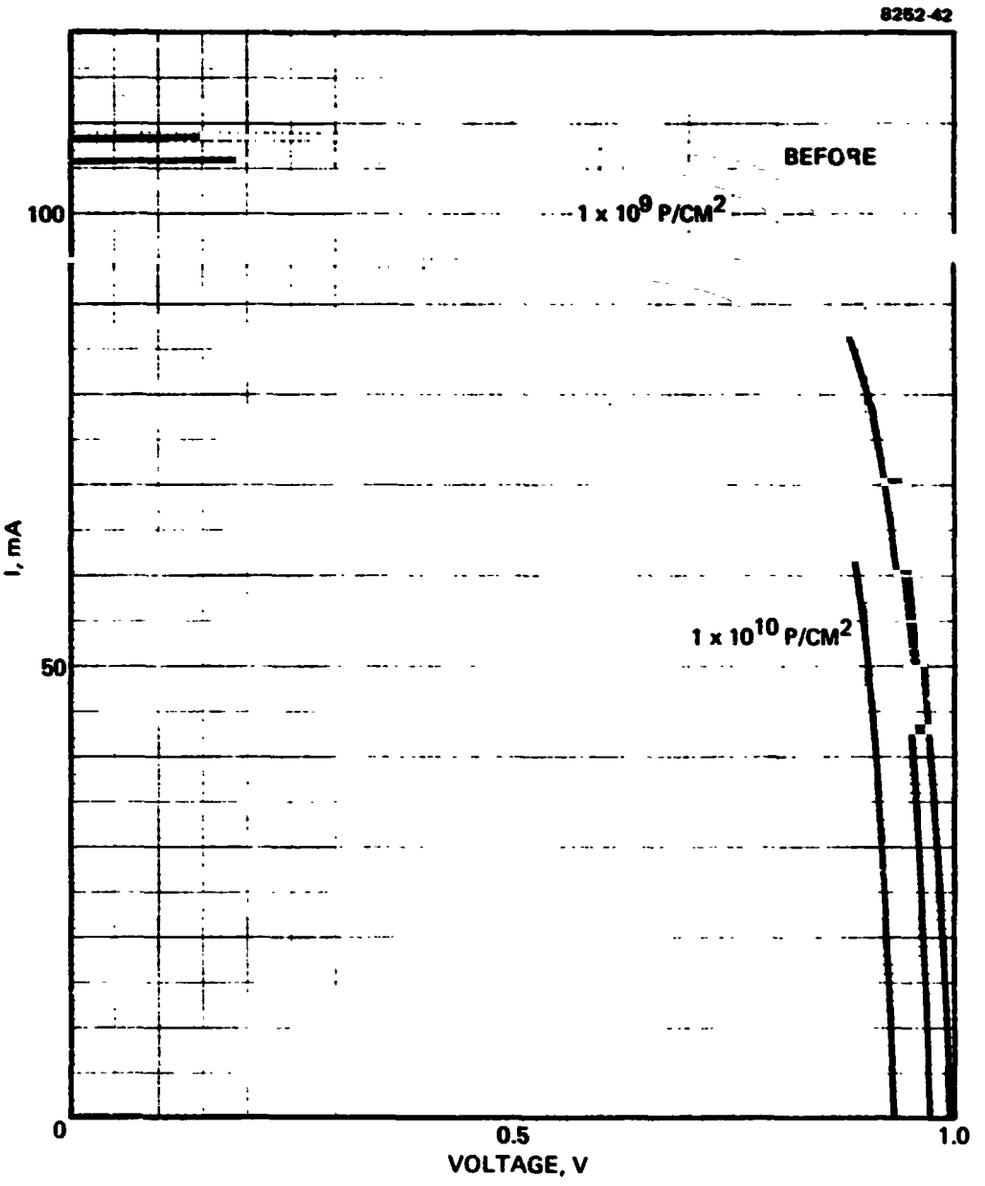

Figure B-18. Photo I-V characteristics before and after proton irradiation; proton energy = 290 keV (cell 2375).

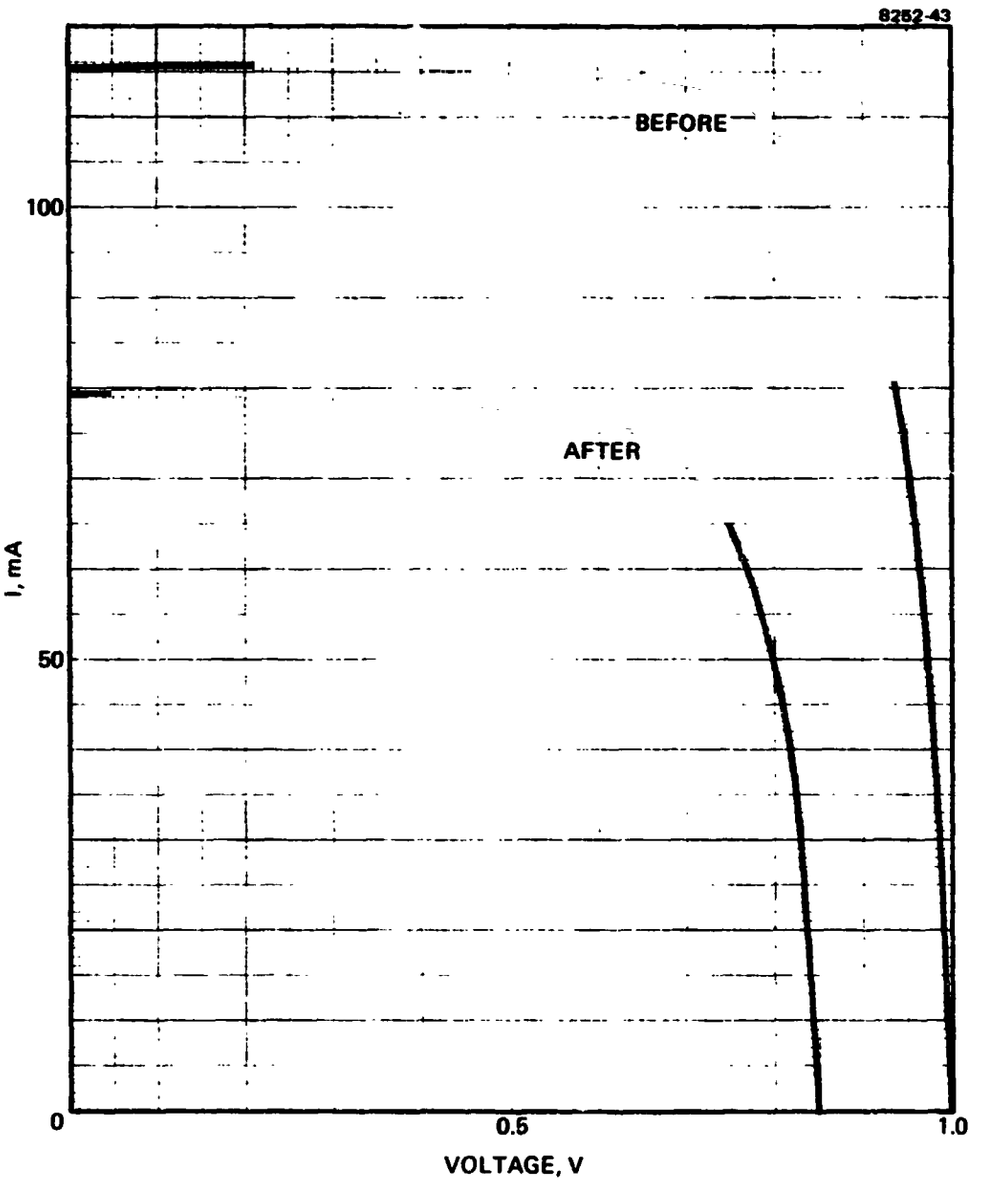

Figure B-19. Photo I-V characteristics before and after proton irradiation; proton energy = 290 keV; 1 x 10^{11} P/cm^2 (cell 2421).

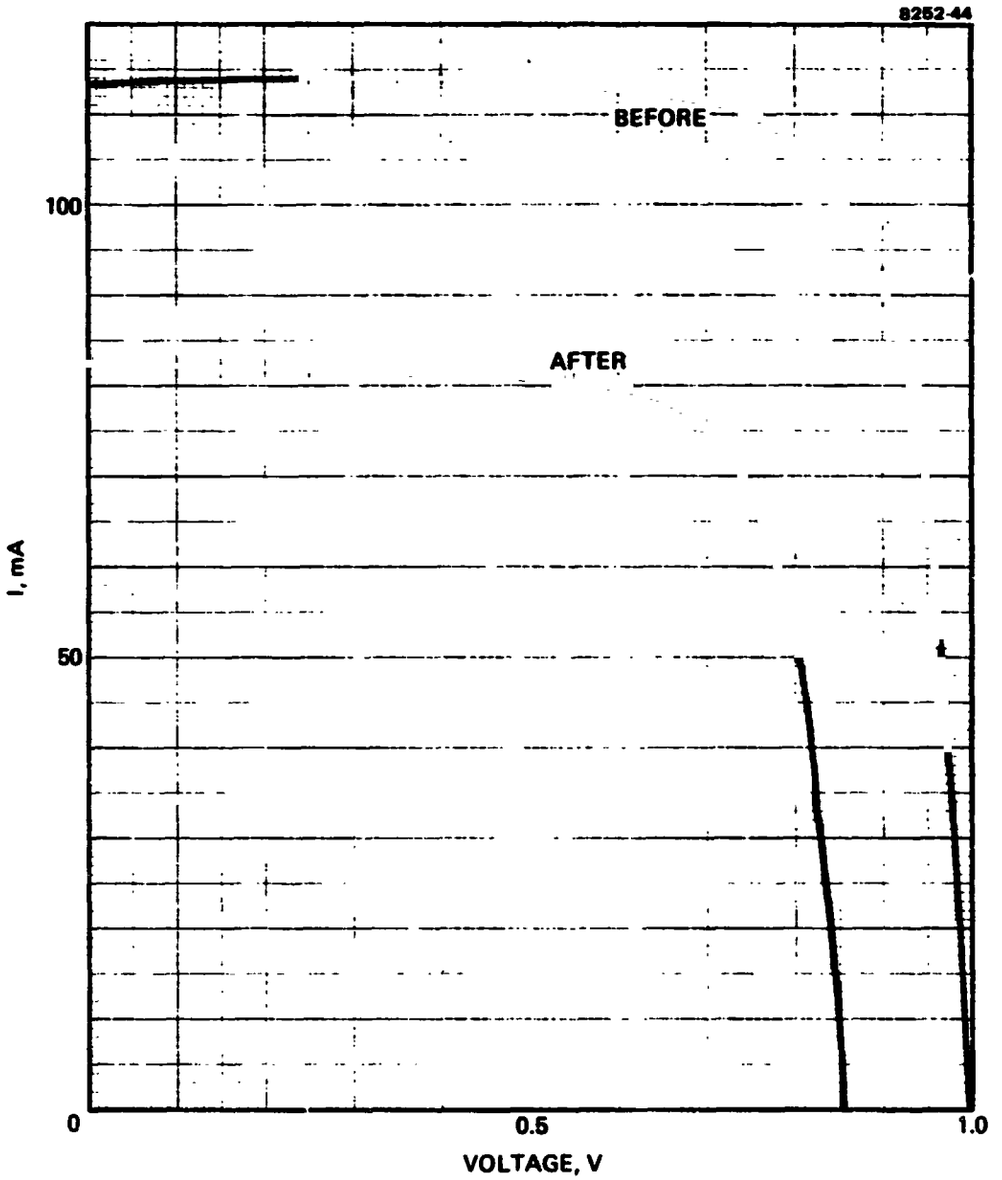

Figure B-20. Photo I-V characteristics before and after proton irradiation; proton energy = 290 keV; 1 x 10^{11} P/cm^2 (cell 2422).

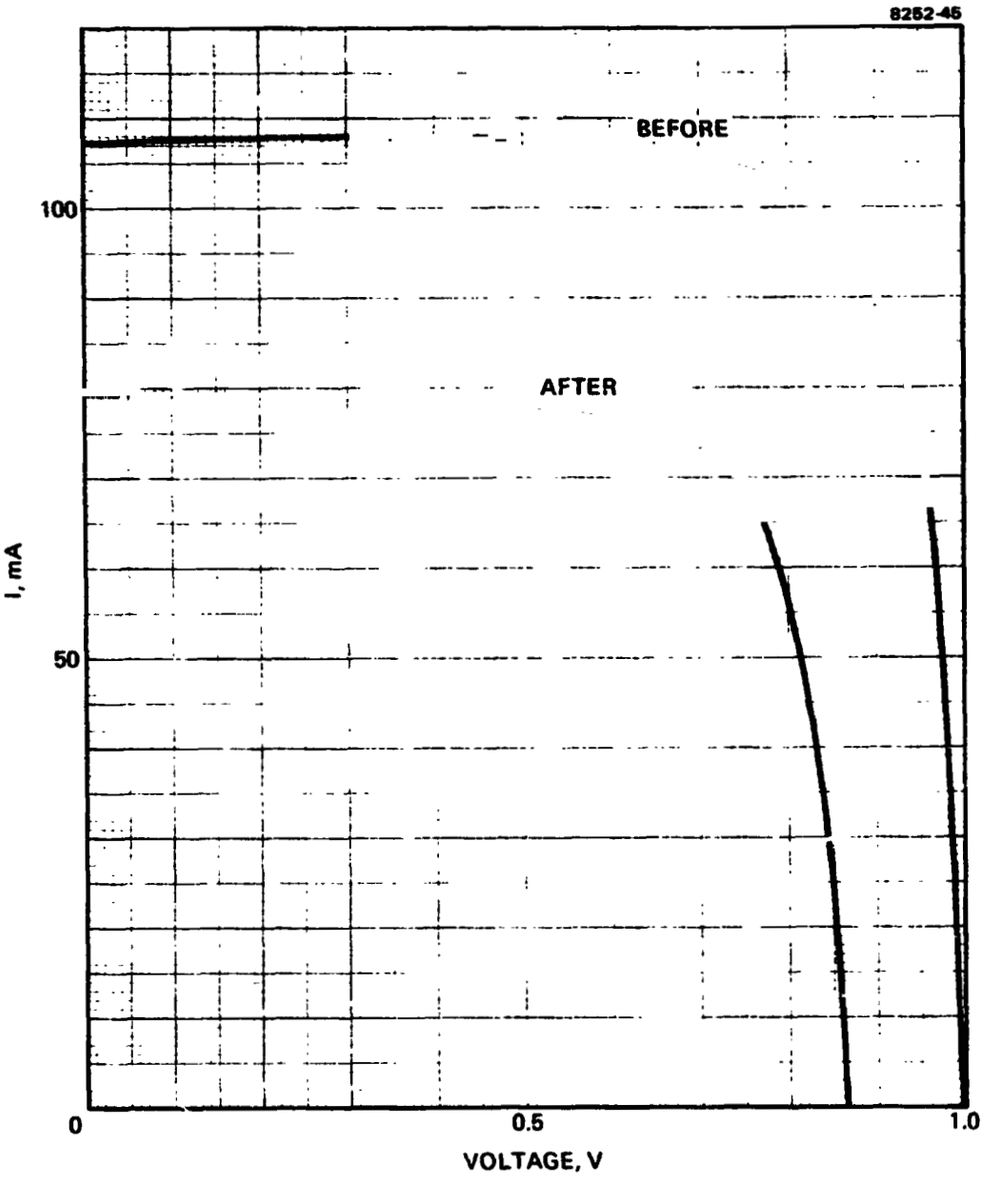

Figure B-21. Photo I-V characteristics before and after proton irradiation; proton energy = 290 keV; 1 x 10^{11} P/cm^2 (cell 2424).

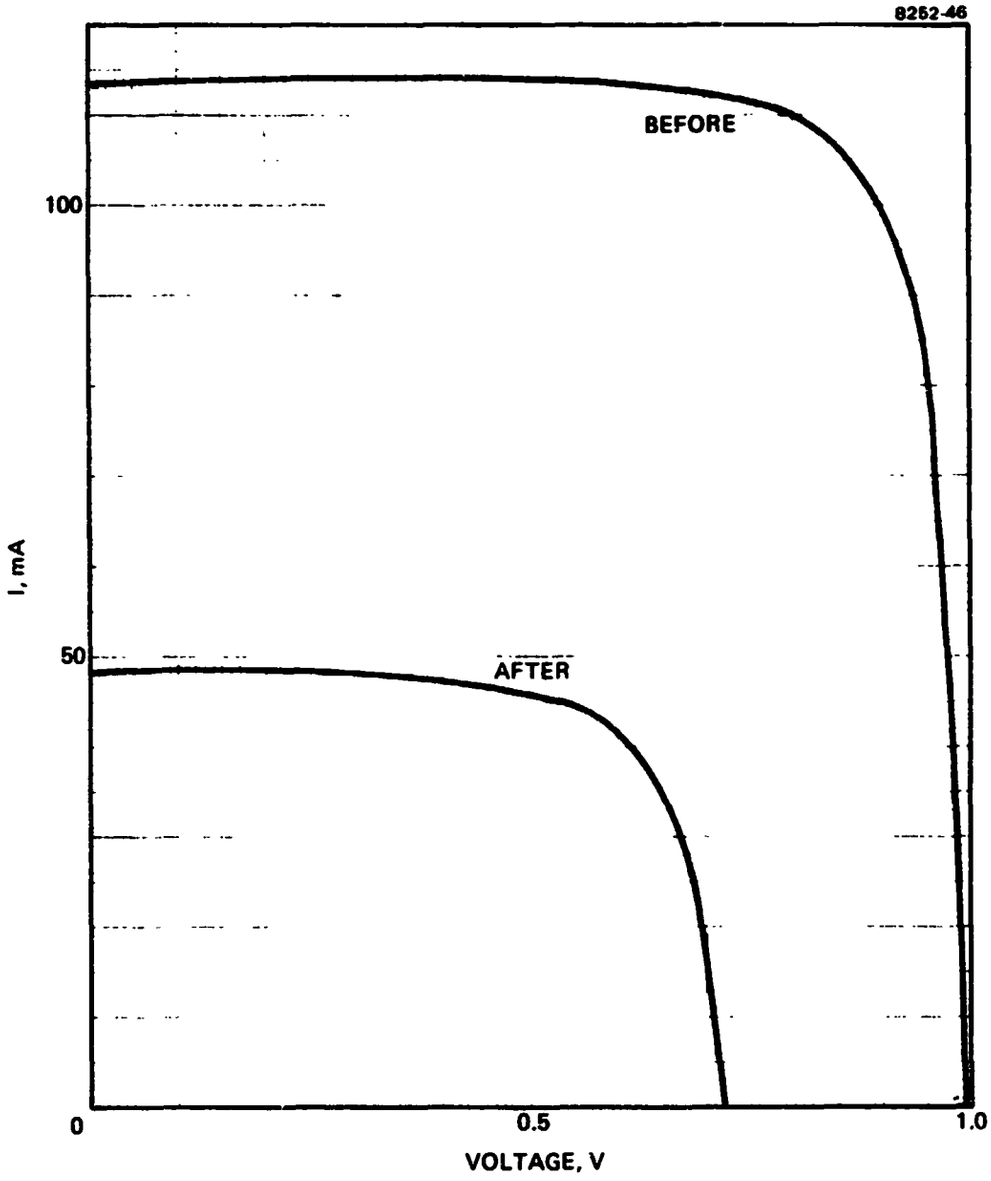

Figure B-22. Photo I-V characteristics before and after proton irradiation; proton energy = 290 keV; 1 x 10^{12} P/cm^2 (cell 2457).

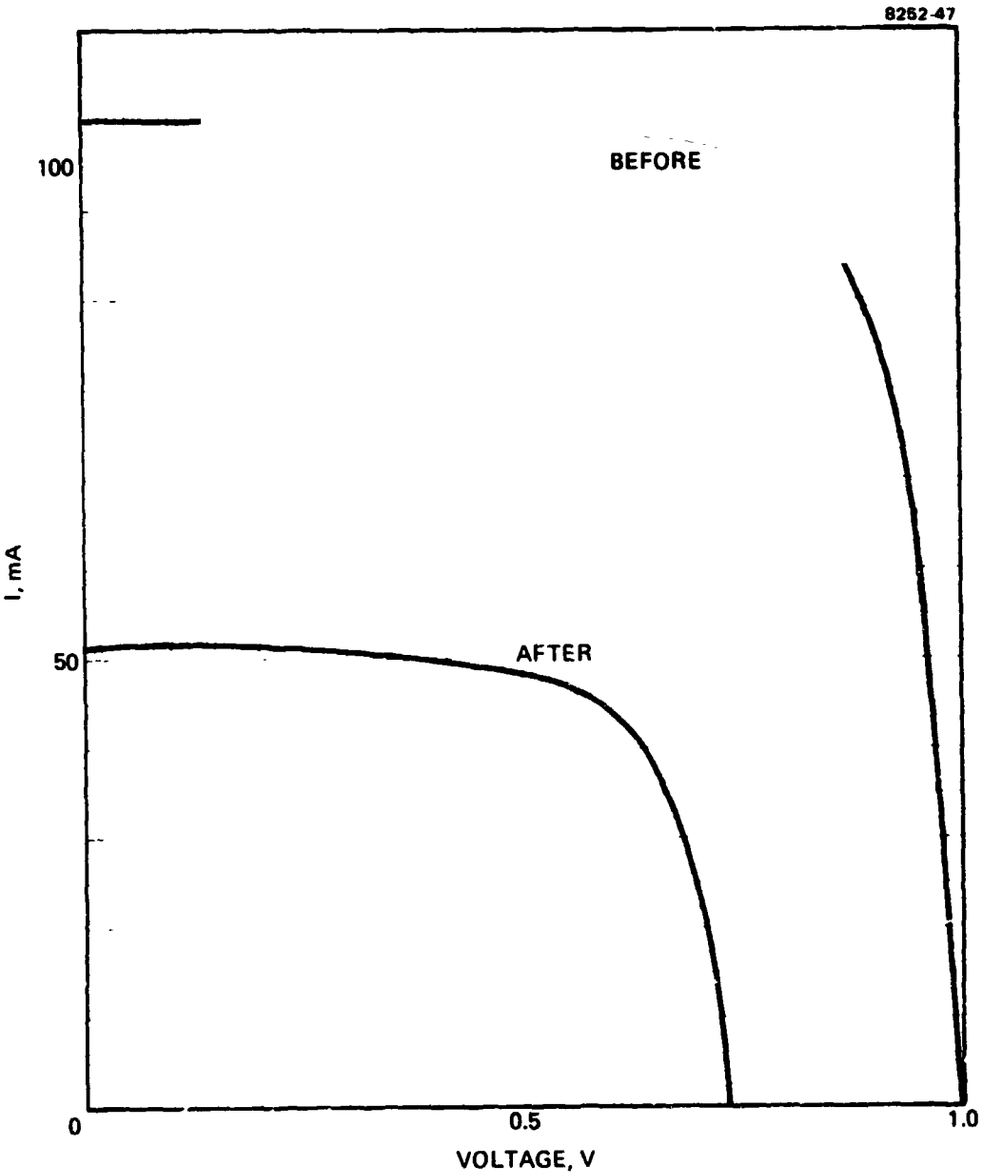

Figure B-23. Photo I-V characteristics before and after proton irradiation; proton energy = 290 keV; 1 x 10^{12} P/cm^2 (cell 2477).

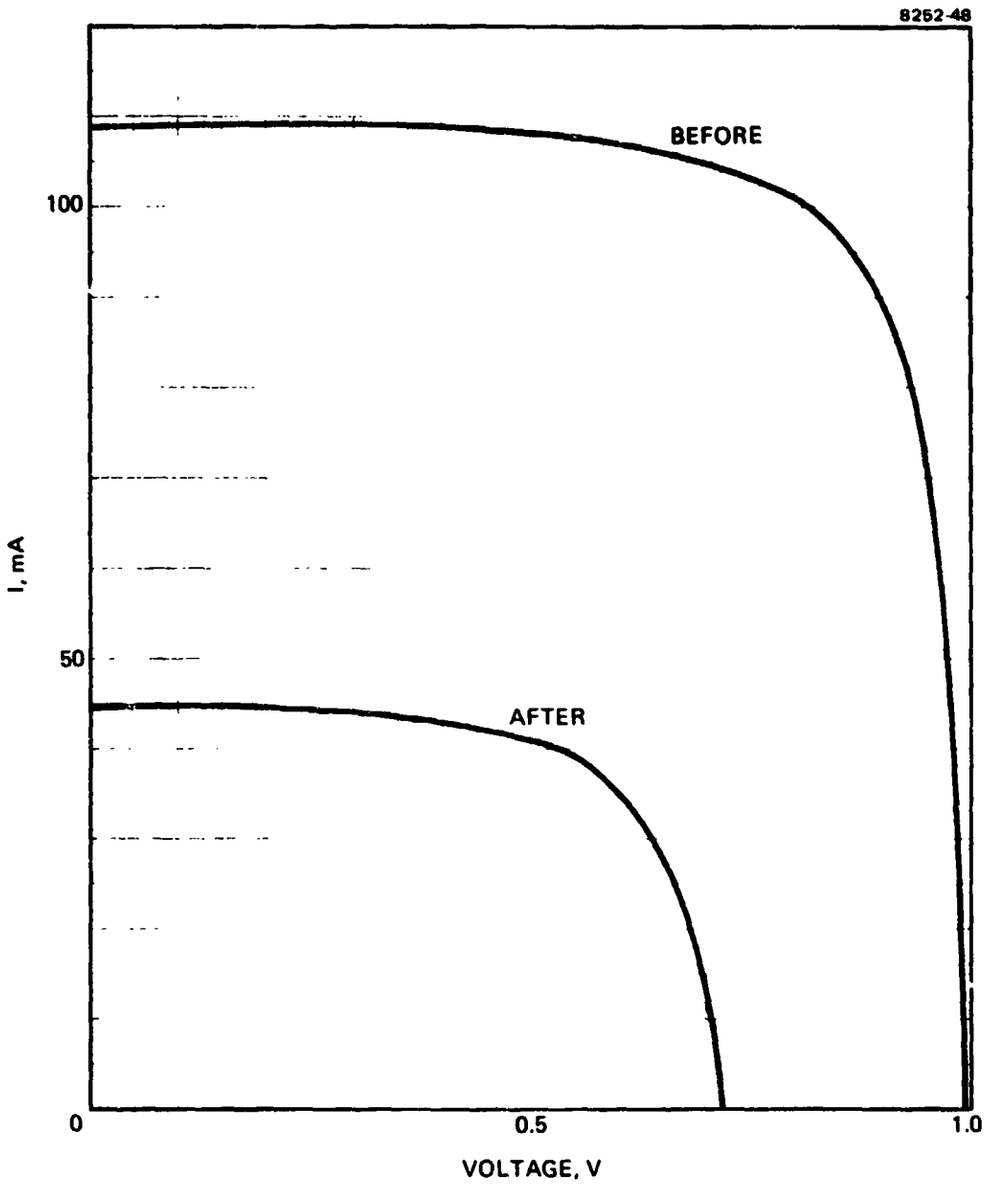

Figure B-24. Photo I-V characteristics before and after proton irradiation; proton energy = 290 keV; 1 x 10^{12} P/cm^2 (cell 2311).

APPENDIX C

PHOTO I-V CHARACTERISTICS OF HIGH EFFICIENCY SILICON SOLAR CELL BEFORE AND AFTER PROTON IRRADIATION

[illegible] PAGE BLANK NOT FILMED

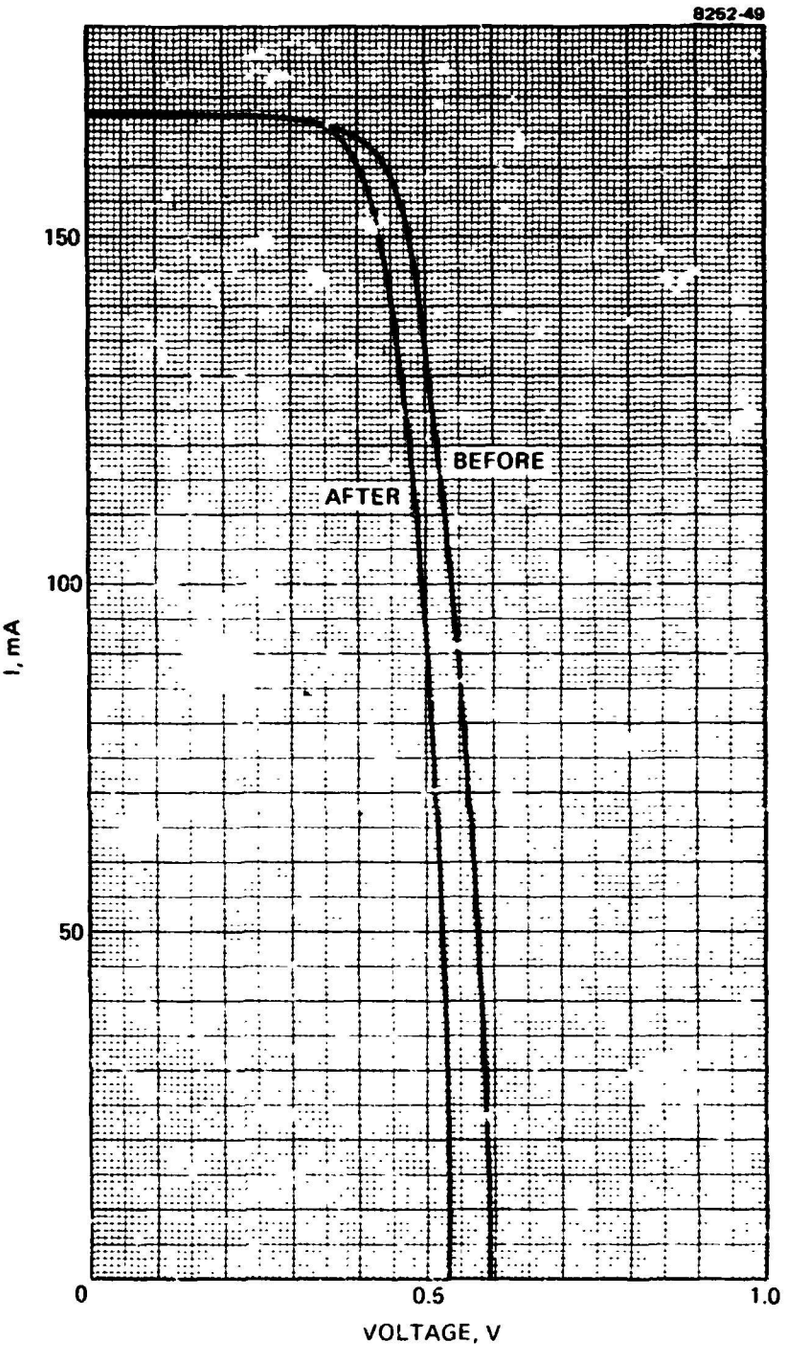

Figure C-1. Photo I-V characteristics of Si solar cell before and after proton irradiation; proton energy = 50 k.V; 1 x 10^{11} P/cm^2 (cell 3).

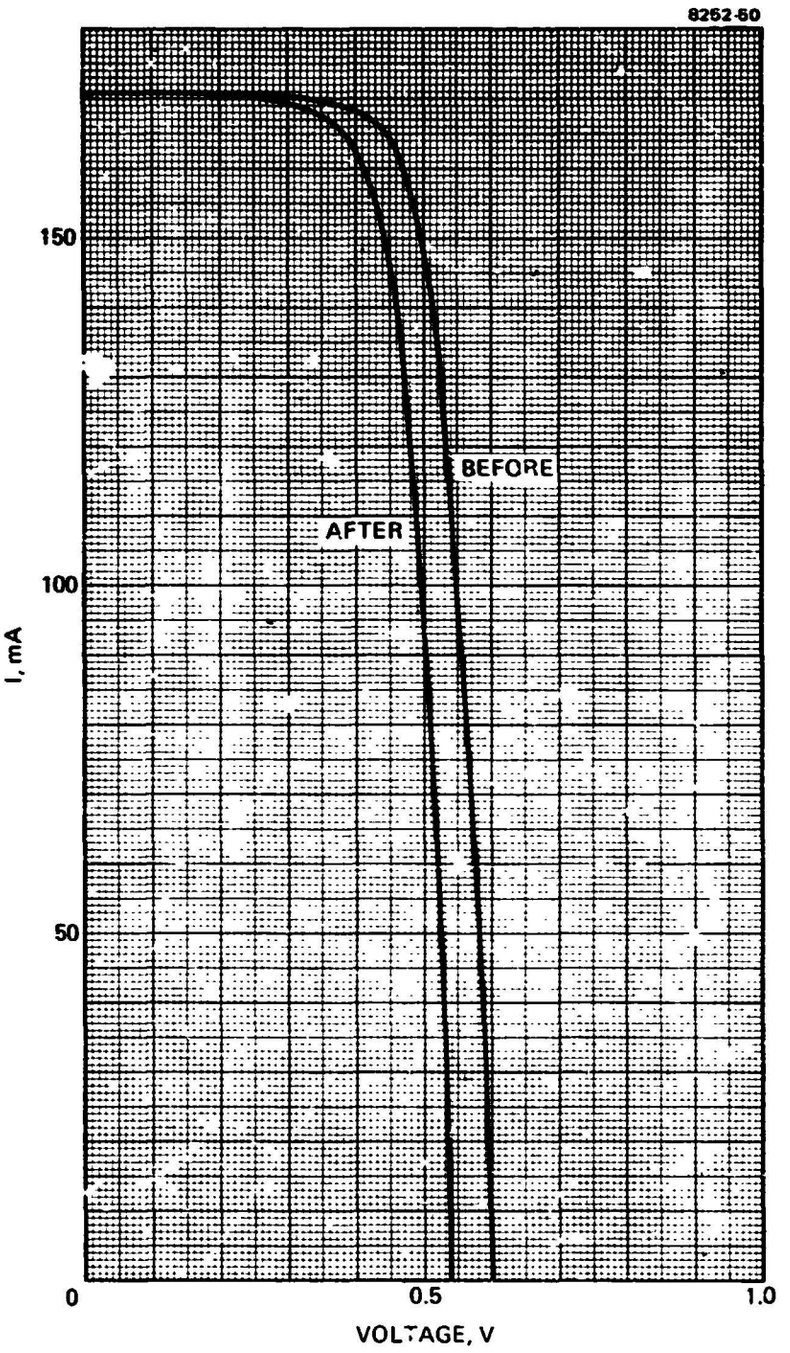

Figure C-2. Photo I-V characteristics of Si solar cell before and after proton irradiation; proton energy = 50 keV; 1 x 10^{11} P/cm^2 (cell 6).

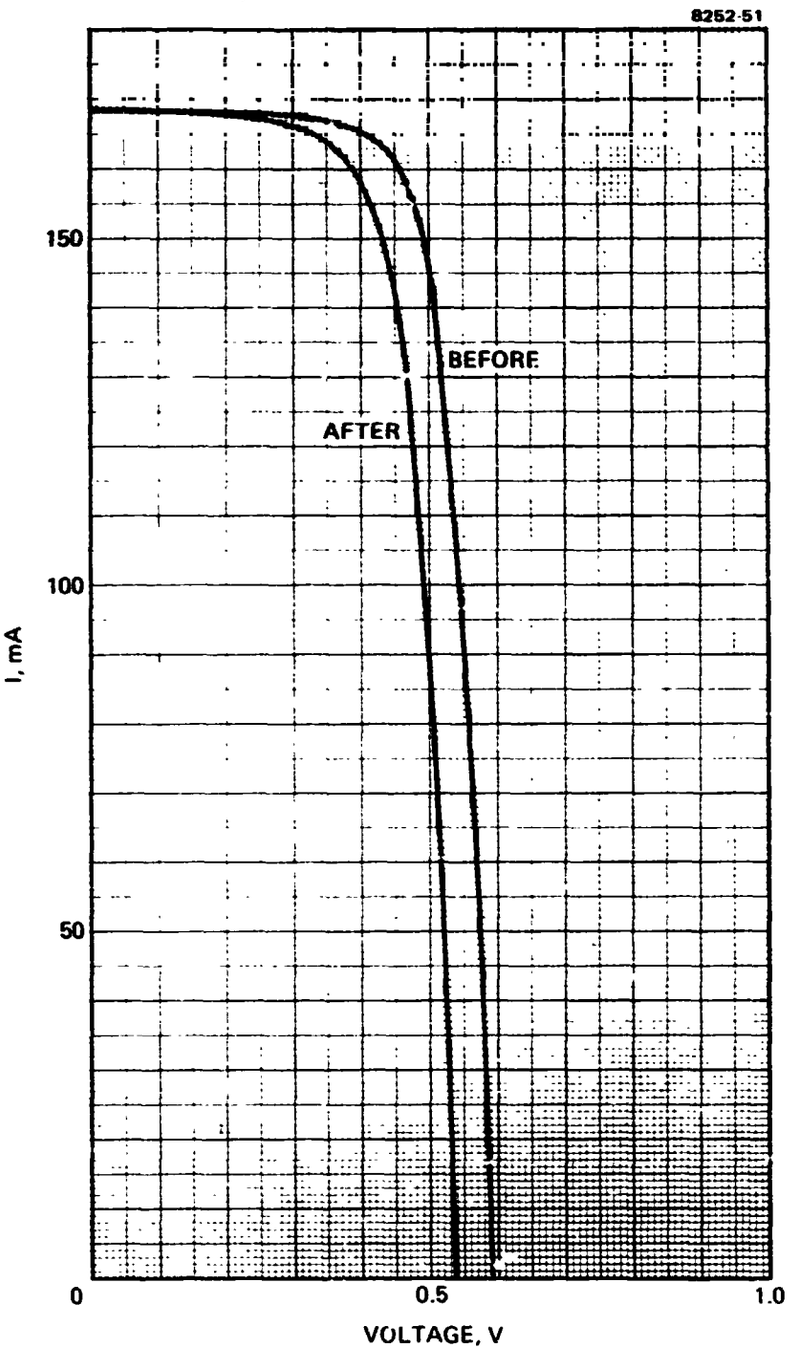

Figure C-3. Photo I-V characteristics of Si solar cell before and after proton irradiation; proton energy = 50 keV; 1 x 10^{11} P/cm^2 (cell 9).

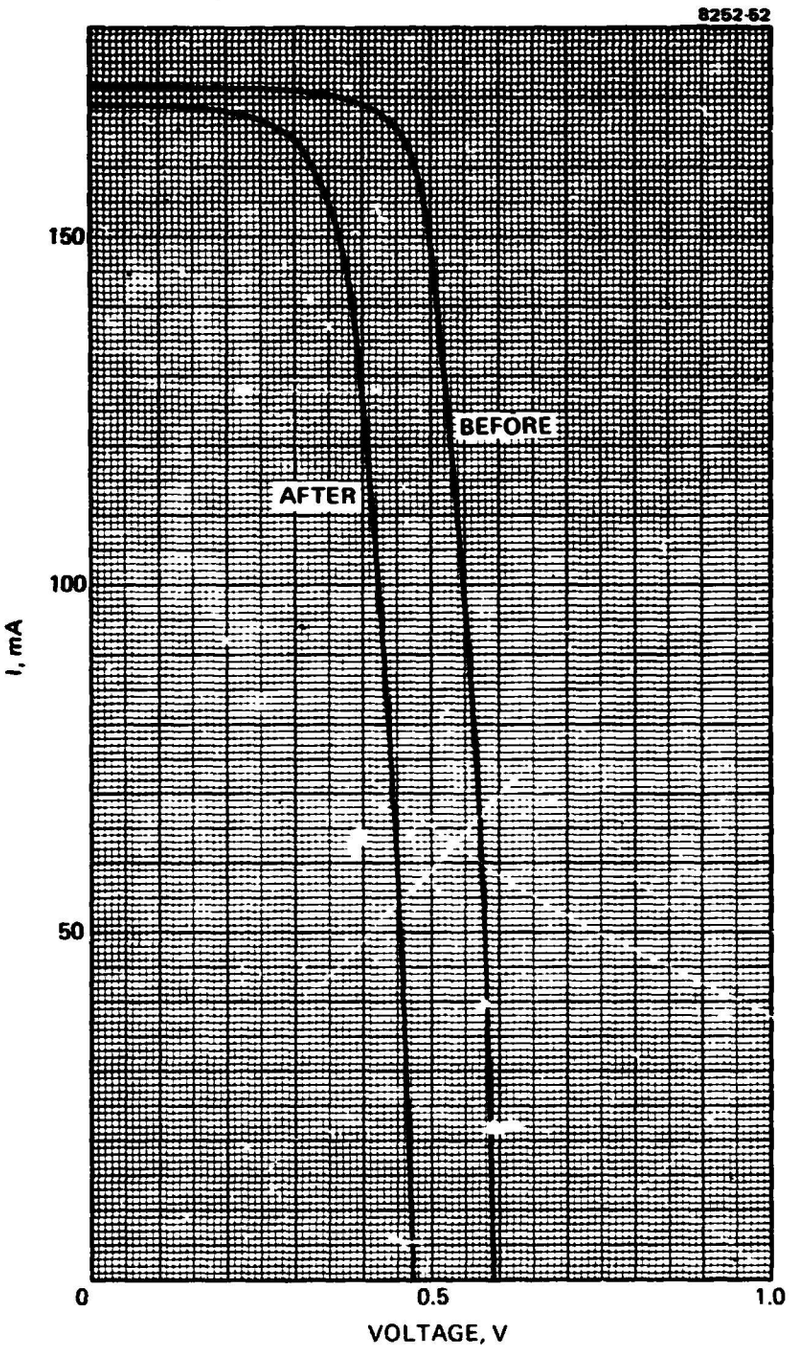

Figure C-4. Photo I-V characteristics of Si solar cell before and after proton irradiation; proton energy = 50 keV; 1 x 10^{12} P/cm^2 (cell 10).

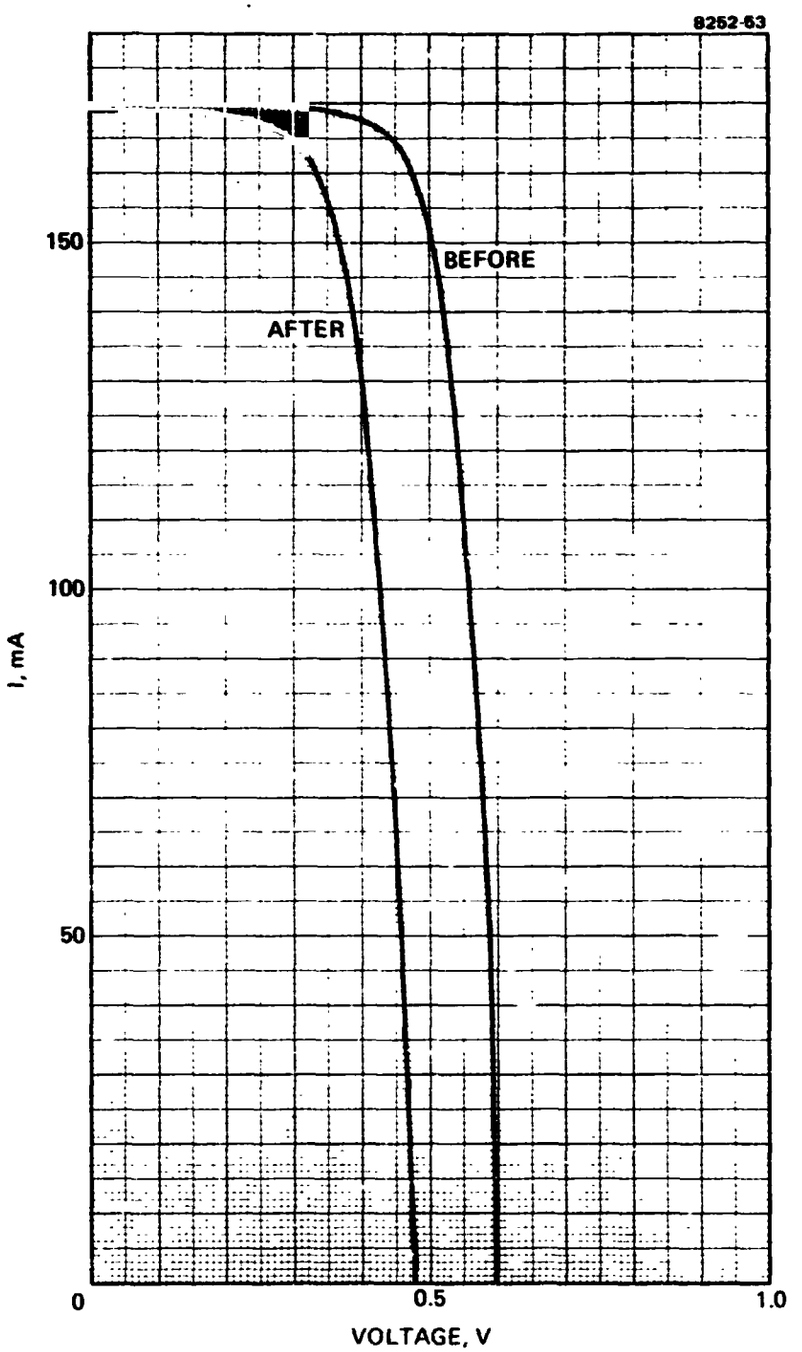

Figure C-5. Photo I-V characteristics of Si solar cell before and after proton irradiation; proton energy = 50 keV; 1 x 10^{12} P/cm^2 (cell 11).

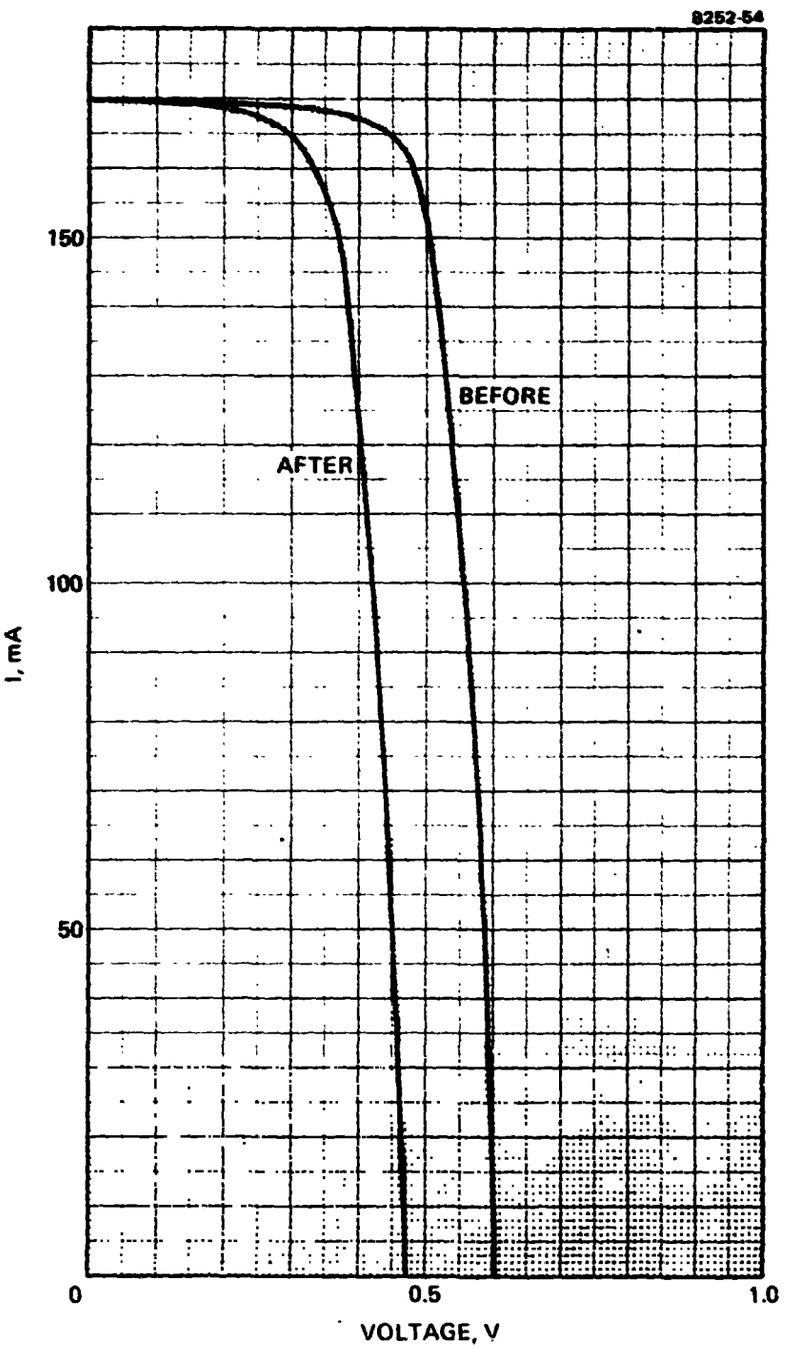

Figure C-6. Photo I-V characteristics of Si solar cell before and after proton irradiation; proton energy = 50 keV; 1 x 10^{12} P/cm^2 (cell 12).

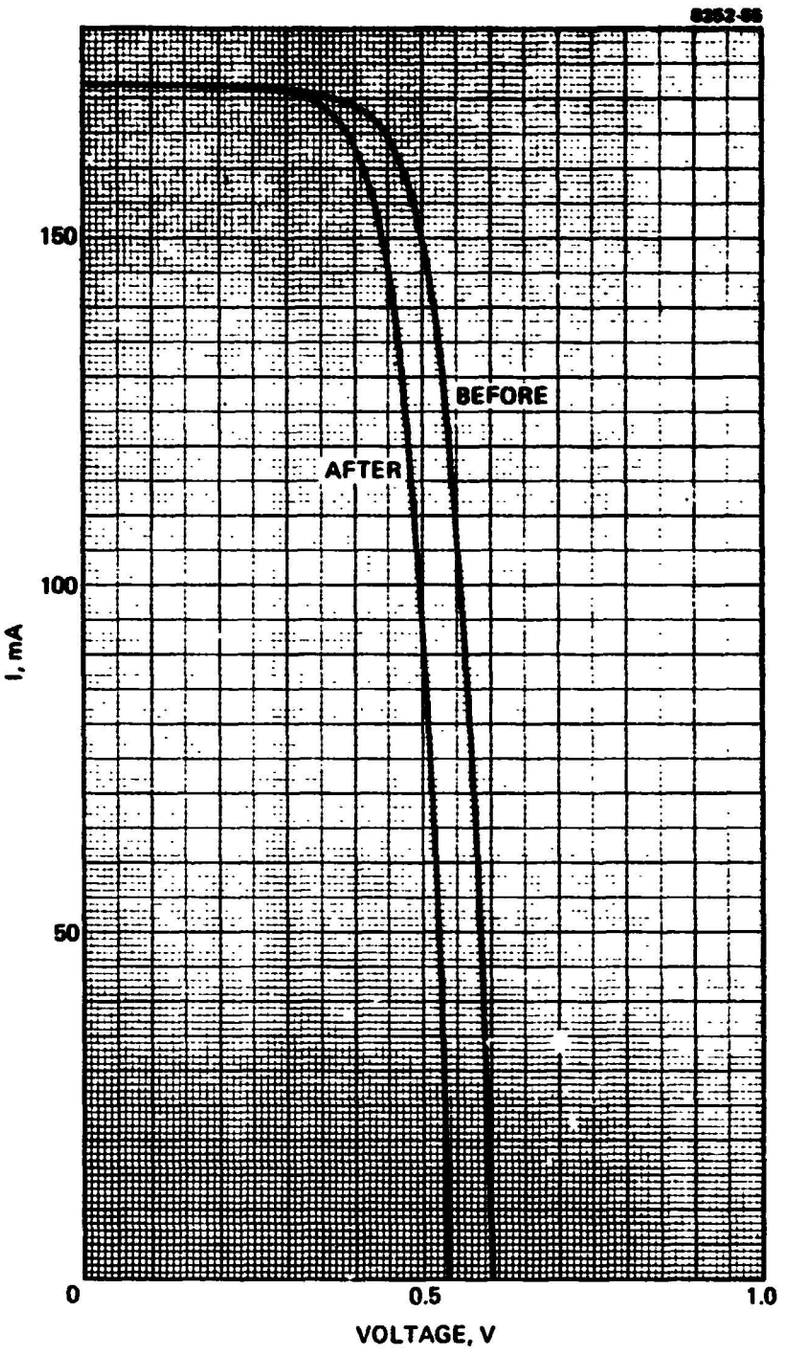

Figure C-7. Photo I-V characteristics of Si solar cell before and after proton irradiation; proton energy = 100 keV; 1 x 10^{11} P/cm^2 (cell 2).

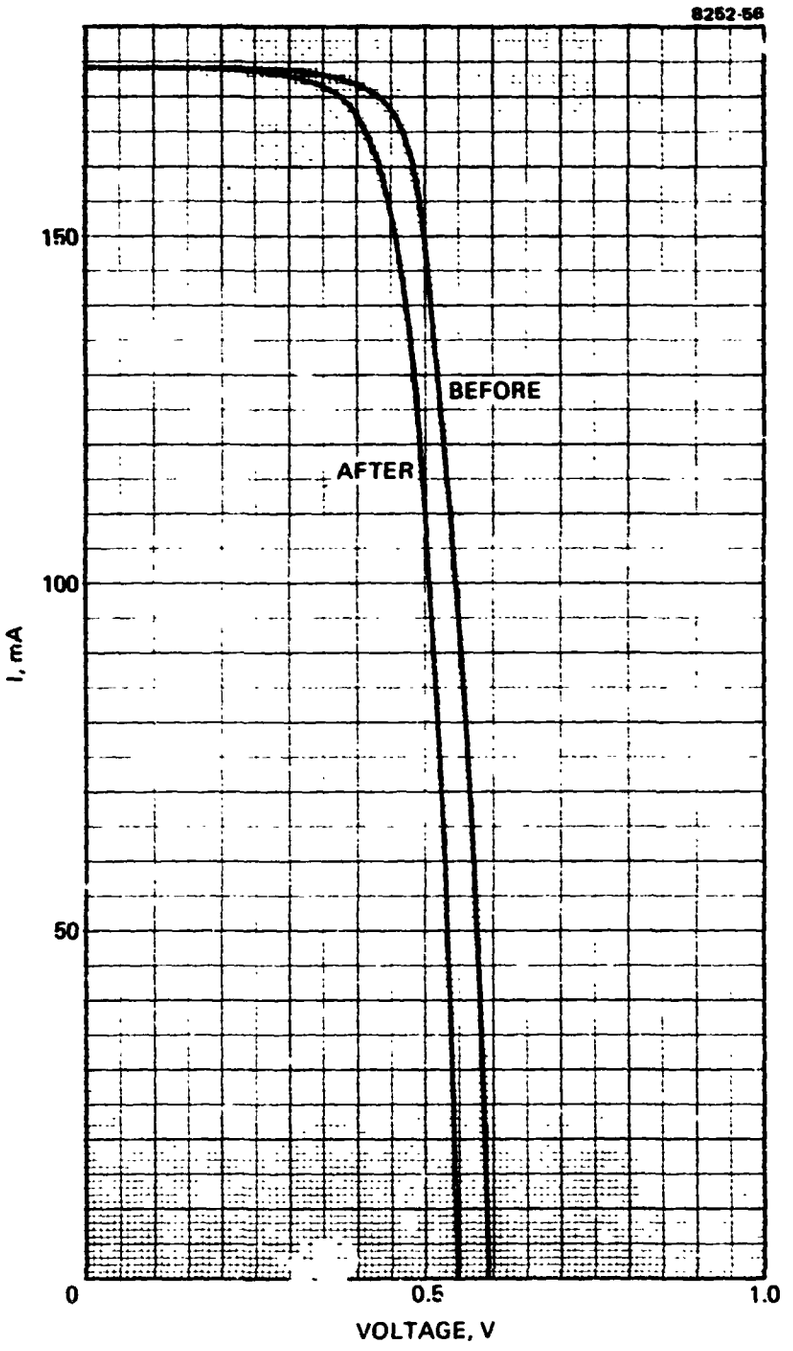

Figure C-8. Photo I-V characteristics of Si solar cell before and after proton irradiation; proton energy = 100 keV; 1 x 10^{11} P/cm^2 (cell 5).

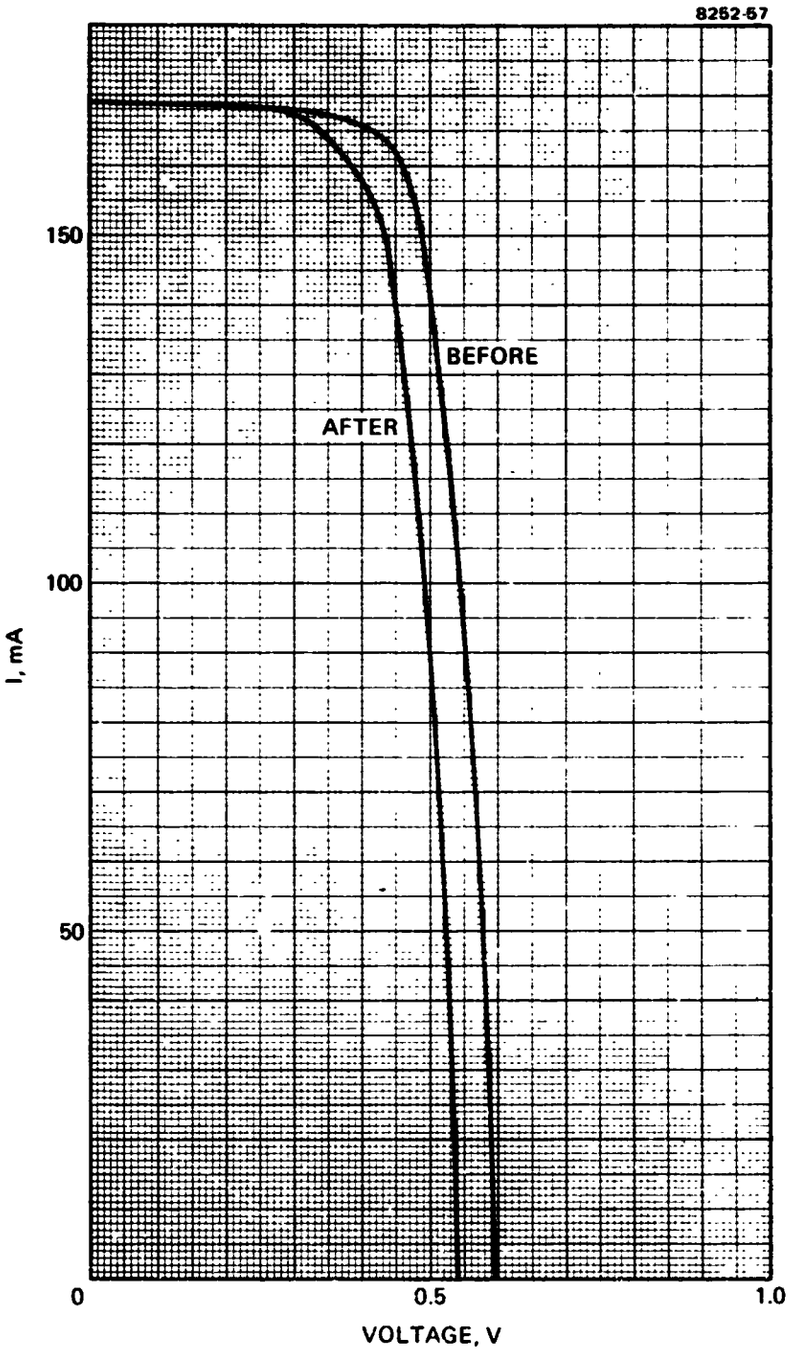

Figure C-9. Photo I-V characteristics of Si solar cell before and after proton irradiation; proton energy = 100 keV; 1 x 10^{11} P/cm^2 (cell 8).

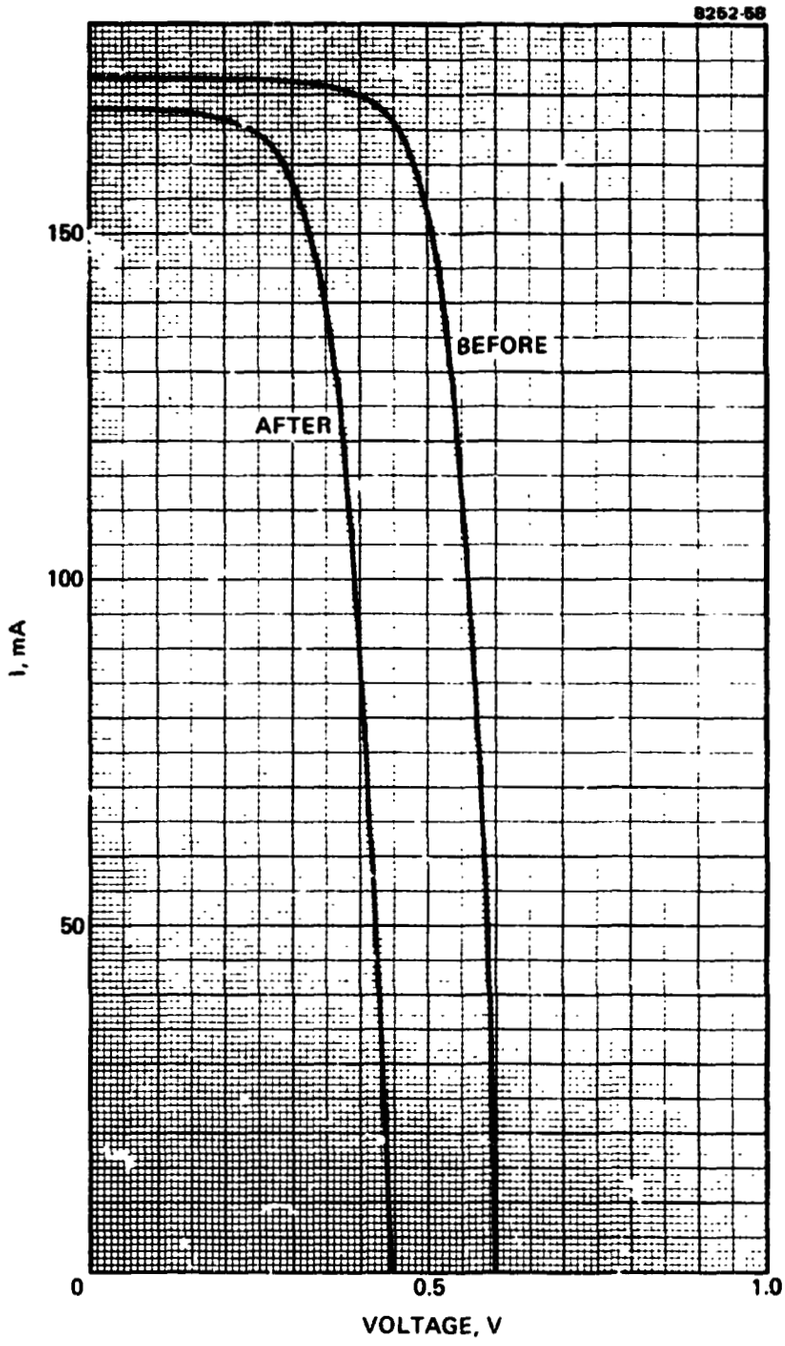

Figure C-10. Photo I-V characteristics of Si solar cell before and after proton irradiation; proton energy = 100 keV; 1 x 10^{12} P/cm^2 (cell 13).

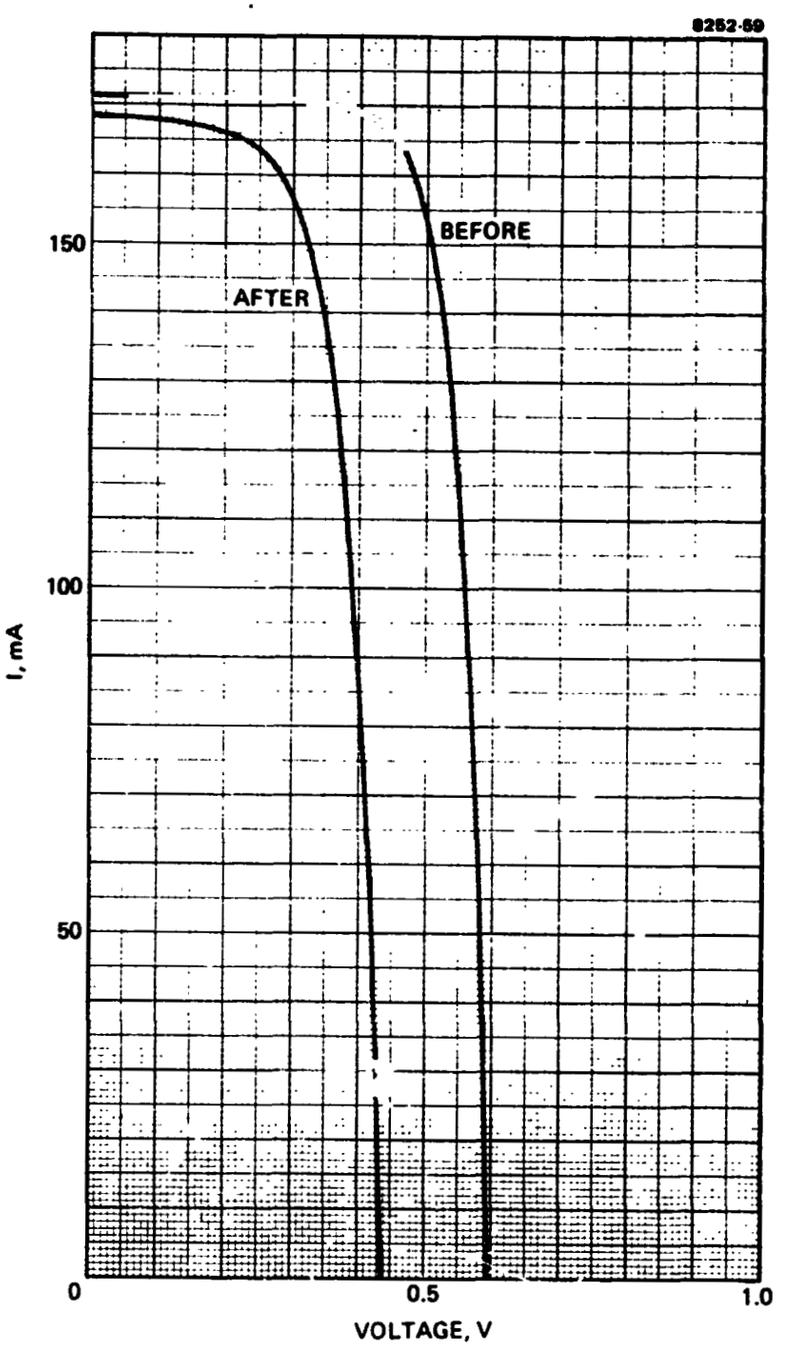

Figure C-11. Photo I-V characteristics of Si solar cell before and after proton irradiation; proton energy = 100 keV; 1 x 10^{12} P/cm^2 (cell 14).

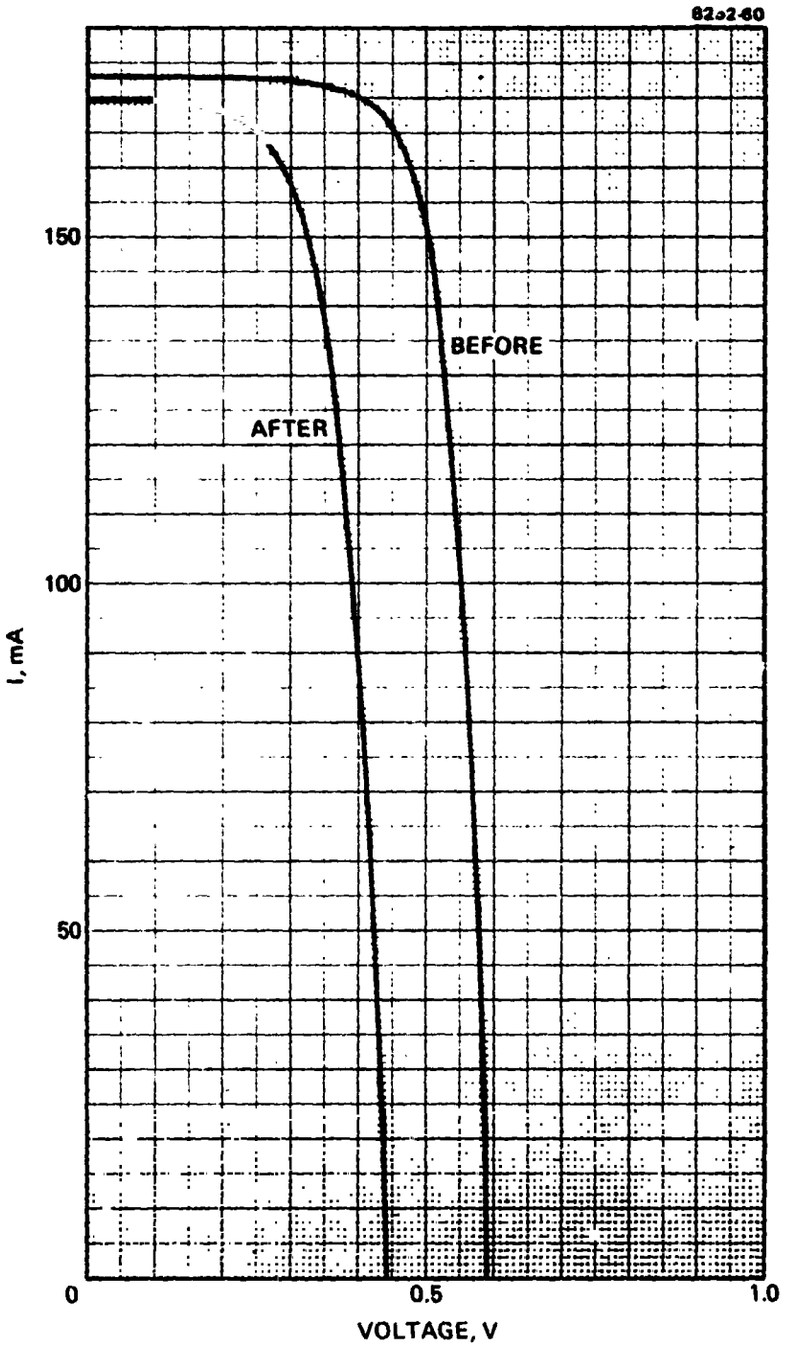

Figure C-12. Photo I-V characteristics of Si solar cell before and after proton irradiation; proton energy = 100 keV; 1 x 10^{12} P/cm^2 (cell 15).

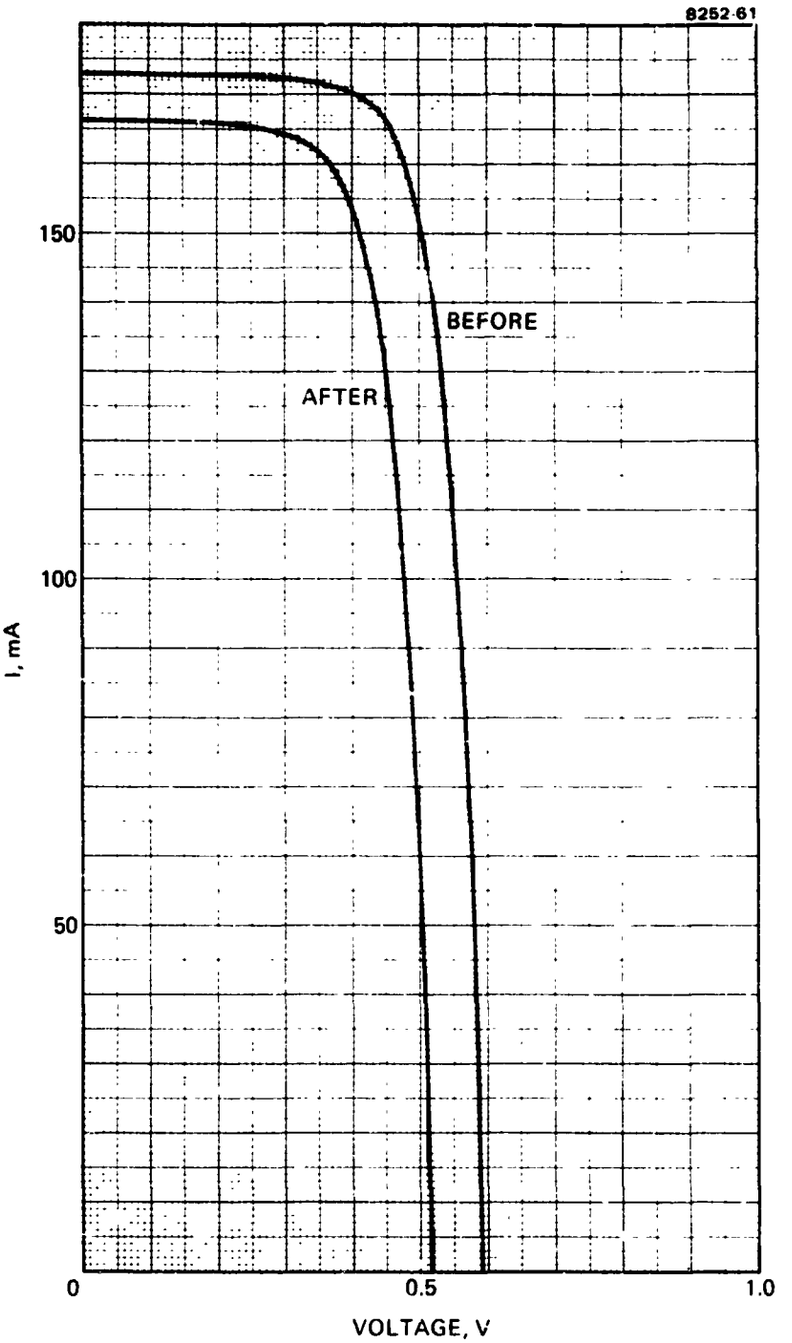

Figure C-13. Photo I-V characteristics of Si solar cell before and after proton irradiation; proton energy = 290 keV; 1 x 10^{11} P/cm^2 (cell 1).

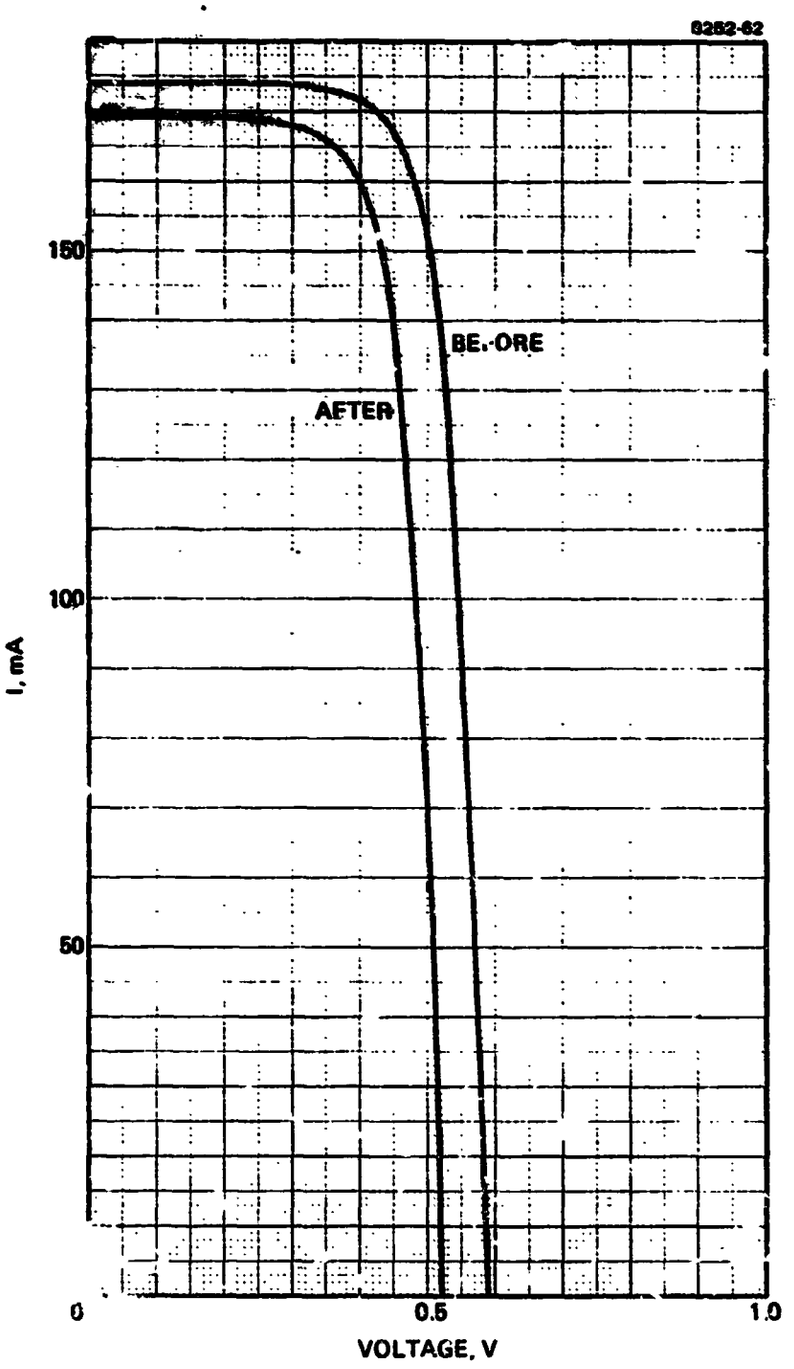

Figure C-14. Photo I-V characteristics of Si solar cell before and after proton irradiation; proton energy = 290 keV; 1 x 10^{11} P/cm^2 (cell 4).

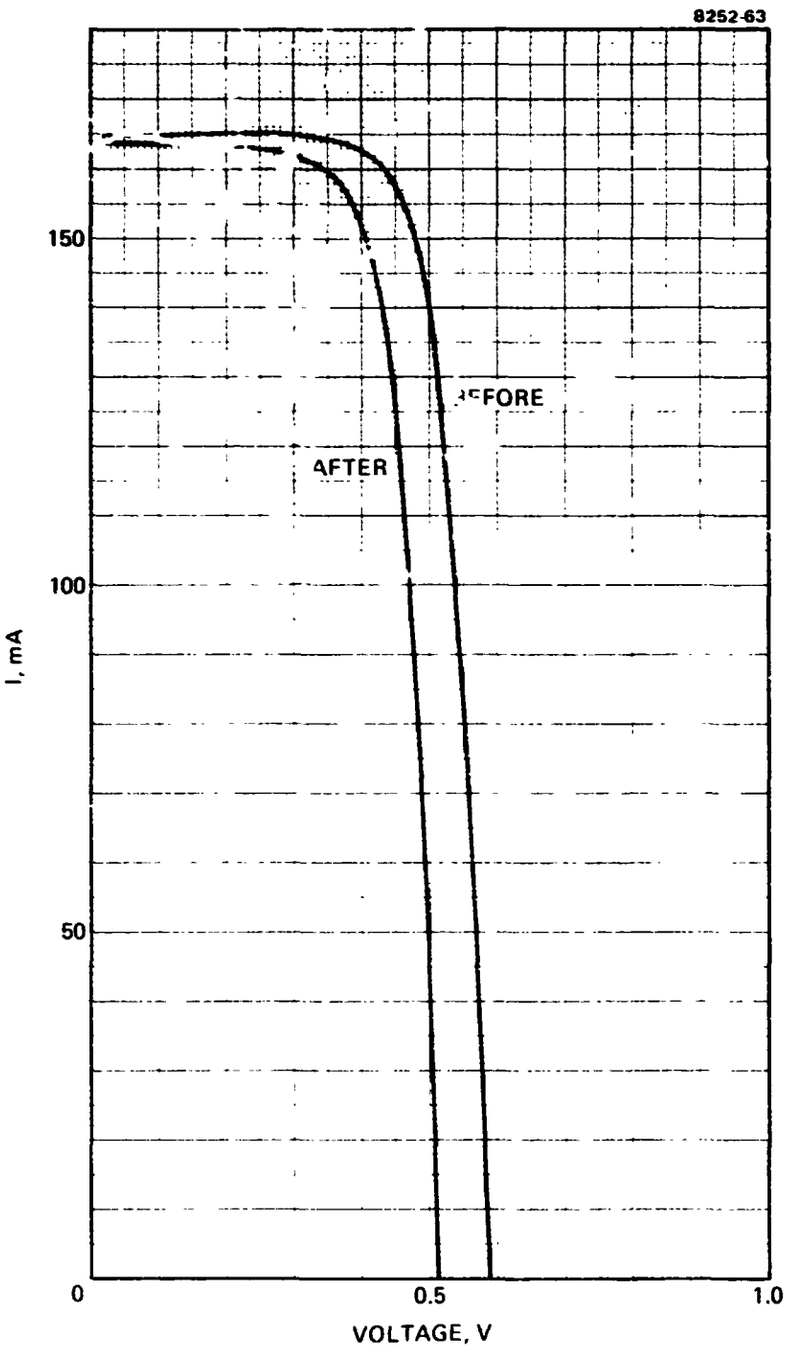

Figure C-15. Photo I-V characteristics of Si solar cell before and after proton irradiation; proton energy = 290 keV; 1 x 10^{11} P/cm^2 (cell 7).

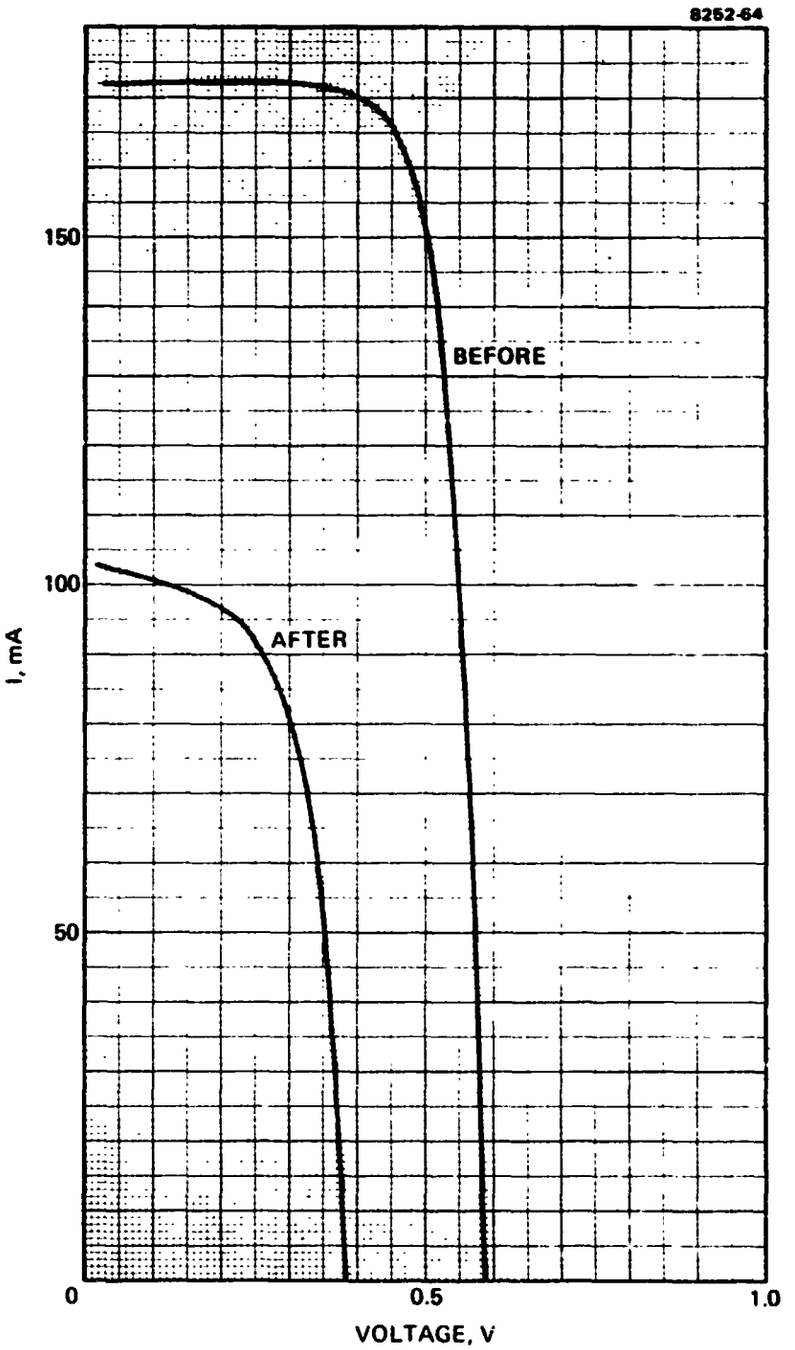

Figure C-16. Photo I-V characteristics of Si solar cell before and after proton irradiation; proton energy = 290 keV; 1 x 10^{12} P/cm^2 (cell 16).

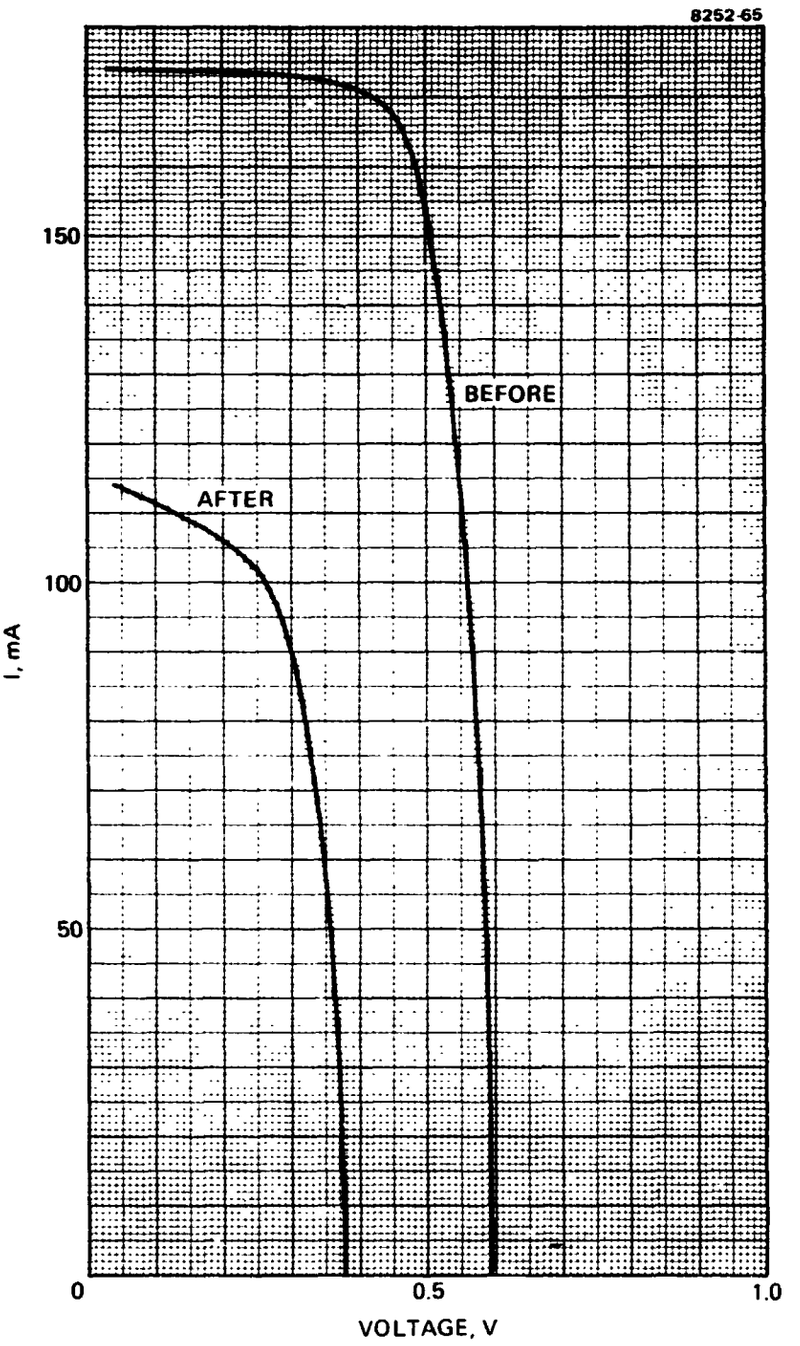

Figure C-17. Photo I-V characteristics of Si solar cell before and after proton irradiation; proton energy = 290 keV; 1 x 10^{12} P/cm^2 (cell 17).

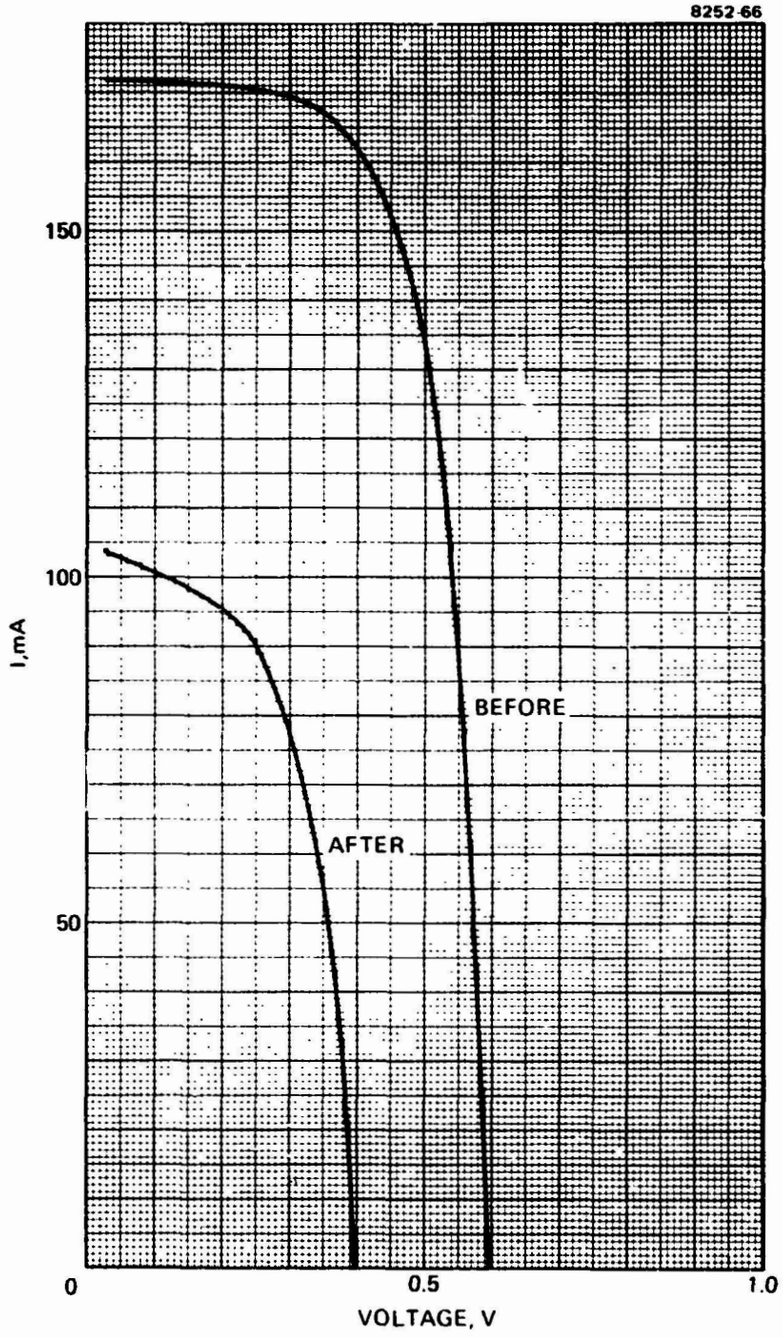

Figure C-18. Photo I-V characteristics of Si solar cell before and after proton irradiation; proton energy = 290 keV; 1 x 10^{12} P/cm^2 (cell 18).